AN EXPERIMENTAL FACILITY FOR MICROCHANNEL RESEARCH AND EVAPORATING R134A IN MICROCHANNEL TUBE

BY

HOUPEI LI

THESIS

Submitted in partial fulfillment of the requirements
for the degree of Master of Science in Mechanical Engineering
in the Graduate College of the
University of Illinois at Urbana-Champaign, 2016

Urbana, Illinois

Adviser:

Professor Predrag S. Hrnjak

ABSTRACT

Microchannel research is important for heat exchanger design. Heat transfer coefficient and pressure drop are the two most important parameters to be measured in an experimental facility. A featured design of heat transfer behavior and pressure drop testing facility for both evaporating and condensing refrigerant in microchannel tubes are made and introduced in this thesis. Details of the installing of the test section, conditioning section, pressure sensors, and other important component of the facility are discussed in section 2. The calibration process of measurement instruments and results are reported in section 3. Heat loss to ambient, effect of thermal paste contact resistance, and temperature uniformity have been discussed in detail. The process of data reduction and uncertainty analysis are discussed. In section 4, testing results of the facility with evaporating R134a are given. Both heat transfer coefficient and pressure drop are measured and reported in this thesis. The conclusion gives a brief summary of this thesis. The appendix has included calibration data from section 2 and raw data from section 4.

Acknowledgments

First of all, I would like to thank my parents. Their elite education and selfless support to me help me to build confidence to conquer problems.

My advisor, Pega Hrnjak, is an intelligent and diligent scientist who guides his student to dig in the earth of truth. I learn not only research but also the attitude to science from him. Professors in our group also give me a lot of help to progress my project including Anthony Jacobi, Clark Bullard, Stefan Elbel, and Xiaofei Wang. Lisa Burdin in ACRC is a generous lady who helps me a lot in administration.

Special thanks to all my colleagues in Air Conditioning and Refrigerate Center: Amir, Bill, Lili, Shenghan, Yu, Neal, Huize, Jun, Wenzhe, Yueming, Hongliang, Andrea, Jiange, Jiu, Cheng-min, Jingwei, Fiona, Yuheng, etc. And all visiting researcher in ACRC bring their new ideas to me: Dong, Nian, Hongliang, Rijing, Lin, Jiao, etc. I really appreciate to William (Bill) Davies who read and corrected my thesis very carefully. My partner in this project, Jiange, contributed his spare time on building the facility.

Great supports from Creative Thermal Solution. Appreciations to everyone in CTS. Specially thanks to Dejan, Dr. Li, Lisa, Ke, Tom, Xida, Hui, John, etc. who directly efforts in my project. Dejan is a creative engineer and worked with me to build the facility, and I have learned a lot of technique skills from him. Dr. Li is a great tutor who guide me in controlling and experiments. Lisa is a beautiful lady who contributed in instruments. Xida is a hard-working engineer who helped me on electrical panel.

Thanks to all our sponsors in ACRC. They give financial help, materials support, and experiences to the facility and project.

Table of Contents

List of Figures

List of Tables

Nomenclatures

Symbol or abbreviation	description	Unit	Type*
Ac	cross sectional area	m^2	C
As	surface area	m^2	C
CS	Conditioning section	-	-
d	diameter	m	C
DP	differential pressure	kPa	M
DP3	differential pressure range 3	kPa	M
DP4	differential pressure range 4	kPa	M
h	enthalpy	$Jkg^{-1}K^{-1}$	C
HTC	heat transfer coefficient	$Wm^{-2}K^{-1}$	C
l	length	m	C
lambda	mean free path	m	C
LMTD	log mean temperautre difference	^oC	C
m	mass flow rate	$g\text{-}s^{-1}$ (M), $kg\text{-}s^{-1}$(C)	CM
M	mass	kg	CM
OCR	oil circulation rate	-	CM
P	pressure	kPa	CM
PD	pressure drop	$kPa\text{-}m^{-1}$	C
Q	heat transfer rate	W	C
QL	heat loss rate	W	C
R_cond	conduction resistance	$K\text{-}W^{-1}$	C
R_cont	contact resistance	$K\text{-}W^{-1}$	C
ρ	density	$kg\text{-}m^{-3}$	C
σ	surface tension	$N\text{-}m^{-1}$	C
T	temperature	^oC	CM
TC	Thermocouple	-	-
TS	Test section	-	-
UA	overall heat transfer coefficient with area	$W\text{-}K^{-1}$	C
V	valve opening	-	T
W	power	W	T
x	vapor quality	-	C

Type*: C=variable for calculation, M=measured variable, T=controlling variable.

Subscripts mainly have three parts: component, refrigerant/material, location. Three parts are separated by their capital initial, as shown below:

$$Variable_{Component\ Refrigerant\ Location}$$

Subscription			
Component	**description**	**Fluid/Material**	**description**
Cs1	conditioning section 1	C	coolant
Cs2	conditioning section 2	G	chiller glycol
Cs3	conditioning section 3	R	refrigerant
Cs4	conditioning section 4	W	Wall
Cs5	conditioning section 5	**Location**	**description**
Csi	conditioning section i	B	bottom
Ev	evaporator	Bi	bottom inlet
Gh	glycol heater	Bo	bottom outlet
Ph	preheater	I	inlet
Phx	plate heat exchanger	O	outlet
Pump	pump	T	top
Ts1	test section 1	Ti	top inlet
Ts2	test section 2	To	top outlet
Ts3	test section 3	To	wall outlet
Ts4	test section 4	Wi	wall inlet
Ts5	test section 5		
Ts6	test section 6		
Tsi	test section i		

1. Introduction

Microchannel with smaller hydraulic diameter can increase in-tube heat transfer coefficient and pressure drop. By installing microchannel tubes instead of conventional tubes, the size and weight of heat exchanger can be decreased. In additional, a microchannel has larger surface-area-to-volume-ratio so that it has a higher boiling effect. The ratio of surface-area-to-volume can be defined as:

$$\frac{A}{V} = \frac{4\pi dl}{\pi d^2 l} \propto \frac{1}{d} \tag{1.1}$$

As the diameter decreased from 10 millimeters to 1 millimeter, which are typical conventional tube diameter and microchannel tube diameter respectively, the ratio increased to 10 times.

A larger surface-area-to-volume-ratio gives higher on-site boiling effect. Also, the smaller hydraulic diameter in microchannel tubes helps the fluid to wet the whole tube surface. In a conventional tube, liquid may only fill half of the tube (stratified flow) because of the gravitational force. However, in a tube with the hydraulic diameter smaller than the capillary length scale L_c, the surface tension force can overcome the gravitational force (Triplett, A. et al. 1999). So in microchannel tubes, an annular flow or slug flow is more likely to be observed than stratified flow.

$$L_c = \sqrt{\frac{\sigma}{g(\rho_l - \rho_g)}} \tag{1.2}$$

Equation 1.2 shows the capillary length scale. It can be reformed into equation (1.3) to show surface tension can balance gravity.

$$L_c{}^3(\rho_l - \rho_g)g = \sigma L_c \tag{1.3}$$

In order to reduce the chance that stratified flow occurs in a microchannel tube, the tube hydraulic diameter is defined by the idea of capillary length scale. Serizawa, A. et al. (2002) defined that a tube with a port diameter at the scale of or smaller than the capillary length scale can be defined as a microchannel tube.

Table 1 shows the calculated capillary length scale for different fluid. For most fluids, the length scale is about 1 millimeter. Investigators also started to give different definition and classification of microchannel tube other than Serizawa's (2002).

Table 1 Capillary length scale of different fluids at different temperature

Fluid	Temperature (°C)	Surface Tension ($mN\text{-}m^{-1}$)	Density Difference ($kg\text{-}m^{-3}$)	Capillary Length Scale (mm)
R134a	10	10.04	1241	0.9082
R134a	20	8.688	1198	0.86
Carbon Dioxide	10	2.674	725.9	0.6127
Carbon Dioxide	20	1.192	579.2	0.4581
Water	10	74.22	999.7	2.751
Water	20	72.73	998.2	2.725
R410A	10	7.684	1087	0.8491
R410A	20	6.154	1027	0.7816

Mehendale, S. et al. (2000) arbitrarily defined small channel tubes by hydraulic diameter.

Micro- heat exchanger	1 μm - 100 μm
Meso- heat exchanger	100 μm - 1 mm
Compact heat exchanger	1 mm - 6 mm
Conventional heat exchanger	>6 mm

Similarly, Kandlikar and Grande (2003)defined tubes as:

Molecular Nanochannel	<0.1 μm
Transitional Nanochannel	0.1 μm – 1 μm
Transitional Microchannel	1 μm - 10 μm
Microchannel	10 μm – 200 μm
Minichannel	200 μm – 3 mm
Conventional Channel	>3mm

Note that Mehendale, S. et al. (2000) stated in their paper that there is not a precise terminology for describing the size of a heat exchanger.

Definition of the microchannel by an arbitrary parameter may not always provide the desired results as shown in table 1. It shows that different fluids under different conditions do not have the same tube size effects. To the best of the author's knowledge, classification of a tube should consider fluid dynamics and heat transfer effects rather than diameter.

Comparing microchannel tubes to macrochannel (conventional channel) tube, the boiling effect is significantly increased by the increase of area and absence of some flow patterns. Pressure drop in the microchannel is the same as in the macrophysical world, that *fRe* is a constant close to 64. Considering the heat transfer effect, capillary length scale can provide an estimated critical diameter.

As diameter decrease, the molecular effect becomes significant. A non-dimensional number to determine whether the molecular effect is significant or not is Knudsen number (*Kn*) (Mehendale, S. et al.).

$$Kn = \frac{\lambda}{d_h} \tag{1.4}$$

Where d_h is hydraulic diameter and λ is the mean free path of molecule defined in equation 1.5:

$$\lambda = \frac{\mu\sqrt{\pi}}{\rho\sqrt{2RT}} \tag{1.4}$$

Where μ-dynamic viscosity, ρ-density, R-gas constant, and T-absolute temperature. Harley, J. C. (1993), J. C. stated in his dissertation that as *Kn* becomes larger than 0.001, continuum flow theory needs to be modified (slip flow); as *Kn* becomes larger than 0.1, flow needs to be studied statistically; and as *Kn* becomes larger than 10, individual molecules must be modeled and treated statistically (free molecular flow). Calculated mean free path and diameter for these criteria have been calculated in table 2.

Table 2 Mean free path and diameter at certain Knudsen number for different gasses

Gas	μ [$gm^{-1}s^{-1}$]	R [J kg^{-1} K^{-1}]	ρ [kg-m^{-3}]	λ [μm]	d_h [μm] Kn=0.001	d_h [μm] Kn=0.1	d_h [μm] Kn=10
Air	0.01854	287.1	1.176	0.06728	67.28	0.6728	0.006728
Nitrogen	0.0179	296.8	1.138	0.06603	66.03	0.6603	0.006603
Oxygen	0.02066	259.8	1.300	0.07128	71.28	0.7128	0.007128
Carbon dioxide	0.01503	188.9	1.796	0.04402	44.02	0.4402	0.004402

As diameter drops to the μm level, it can be predicted that molecular effects will increase dramatically.

In order to quantify heat transfer and hydraulic behavior, heat transfer coefficient (HTC) and pressure drop (PD) are the most important parameters to be investigated experimentally or theoretically.

Heat transfer coefficient measurements are generally conducted in one of two conditions: constant heat flux or constant wall temperature. The constant heat flux method is more commonly used due to more convenient and accurate control. However, in reality, because of the temperature change of the single phase secondary fluid, neither constant heat flux nor constant wall temperature can be achieved. In two-phase flow, since the bulk temperature of the refrigerant is constant, constant wall temperature is considered to better resemble reality. The challenge of holding wall temperature constant is keeping wall temperature uniform throughout the test sections while being able to measure heat flux accurately. Besides, it is preferred to collect data from quality zero to one in one pass. Pressure drop is usually measured adiabatically. The difference between adiabatic pressure drop and diabatic pressure drop is that evaporation is an accelerating process and condensation is a decelerating process.

A new experimental facility has been designed and built to study heat transfer and hydraulic behavior of refrigerants in microchannel tubes. The facility can measure heat transfer coefficient with desired heat flux, mass flux, and wall temperature. In the meantime, diabatic pressure drop can be collected. Adiabatic pressure drop can be measured separately. Oil circulation and potential ports at each test section for fluid sample are included on it.

There are three loops in this facility: refrigerant loop, coolant (water) loop, and chiller (glycol) loop. The refrigerant loop is used to determine the condition of refrigerant and pressure drop across test sections. Heat flux is determined in coolant loop by measuring the temperature difference between inlet and outlet coolant and the mass flow rate. Constant wall temperature is controlled by heating water before the inlet of test sections. Wall temperature is determined by inserting thermocouples into an aluminum block between the tested tube and the secondary fluid tube. The large thermal capacity of aluminum should give a relatively uniform wall temperature. The function of the chiller loop is to cool the water to set the condition. In additional, the chiller loop will be used to condense refrigerant in evaporating mode.

The first fluid tested on the facility is R134a. 1,1,1,2-tetrafluoroethane, also known as R134a, is a fluid that has much lower ozone depletion potential, but relatively high global warming potential. It is fading out in recent years and probably will be replaced by refrigerant with much smaller Global Warming Potential such as R1234ze(E) or carbon dioxide.

In this thesis, a general introduction to the experimental facility for evaporating research and details of how the new experimental facility was designed and built will be delivered first. Secondly, important calibration processes will be explained and parameters will be given. A literature review of R134a prediction model will be made. Tested data of R134a on the new facility will be shown and discussed. At the end will be the conclusion of this thesis.

2. Experimental Facility for Microchannel

2.1 Literature study of designing an experimental facility for evaporation

Generally, there are different approaches to conducting an evaporation experiment in tubes. Different approaches could give different results. Some results may be closer to engineering realistic applications and some may be too idealistic to be applied to. Sometimes an ideal situation may be easier to be approached than a real situation. The term easier here could mean less cost, more stable, simpler construction, and so on. Researchers may balance between idealistic and realistic when building an experimental facility.

Heat transfer coefficient, which can be defined in equation 2.1, is the main product from heat transfer behavior experimental research.

$$HTC = \frac{Q}{A_s(T_{wall} - T_{fluid})} \tag{2.1}$$

Here, Q is the heat transfer rate. T is temperature at wall or the bulk temperature of fluid, A_s is the surface area. The way to generate and determine heat transfer rate can be performed many different ways. How temperature is measured, or what instrument is used to determine temperature can also be different and give very different result of heat transfer coefficient. Instead of determining heat transfer coefficient by definition, the Wilson plot method (Wilson, E. 1995) could also be used to determine heat transfer coefficient when the information outside the microchannel tube is known and the wall temperature is hard to measure correctly.

2.1.1 Heating methods

There are many different ways to generate heat transfer from outside of the tube to fluid in the tube. Table 2 has listed several methods of heating, a brief schematic of the heating tools, and examples of facilities using each kind of method.

Table 3 Heating Methods

Fluid Heating	Direct Fluid (Water Bath)	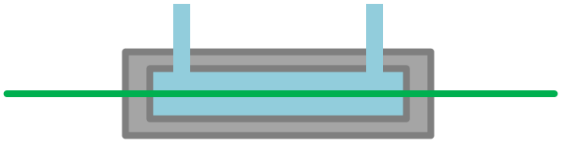	Anowar, M. et al. (2013)
	Indirect Fluid (Heat Exchanger)	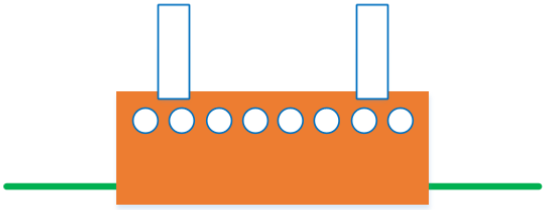	This Thesis
Electrical Heating	Direct Current	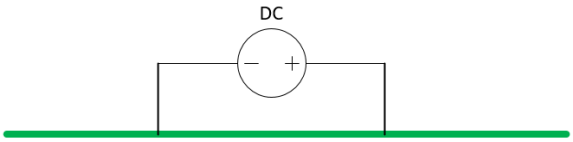	Anwar, Z. et al. (2015)
	Indirect Heater		Mortada, S. et al. (2012)
	Multiple Heaters		Qu, W., and Mudawar, I. (2003)

Fluid heating is to run a warmer fluid and transfer heat from the fluid to the refrigerant. In order to determine heat transfer rate, a heat balance method is always used. By knowing the flow rate and temperature difference from inlet to outlet of fluid, the heat transfer rate can be calculated with known heat capacity. So in this method, a well-researched fluid such as water or ethanol is used in the liquid phase in the secondary loop. However, in the indirect fluid heating method, two-phase refrigerant might be used to research a heat exchanger product.

Anowar, M. et al. (2013) have test sections like a tube-in-tube heat exchanger, with refrigerant flows in a smaller tube, and water flows in a larger tube. Mass flow rate and water temperature at the inlet and outlet are measured to determine heat flux. Wall temperature and refrigerant temperature are measured to determine temperature difference. With these two determined values, heat transfer coefficient can be calculated.

A problem may effect the accuracy in direct fluid heating is that the tube temperature might be different along the tube length since fluid temperature will change. In order to reduce the effect of non-uniformity of wall temperature, Garimella, S. and Bandhauer, S. (2001) came up with the idea of the thermal amplification method. In this method, they applied a tertiary loop to bring or remove heat from the secondary loop. In the secondary loop, water flow rate can be very high to reduce temperature change; and in the tertiary loop, the flow rate is adjusted to be very low to reduce the temperature uncertainty level.

Another way to reduce the non-uniform wall temperature effect is to add conduction distance from the secondary loop to the refrigerant loop. A heat transfer block is designed to achieve this approach and will be discussed later in this thesis.

Usually, a facility with fluid heating can conduct cooling experiments as well. Those facilities with electrical heating are most likely heating/evaporating only. Anwar, Z. et al. (2015) applied DC voltage on a stainless steel refrigerant tube. The tube is resistively heated.

Different from using the tube as a resistance heater, Mortada, S. et al. (2012) used thermal foils to heat one surface of aluminum blocks. A microchannel with a hydraulic diameter of 1.1 mm was machined on the other side of the aluminum blocks. Comparing this indirect heater method to direct current on the tube, heat flux could be more uniform to the refrigerant.

The other way to supply uniform heat flux is to use multiple heaters as in Qu, W., and Mudawar, I. (2003) A 3×4 cartridge heaters pattern inserted in a heat sink was used to heat the microchannel on their facility.

2.1.2 Microchannel selection

Basically, a microchannel tube can be procured from a manufacturing supplier or made in a lab. A lab-made microchannel tube can be made of non-engineering material. So heat transfer and hydraulic behaviors of the lab-made tube can be very different from a commercial tube. However, it's easier to control the geometric parameter on a lab-made tube.

A lab-made microchannel tube can be a circular metal tube with a small diameter. This type of tube can be easily heated by direct current heating as shown in the facility from Anwar, Z. et al. (2015). They used a 245 mm long stainless steel tube with 1.60 mm inner diameter. Triplett, K. a. et al. (1999) used Pyrex circular channels in order to study flow patterns. This is another category of material to use for lab-made microchannels: transparent material.

A lab-made microchannel tube can also be channels machined on a piece of material. As shown in Zhang, J. et al. (2010), U-shape channels are wet etched on silicon. Szczukiewicz, S. et al. (2012) applied Deep Reactive Ion Etching method to etch 67 parallel microchannels on a polished silicon wafer. Tu, X. and Hrnjak, P. (2004) machined a single-channel test section on clear PVC block.

The other major category of tubes is commercial products on the market. For example, the microchannel studied in this thesis is a 24-channel aluminum tube with a hydraulic diameter of 0.6 mm manufactured by the extruding method.

2.1.3 Number of test section(s)

An experimented facility may have multiple test sections that could collect multiple data points at one pass, or just one test section that collects fewer data points.

Qu, W., and Mudawar, I. (2003) used only one test section. Since heat transfer coefficient is typically plotted versus vapor quality, the inlet quality of the test section is changed by a pre-conditioning section.

Anowar, M. et al. (2013) had a 6.59 m test line where the effective heat transfer length is 3.6 m. And the whole test line is split into 12 test sections which are 300 mm long. They also separate the 12 test sections into two parts connected with a U-bend in order to reduce the total length of the facility.

Table 4 Comparison of test section number

	One test section	Multiple test sections
Cost to build	Less	More
Complexity	Simple	Complex
Time to steady	Shorter	Longer
Data points gained one pass	Fewer	More
Local condition	More ideal	More realistic
Uncertainty	Less	Accumulative

Table 4 gives a general comparison of test section number difference. Since there are less instruments used on one test section facility, it is typically less expensive than a multiple test sections facility. A multiple test sections facility is more complicated than a one test section facility. Because of its complexity, time waiting to reach steady state is longer. However, more data points could be gained by a multiple test sections facility. Since the flow is continued conditioned by test sections, the local condition like concentration is more realistic to a heat exchanger. The vapor quality is usually determined by heat balance in the test section and pre-conditioning section, and the uncertainty is accumulated from the first section to the last one. There are more discussions which could be made between a one test section and a multiple test sections facility, but there is not preference to say which one is better.

2.1.4. Important factors to heat transfer coefficient and pressure drop

There are a lot of effects that can influence the heat transfer coefficient and pressure drop. As shown below:

Geometry	**Fluids**	**Operation Conditions**
Channel geometry	Single/multiple Component	Heat Flux
Hydraulic diameter	One/two-phase	Saturation Temperature
Roughness	With/without oil	Mass flux
Channel Numbers		Adiabatic/diabatic
		Wall Temperature
		Concentration

These factors can be all considered in designing test matrix.

2.2 Test Facility

An experimental facility for microchannel has been designed and built. Figure 1 and 2 have shown a real photo and a functional schematic of the facility. This facility is over 6 meters long with three cycles. Figure 2 shows the refrigerant cycle (green), coolant cycle which is running water now (blue) and chiller cycle with ethylene-glycol water mixture now (purple).

Six test sections and five conditioning sections have been insulated in the pink insulation box as shown in figure 1. Pressure transducers nearby the insulation box are used to measure pressure and pressure drop. T-Type thermocouples are used to measure temperature. All flow rates are measured by mass flow meters.

Figure 1 Photos of the facility

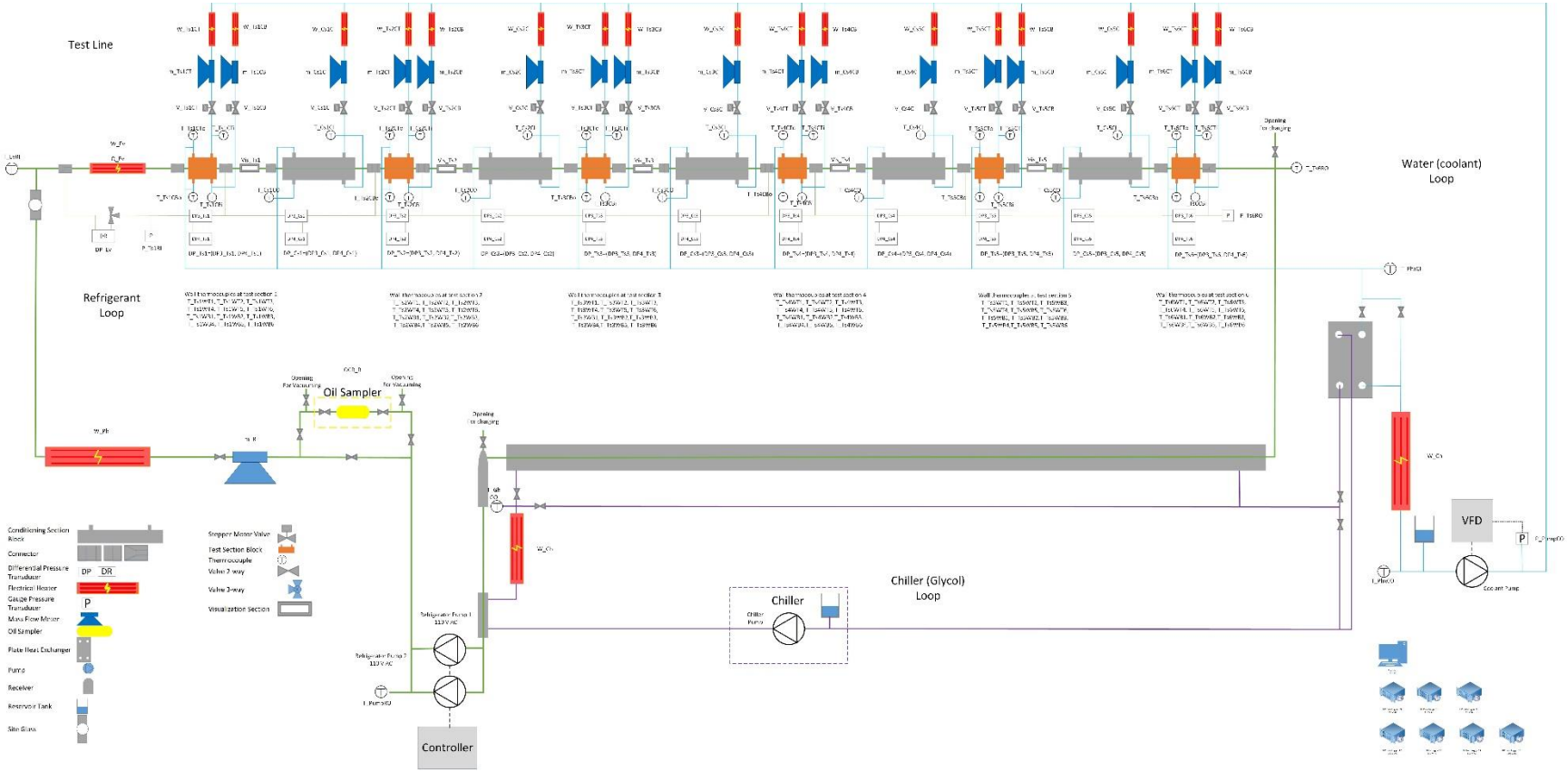

Figure 2 Functional schematic of the facility

This facility is built for multiple purposes that can be summarized as:

a) Pressure range: testing pressure can be up to 3500 kPa.
b) All refrigerants including hi-glide mixtures and ammonia: O-Rings used can resist ammonia.
c) Minimize system volume to handle mixtures and oil sampler setup added.
d) One pass multiple data points design. There are six test sections and five conditioning sections to adjust inlet condition.
e) Heaters, pumps, valves are controlled by the data loggers. A pre-programmed measurement interface uses PID subprogram to adjust all testing conditions instead of manually controlling.

With the PID subprogram, several testing situation can be adjusted automatically by data logger and computer including:

a) Constant wall temperature evaporation/condensation.
b) Constant heat flux evaporation/condensation.
c) Constant wall superheating in evaporation or subcooling in condensation.
d) Adiabatic/diabatic pressure drop.

A brief introduction of three loops has been made in this subsection and details can be found in the later text of this section.

2.2.1 Refrigerant loop

Subcooled refrigerant (observed by a sight glass) is pumped by a bi-gear-pump setup to make sure there is enough pumping power. An inline OCR measurement sampler with bypass is installed after the pump. A Micro Motion Elite CMF010 mass flow meter with the RFT9739 transmitter is used to measure refrigerant flow rate (m_R) and density (ρ_R). A pre-heater (Ph) of 2 kW is used to adjust the inlet condition of the test line where temperature (T_{EvRI}) and pressure (P_{EvRI}) are measured to determine enthalpy (h_{EvRI}). In the test line, there are an evaporator, six test sections, and five conditioning sections to measure heat transfer coefficient and pressure drop. The evaporator and conditioning sections are used for adjusting inlet condition of the following test section. Heat transfer rate of the evaporator is determined by tge DC system power supply, and the heat transfer rate of the

conditioning section is determined by the flow rate of coolant into the heat transfer block and coolant temperature difference from the outlet to inlet of the block. With determined enthalpy and measured pressure, the inlet condition is calculated. The details of test line will be introduced later in this section. An opening located at the outlet of the test line is for charging and evacuating. A co-axial design condenser (round tube to microchannel) working with chiller loop is used to condense the refrigerant. A shell and tube design sub-cooler is to subcool the refrigerant. An external receiver is used to control system pressure.

2.2.2 Coolant loop

In most cases, water is the coolant used in the coolant loop. If temperature requirements are changed, water in the coolant loop could be replaced by ethanol or glycol mixture. A pump with VFD controller is used to pump the fluid. A reservoir tank is installed at the suction of the pump in order to maintain a minimum suction pressure. Pressure at the discharge is measured by a pressure sensor and this signal is used to adjust the pump to maintain discharge pressure steady. Fluid is supplied to an inlet header to provide a parallel line to each test section and conditioning section. The fluid temperature is adjusted by a 208 V AC 530 W heater and the flow rate is adjusted by a Danfoss ETS-6 stepper motor valve. The mass flow rate is measured by a CMF010 mass flow meter in the test section and a DS006 mass flow meter in the conditioning section. Temperature measurement is done by T-Type thermocouples inserted into the coolant tube. All coolant from test sections and conditioning sections return to an outlet header. A plate heat exchanger and a 1.5 kW heater are installed after the header to adjust coolant temperature supplied to the pump.

2.2.3 Chiller loop

The chiller loop provides cooling to the refrigerant sub-cooler, refrigerant condenser, and brazed plate heat exchanger in the coolant loop. The chiller loop consists of a chiller with pump and reservoir tank and now is running with 50%-50% ethylene-glycol water mixture. After the pump, glycol flows to a sub-cooler which subcools the refrigerant to make sure that liquid refrigerant flows into the gear pump. A 1.5 kW heater is used to adjust the condenser inlet temperature of glycol. A bypass has been made for the condenser because the condenser is only needed in evaporation mode. A plate heat exchanger is used for glycol so that the coolant loop can be cooled.

2.3 Test line

From inlet to outlet in the test line, there are evaporator (*Ev*), six test sections (*Tsi*, i=1:6), five conditioning sections (*Csi*, *i*=1:5), connectors, a visualization section placeholder, and pressure transducers.

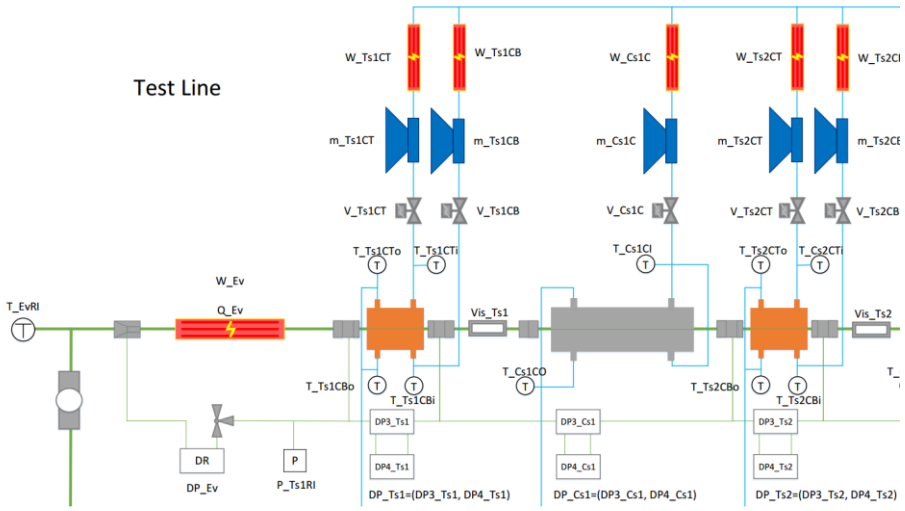

Figure 3 Schematic of inlet part in test line

As shown in figure 3, the first connector (left) is used to connect the round tube and the microchannel tube. A thermocouple inserted in the round tube close to the connector is used to measure the temperature of the refrigerant. After the connector, an evaporator is used to adjust the inlet condition of the first test section (Ts1). Figure 4 shows a real photo of inlet connector and the evaporator. A connector is used to connect two microchannel tubes with a small opening to measure the pressure. After the test section, a space is left for the visualization section which is still under construction. A conditioning section follows, which is similar to the test section but with a longer length to adjust the condition for the next test section. The test sections along the test line can provide measurements of heat transfer coefficient (HTC) and pressure drop (PD). Each of the test sections will have exactly the same mass flow rate, oil circulation rate (OCR), and composition (C) under the ideal running assumption. In the tests with oil or mixtures, the actual composition of refrigerant and OCR can be measured. The measurement of the composition is achieved by a port near the pressure transducer from which a sampler can take a refrigerant sample from the port and later be tested with spectrum analysis instrument.

Figure 4 Photo of un-insulated test line inlet

As refrigerant flows in, the test line inlet condition is set by the pre-heater (*Ph*, shown in figure 2 left bottom corner of the refrigerant line). In evaporation mode, the inlet condition will be subcooled liquid phase and inlet quality of the first test section (x_{Ts1RI}) can be adjusted by the evaporator. Inlet quality of the second test section (x_{Ts2RI}) can be adjusted by conditioning section one (*Cs1*). The same process will be made for all the rest of the sections in the test line. In condensation mode, the inlet condition of the test line is set by the pre-heater and superheated-vapor. The evaporator is turned off and the first test section (*Ts1*) is used to measure heat transfer data from super heat to two-phase. Similar to evaporation mode, conditioning section *i* (*Csi*) will adjust the inlet condition of the next test section (*Ts(i+1)*). By a proper adjustment, the six test sections will measure HTC and PD from vapor quality 0 to 1 in one pass.

The evaporator is made of two aluminum blocks that sandwich the microchannel tube. Each block has two holes. There are 4 DC electrical heaters inserted in the two blocks to provide the desired heating power to the refrigerant. The test section 1 is right after the evaporator. Refrigerant inlet enthalpy of test section 1 can be determined with knowing

enthalpy inlet of the evaporator, heat transfer rate of the evaporator, and mass flow rate of refrigerant.

The six test sections have the same design. Each of the test section consists of two aluminum blocks (6 by 3 by 1.5 inches), designated top block (TB) and bottom block (BB) as shown in figure 5. A water jacket design is machined in the block for the coolant loop. TB and BB sandwich a microchannel tube to transfer heat from coolant to refrigerant. Four long screw bolts with nuts are used to tighten the two blocks with the same torque (7.6 N-m) on each bolt in all test sections. Between microchannel and blocks, the surface cavities are filled with thermal paste CHEMPLEX 1381 DE with reported thermal conductivity of 0.75 $W\text{-}m^{-1}K^{-1}$.

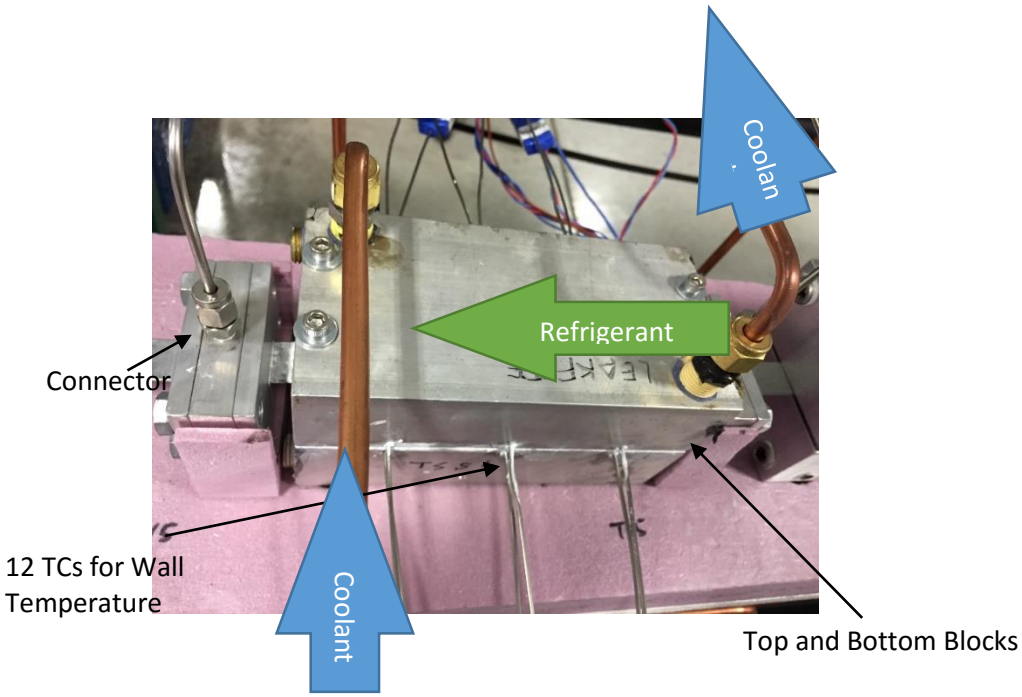

Figure 5. Photo of a test section

On each block, three thermocouple wells have been made on one side and six in total for inserting thermocouples to measure the wall temperature. A unique calibration method for the effect of contact resistance of the thermal paste has been conducted and will be discussed in detail in section 3.

Figure 6 shows a detailed schematic of one test section with thermocouple inserted position and insulation. The two blocks are made of aluminum to make sure of good

thermal conductivity. Six thermocouples (TC) are inserted into the block's well with a diameter of 1.6 mm. The probe wells are designed to be 0.13 mm from the contact surface so that the temperature has a better representation of the wall temperature of the microchannel. The three thermocouples on one side are distributed almost equally to cover the 6 inches of length. The first TC well is 20.8 mm from the front surface, the second TC well is at the center which is 30 mm from the first one, and the third one is 30 mm from the second one.

The coolant channel is machined and the design can be seen in figure 6. The coolant mass flow rate is measured by a Micro Motion elite mass flow meter ($m_{TsiCT/TsiCB}$, i=1:6) and adjusted by a Danfoss ETS 6 thermal expansion valve ($V_{TsiCT/TsiCB}$). Coolant temperature ($T_{TsiCTi/TsiCTo/TsiCBi/TsiCBo}$) is measured by thermocouple and adjusted by a heater ($W_{TsiCT/TsiCB}$). The mass flow rate is maintained to keep a reasonable temperature difference among wall temperature readings (within 0.5 ^{o}C) and a reliable inlet to outlet difference (around 3 ^{o}C). The heater adjusts the coolant temperature so that heat flux is controlled. All control signals are supplied by an HP 3852A data logger and PID subprogram in the measurement program.

The installation of pressure transducers will be discussed later in this section.

The conditioning section has the same design as the test sections, but is longer in length (400mm). And there is not a wall TC well in the conditioning sections. And the section is not tightened with bolts. The function of the conditioning section is that the heater (W_{CsiC}) will adjust the temperature ($T_{CsiCI/CsiCO}$) in order to adjust heat transfer rate from coolant to refrigerant line. In this way, the inlet quality for the next test section can be controlled to the desired value. Figure 7 shows a top view mechanical drawing of a conditioning section block. Details of the calculation of quality will be mentioned in section 3.

In test sections, the top and bottom blocks have two different coolant flow directions. TB is counter flow to the refrigerant and BB is parallel flow to the refrigerant. This design helps to reduce the effects of coolant temperature distribution on wall temperature uniformity. Temperature uniformity will be discussed in section 3 in this thesis. In the conditioning section, both the top and bottom block are counter flow design to

refrigerant for a better heat transfer. The tubing method could be read from figure 6 and a photo has been shown in figure 5.

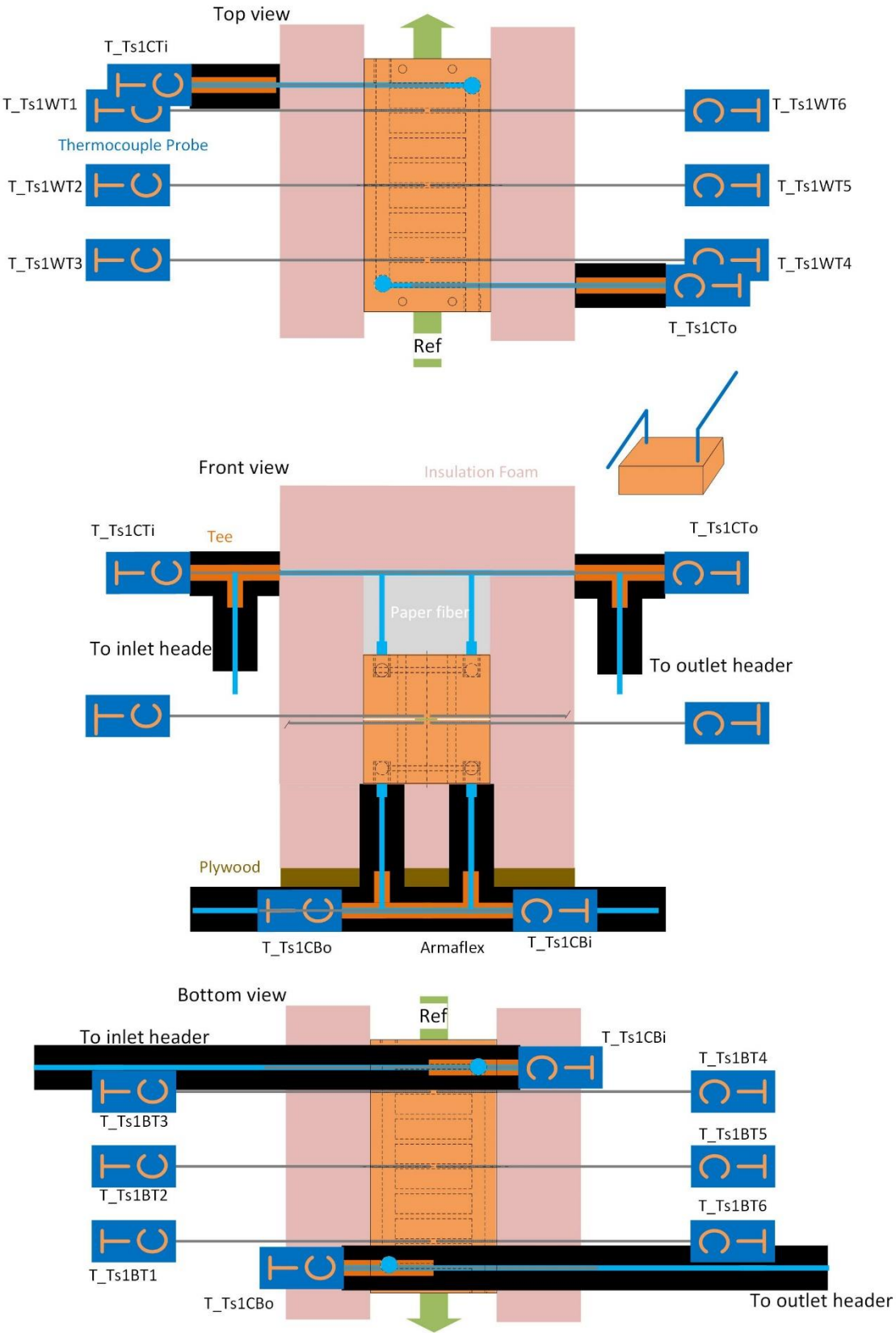

Figure 6 Schematic of one test section with TCs and insulation

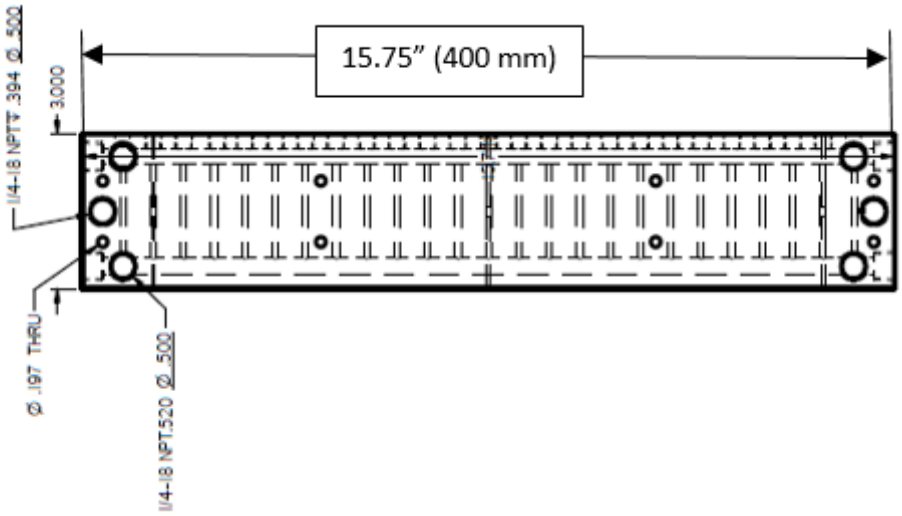

Figure 7 Conditioning section block

The microchannel used here is a 24-port flat tube and each tube has a hydraulic diameter of 0.65 mm for main port and 0.60 mm for the whole tube as shown in figure 8. Figure 9 shows the photo of the tube and inner channels.

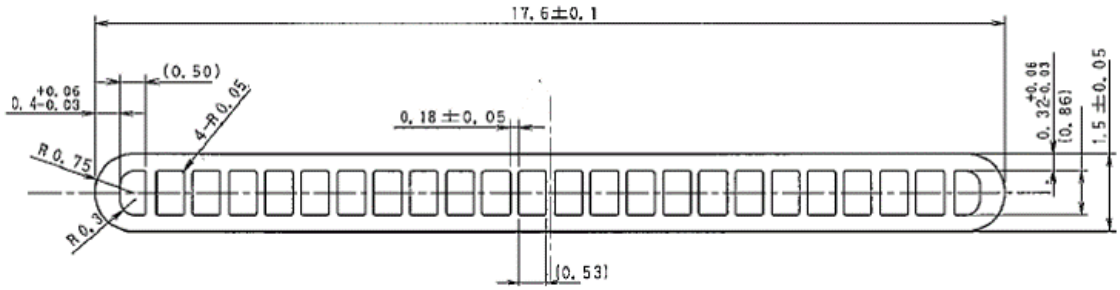

Figure 8 Cross sectional view of microchannel tube

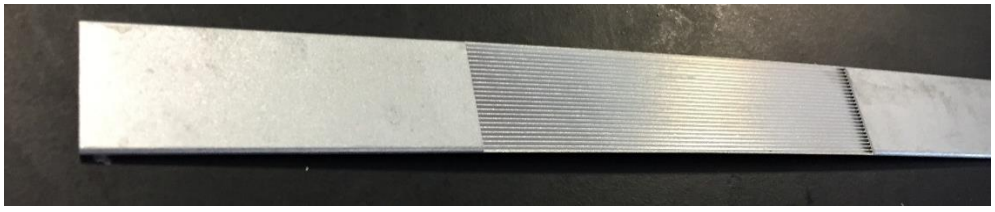

Figure 9 Photo of microchannel tube and inner channels

In between the test section and conditioning section, a short microchannel tube has been placed as a placeholder for future improvement of visualization sections. The author has tried many different ways for the microchannel visualization part that can hold pressure

up to 3500 kPa. Figure 10 shows two designs of the visualization section. This work will be continued.

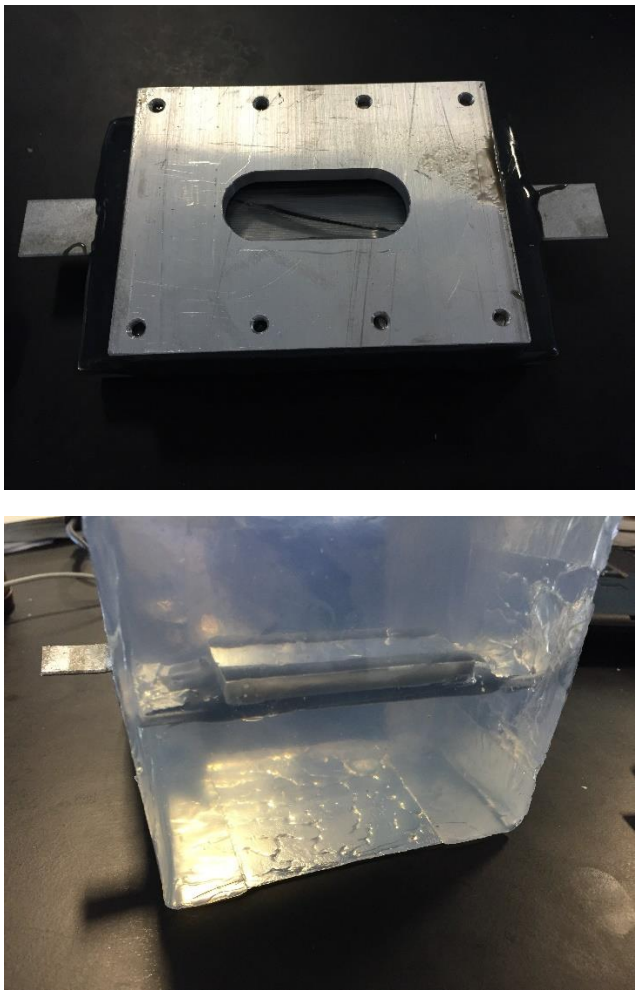

Figure 10 Photo of visualization section

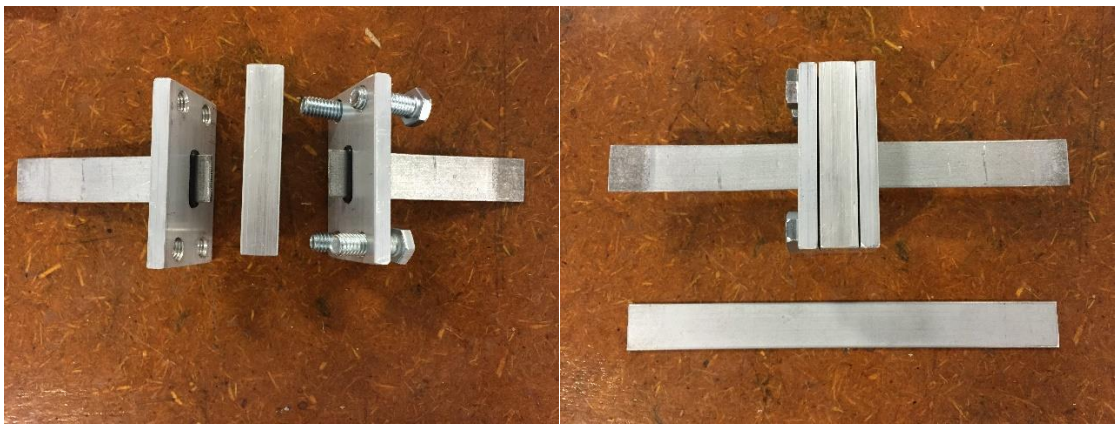

Figure 11 Connector

Figure 11 shows the design of the connector which connects two microchannel tube into one and reduces effect of re-develop of fluid. The connector is made of three pieces and tightened by four bolts. The three pieces from left to right in figure 11 are a cover with thread, a middle part without port, a cover without threads. On the cover, a round chamfer has been machined for an O-ring. Between the cover and middle part, an O-ring is used to prevent leaking. Another design of the middle part is that with a port for connection to a pressure transducer.

2.4 Pressure transducers

There are in total 26 pressure sensors on the facility and 25 of them are installed on the refrigerant line. The installation is described in Figure 5.1.

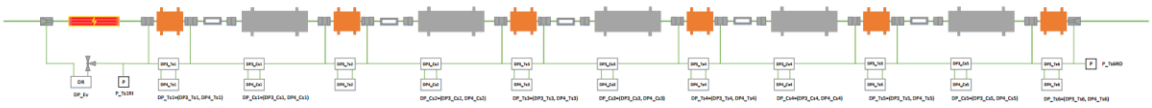

Figure 12 Schematic of installation of pressure sensors

In Figure 12, 11 of the pressure sensors are Rosemount 1151 DP3 (range code is 3). 11 of them are Rosemount 1151 DP4 (range code is 4). For the same tube section, one DP3 sensor and one DP4 sensor are installed in parallel to measure the pressure difference at inlet and outlet of the section. The reason to have two sensors for each section is to make sure the uncertainty for low-pressure difference is small enough, and the range is large enough for higher pressure difference. For example, in condensation mode, the first test section will have a larger pressure difference than the last test section since the fluid in the first test section has higher quality. In contras, the first test section will have smaller

pressure difference than the last section in evaporation mode. So a calibrated DP4 sensor will measure the pressure difference of high-quality fluid. The calibrated DP3 sensor will measure the pressure difference of low-quality fluid.

There are two Rosemount GP8 sensors to measure the gauge pressure in the system. The atmospheric pressure will be collected from an online weather server such as 'UIUC Weather'. These two Rosemount GP8 sensors have been calibrated with a span range of 3500kPa.

One Rosemount DR2 sensor is installed to measure the pressure change in the evaporator. With the gauge pressure sensor and the differential pressure sensor, the absolute pressure at the inlet of the evaporator can be calculated. The enthalpy can then be determined with temperature measurement by TC when the fluid is at SC liquid state. As the input power of evaporator and flow rate of refrigerant are also measured, the enthalpy/quality at evaporator outlet (test section 1 inlet) can be calculated. This sensor has a span range of 2 [kPa].

There is a gauge pressure sensor installed on coolant pump discharge shown in Figure 13. This is a Sensotec pressure sensor with amplified transmitter built in.

Figure 13 Coolant loop pressure sensor

This pressure sensor is installed at the discharge of the coolant pump. The signal will be used to control the coolant pump. A water reservoir installed at pump suction line so that the pressure at pump inlet is fixed almost at atmosphere pressure. The gauge pressure sensor is used to fix the pump outlet pressure by controlling the water pump VFD.

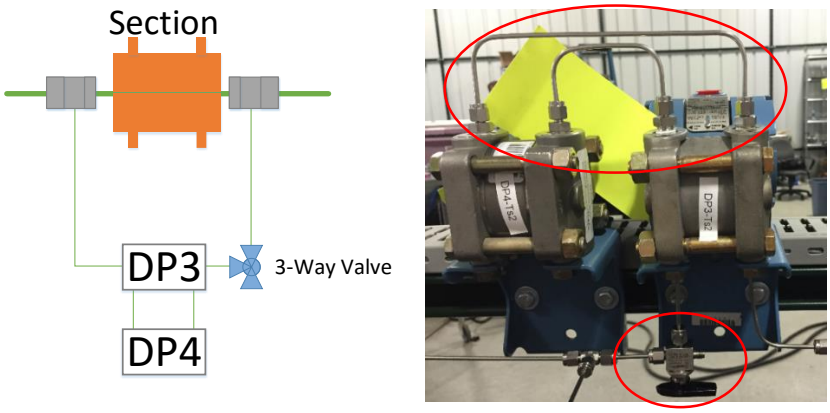

Figure 14 Three-way-valve and connection between two sensors

All Rosemount pressure transducers are calibrated online. The design is shown in Figure 14.

As shown in Figure 14, Rosemount DP3 and DP4 sensors are installed in parallel to a section. Test sections and conditioning sections have different lengths, so they have a different range of differential pressure sensors. At the low side of the DP3 sensor, a three-way valve is connected to the tube to change the low side pressure connection. As Figure 14 shows, the valve makes the low side of sensor connected to the system, which corresponds to the working position. Low sides of DP3 and DP4 sensors are connected by tube and similar connection on high sides of the two sensors. The low side of the DP3 sensor is also connected to the high side of the next DP3 sensor. In calibration, the valve will connect the low side to atmosphere. As the high side is still connected to the system, the pressure difference in the DP sensor will be adjusted by changing the system pressure. The calibration results will be reported in section 3 of this thesis.

2.5 Other important parts

2.5.1 Refrigerant pumps

The pumping system on the refrigerant loop is mainly pumped by a micro gear pump. Another gear pump is installed in parallel to the main pump for extra power when it is needed. Figure 15 shows how the pumping on the refrigerant loop is set up. The blue pump is the main pump with higher power and signal input so it can be controlled in percentage power from 0 to 99. The gray pump can be manually controlled and is by-passed to the main pump.

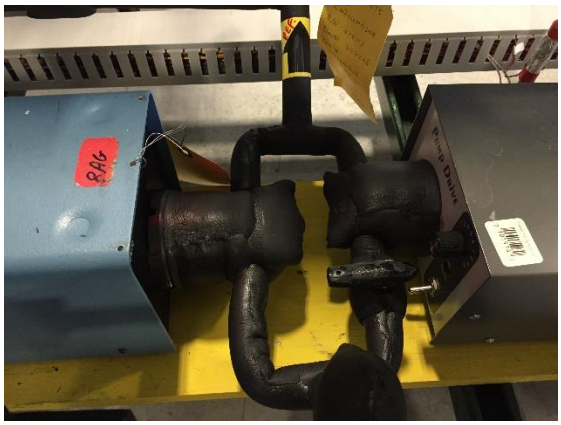

Figure 15 Gear pumps in refrigerant loop

2.5.2 Oil sampler

An oil sampler setup with bypass is installed on refrigerant loop as shown in figure 16.

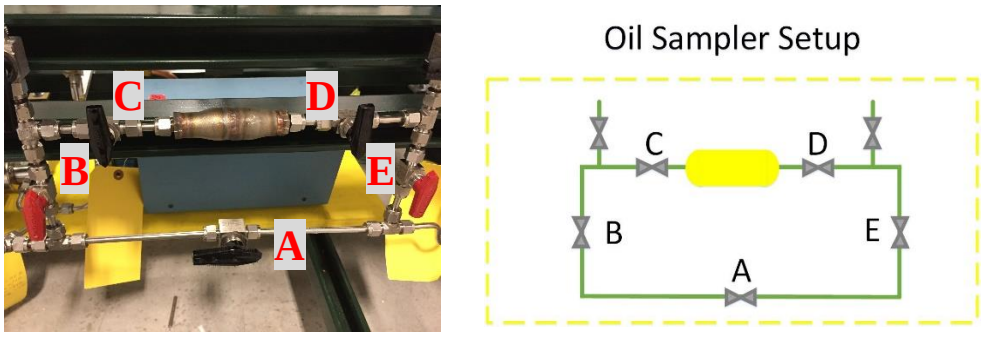

Figure 16 Oil sampler

The oil sampler can be used to measure oil circulation rate in the system. By closing the valve under the sampler (A in figure 16) and opening the other four valves (B, C, D, and E), the refrigerant will flow through the sampler. After running, by closing valve B, C, D, and E, the sampler can be taken off from the system. The sampler will be connected to a capillary tube and a needle valve. With this setup the refrigerant in the sampler can be slowly released in the vapor phase and oil will remain in the sampler. By comparing the weight of the sampler with oil and refrigerant (M_{SOR}), the weight of sampler with oil only (M_{SO}), and empty sampler (M_S), the oil circulation rate can be calculated as shown equation 2.2.

$$OCR = \frac{\mathrm{M}_{SO} - M_S}{M_{SOR} - M_S} \tag{2.2}$$

2.5.3 Chiller

A chiller is specially made for the system. The chiller is mainly made of a residential air conditioning unit, a receiver, a plate heat exchanger, a reservoir tank, and a pump. R22 in the residential unit evaporates in the plate heat exchanger and cool down the glycol. Glycol is forced by a pump to flow through the system. The chiller sub-cools the refrigerant to a sub-cooled liquid and cools the warm water to low temperature. The chiller is movable and not built within the system so that it can be easily changed when the cooling load is changed. Figure 17 shows the chiller.

Figure 17 Chiller

2.5.4 Instruments

A schematic of all instruments name and model number is shown in figure 18. Model numbers, nomenclature, and explanation of nomenclature are listed in table 5 for pressure transducers, table 6 for mass flow meters, and table 7 for stepper motor valves.

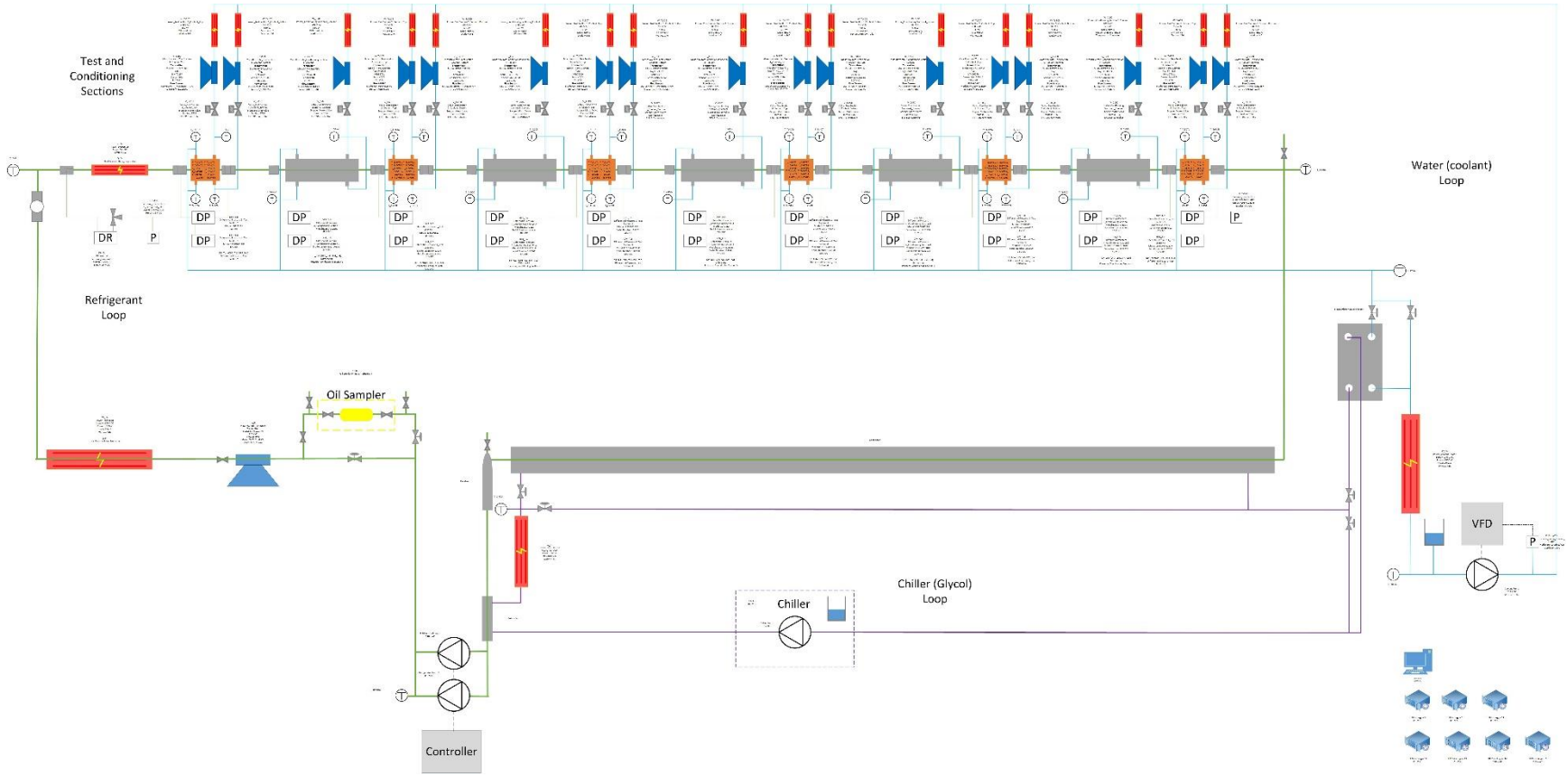

Figure 18 Detailed schematic with all instruments and nomenclature

Table 5 Pressure transducers list

Gauge pressure transducer					
Name	Component	Fluid/Material	Location	Model Number	Supply
P_Ts1RI	Test Section 1	Refrigerant	Inlet	GP8M53B1I6	12
P_Ts6RO	Test Section 6	Refrigerant	Outlet	GP8M12B1I6	12
P_PumpCO	Water Pump	coolant	Outlet	Sensotech Z/718	24
Differential pressure transducer					
Name	Component	Fluid/Material	Location/Range	Model Number	Real Supply
DP3_Ts1	Test Section 1	Refrigerant	-	S12B1	24
DP3_Cs1	Conditioning Section 1	Refrigerant	-	G22B2	48
DP3_Ts2	Test Section 2	Refrigerant	-	E12	24
DP3_Cs2	Conditioning Section 2	Refrigerant	-	E12	48
DP3_Ts3	Test Section 3	Refrigerant	-	S12B1	24
DP3_Cs3	Conditioning Section 3	Refrigerant	-	S52	24
DP3_Ts4	Test Section 4	Refrigerant	-	E12	24
DP3_Cs4	Conditioning Section 4	Refrigerant	-	G22B2	48
DP3_Ts5	Test Section 5	Refrigerant	-	J22	24
DP3_Cs5	Conditioning Section 5	Refrigerant	-	S12B1	24
DP3_Ts6	Test Section 6	Refrigerant	-	E22	24
DP4_Ts1	Test Section 1	Refrigerant	-	E12B1	12
DP4_Cs1	Conditioning Section 1	Refrigerant	-	E22T0085B3	24
DP4_Ts2	Test Section 2	Refrigerant	-	M12B1I6	12
DP4_Cs2	Conditioning Section 2	Refrigerant	-	M12B1I6	12
DP4_Ts3	Test Section 3	Refrigerant	-	M12B1I6	12
DP4_Cs3	Conditioning Section 3	Refrigerant	-	M12B1I6	12
DP4_Ts4	Test Section 4	Refrigerant	-	M12B1I6	12
DP4_Cs4	Conditioning Section 4	Refrigerant	-	M12B1I6	12
DP4_Ts5	Test Section 5	Refrigerant	-	E22	24
DP4_Cs5	Conditioning Section 5	Refrigerant	-	M12B1I6	12
DP4_Ts6	Test Section 6	Refrigerant	-	M12B1I6	12
DP_Ev	Evaporator	Refrigerant	-	DR2F22B1	24

Table 6 Mass flow meters list

Mass flow meter						
Name	Component	Fluid /Material	Location	Transmitter model:	Flow sensor model:	SENSOR S/N
m_R	-	Refrigerant	-	RFT9739	CMF010N323NU	355474
m_Ts1CT	Test Section 1	Coolant	Top	RFT9739	CMF010M313MU	454717
m_Ts1CB	Test Section 1	Coolant	Bottom	RFT97121PNU	CMF010M313MRAUEZZZ	11013107
m_Cs1C	Conditioning Section 1	Coolant	-	RFT97121PNU	DS012S109SU	231388
m_Ts2CT	Test Section 2	Coolant	Top	RFT97121PNU	CMF010M313MRAUEZZZ	460720
m_Ts2CB	Test Section 2	Coolant	Bottom	RFT97121PNU	CMF010M313MU	375953
m_Cs2C	Conditioning Section 2	Coolant	-	RFT97121PNU	DS012S109SU	212333
m_Ts3CT	Test Section 3	Coolant	Top	RFT97121PNU	CMF010M999NRAUEZZX	198531 7542
m_Ts3CB	Test Section 3	Coolant	Bottom	RFT97121PNU	CMF010M313MU	452256
m_Cs3C	Conditioning Section 3	Coolant	-	RFT97121PNU	D3012S109SU	200812
m_Ts4CT	Test Section 4	Coolant	Top	RFT97121PNU	CMF010M520MU	384735
m_Ts4CB	Test Section 4	Coolant	Bottom	RFT97121PNU	CMF010M313MU	371257
m_Cs4C	Conditioning Section 4	Coolant	-	RFT97121PNU	DS012S109SU	197102
m_Ts5CT	Test Section 5	Coolant	Top	RFT97121PNU	CMF010M321MU	364349
m_Ts5CB	Test Section 5	Coolant	Bottom	RFT97121PNU	CMF010M321MU	362352
m_Cs5C	Conditioning Section 5	Coolant	-	RFT97121PNU	DS012S109SU	204699
m_Ts6CT	Test Section 6	Coolant	Top	RFT9739	CMF010M321NRAUE22	14164795
m_Ts6CB	Test Section 6	Coolant	Bottom	RFT9739	CMF010M321MU	371103

Table 7 Stepper motor valves list

Valve			
Name	Component	Fluid/Material	Location
V_Ts1CB	Test Section 1	Coolant	Bottom
V_Ts1CT	Test Section 1	Coolant	Top
V_Cs1C	Conditioning Section 1	Coolant	-
V_Ts2CB	Test Section 2	Coolant	Bottom
V_Ts2CT	Test Section 2	Coolant	Top
V_Cs2C	Conditioning Section 2	Coolant	-
V_Ts3CB	Test Section 3	Coolant	Bottom
V_Ts3CT	Test Section 3	Coolant	Top
V_Cs3C	Conditioning Section 3	Coolant	-
V_Ts4CB	Test Section 4	Coolant	Bottom
V_Ts4CT	Test Section 4	Coolant	Top
V_Cs4C	Conditioning Section 4	Coolant	-
V_Ts5CB	Test Section 5	Coolant	Bottom
V_Ts5CT	Test Section 5	Coolant	Top
V_Cs5C	Conditioning Section 5	Coolant	-
V_Ts6CB	Test Section 6	Coolant	Bottom
V_Ts6CT	Test Section 6	Coolant	Top

2.6 Insulation

The whole system is insulated by insulation foam, Armaflex, and paper fiber. Some cavity of insulation foam is filled with silicone. Silicone is also used to glue insulations except Armaflex is glued by Armaflex 520 adhesive.

The test line is mainly insulated by insulation foam box filled with paper fiber. Another tubing on the refrigerant loop is insulated by Armaflex. Coolant loop and chiller loop are insulated by Armaflex.

2.6.1 Test line insulation

The Microchannel (MC) tube, test sections, conditioning sections, and the evaporator are insulated by 2-inch insulation board. Several boards cover the sections to form a box to prevent heat loss. Boards are glued by silicone gel. Inside the box, paper fiber is used to prevent inside natural convection and limit conduction. Table 8 listed the thermal information from manufacture's manual. Figure 19 shows how insulation is made for test sections.

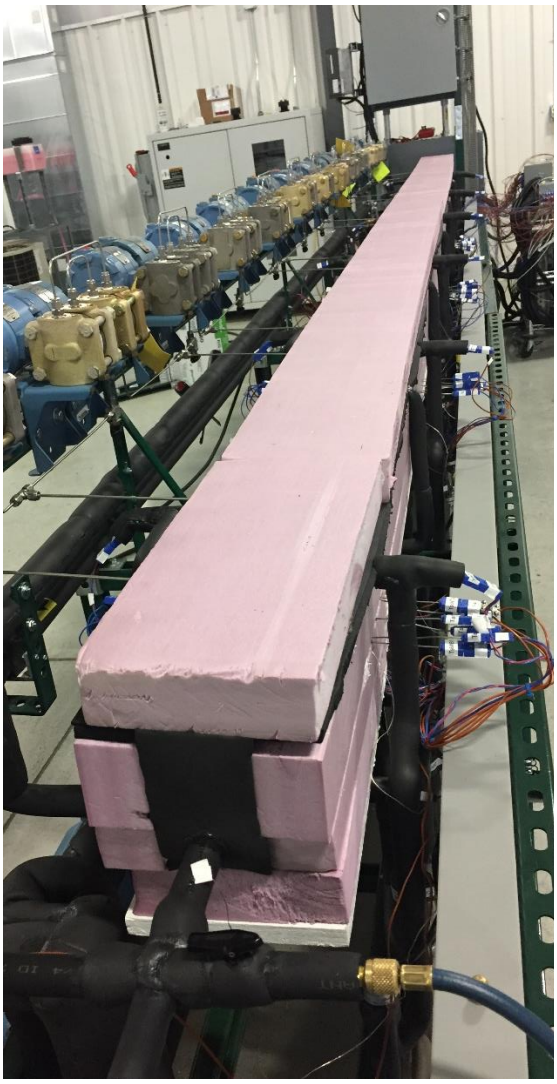

(a)

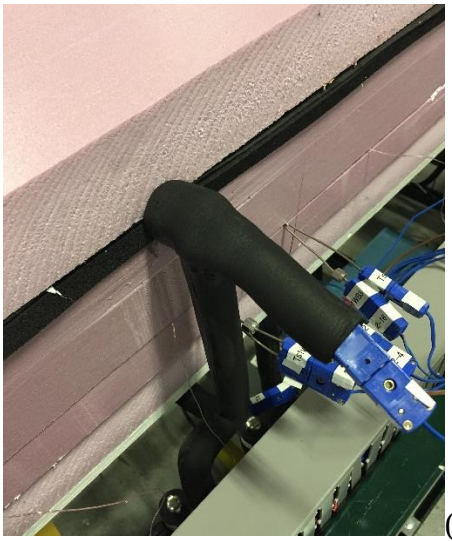

(b)

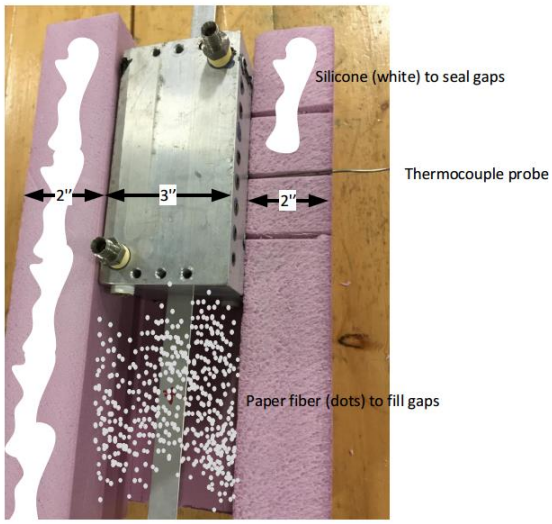

(c)

Figure 19 Test line insulation

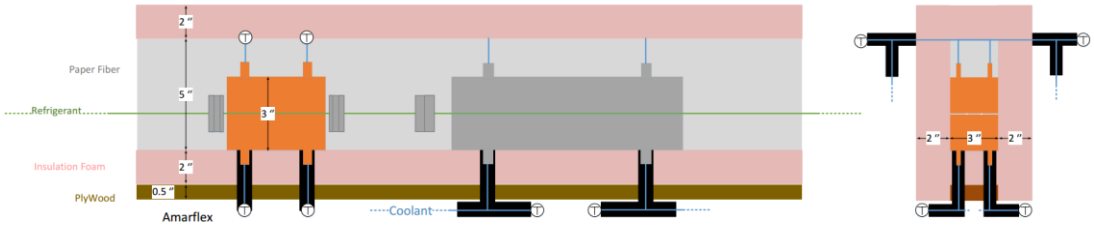

(d)

Figure 19 (cont'd)

Table 8 Reported thermal conductivity of insulation materials

Material	Thermal Conductivity [W-m^{-1}-K^{-1}]
Armaflex	0.036
Insulation Foam	0.014
Paper Fiber	0.0395

In figure 19 (a), the test line is covered by the pink insulation box which consists of several insulation foam. The box is lying on white plywood. Inlet and outlet of the box are covered by a thick piece of Armaflex sheet.

One special treatment has been made for the coolant tube outlet as shown in figure 19 (b). The coolant tube carries coolant fluid to transfer heat to the refrigerant loop. This tube lies on the insulation foam. The top foam lies on the tube as a lid to close the insulation box. In order to fill the big gap caused by the quarter-inch tube, a quarter inch thick Armaflex sheet is used. Silicone is used to glue the Armaflex sheet to the insulation foam. And the tube is insulated by Armaflex as well.

Another special treatment is the slots for thermocouples (TCs). In figure 19 (c), three slots have been made on the insulation foam so that TCs can be inserted into the test line insulation box and the heat transfer blocks. White silicone is used to fill all the gaps and glue all insulation foam contact surfaces.

In addition, the bottom block with two coolant inlet/outlet needs an opening on the insulation box. As shown in figure 19 (d), 1-inch holes have been drilled in the insulation foam and plywood. In order to reduce heat loss here, Armaflex tube insulation covered the coolant tube and fill the holes. Unoccupied space in the insulation box is filled with paper fiber in order to reduce natural convection inside the box. Under the BB, there is a total of 2.5 inches of protection consisting of 2 inches of insulation foam and a half inch of plywood.

Above the TB, there is a total of 4 inches thick protection consisting of 2 inches of paper fiber and 2 inches of insulation foam. The box has a side thickness of 2 inches.

2.6.2 Test section insulation

Additional information about test section insulation is shown in figure 20. Nomenclature of test section 1 (Ts1) is used here as an example to illustrate the position relationship of thermocouples.

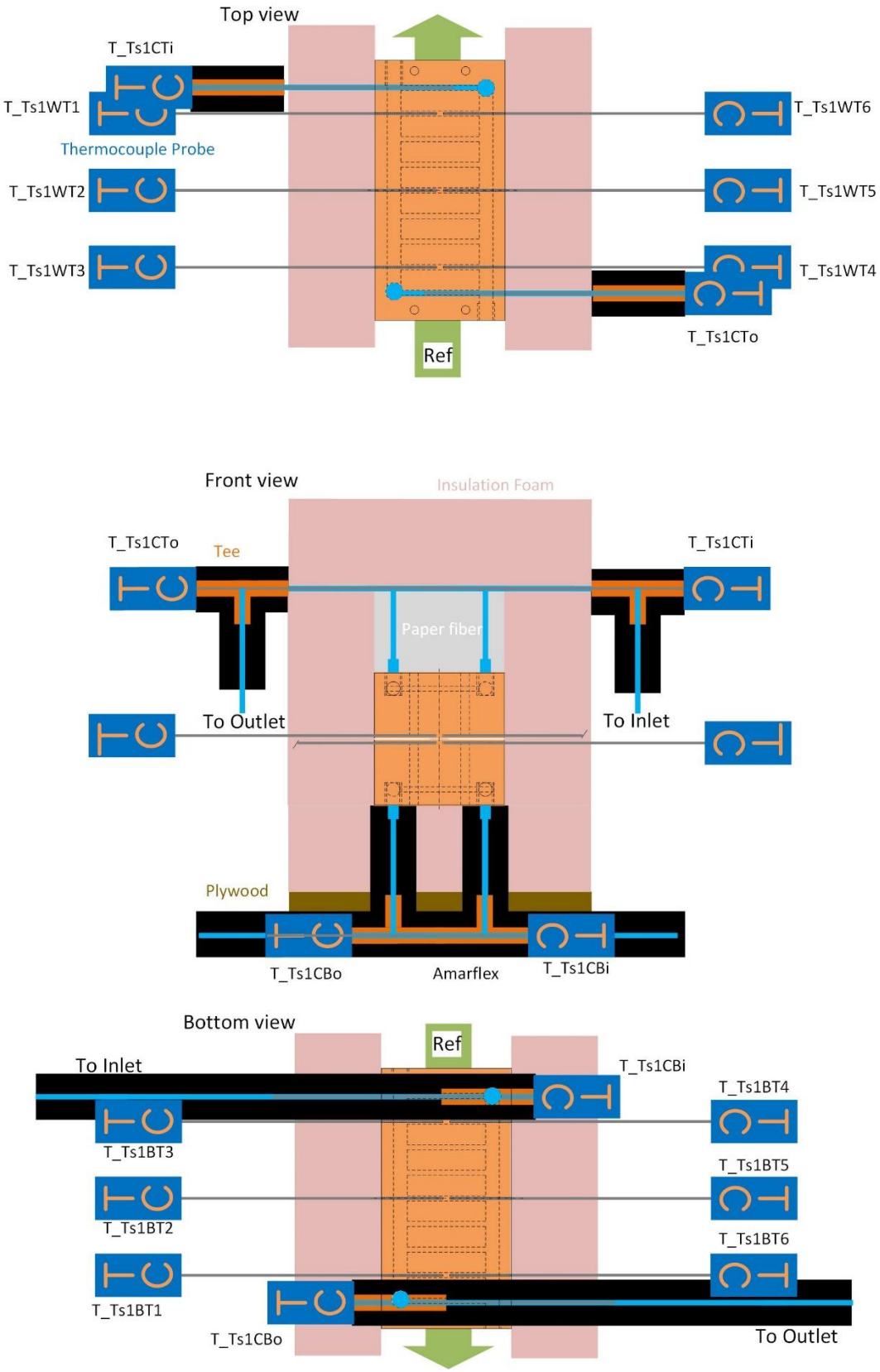

Figure 20 Test section insulation

Top cover insulation foam is removed from top view in figure 20 for better illustration. Outside of the box, the coolant tube is covered by black Armaflex insulation. Thermocouples (blue with “TC”) are inserted in a Tee into the box to measure inlet and outlet temperature. Thermocouples inserted into the top block (orange) measure wall temperature. Besides the top block, there are two 2-inch insulation foams to prevent heat loss. The top view also shows how coolant flows as counter flow to the refrigerant.

In the front view of figure 20, it shows the vertical relationship of thermocouples and insulation.

In the bottom view of figure 20, the bottom insulation foam and plywood have been removed for better illustration. Different from the top block, thermocouples in the coolant loop at the bottom block are not inserted into the insulation box. A tee is used to connect the thermocouples, tube from tee to BB, and the tube connected to coolant inlet/outlet. All tube is insulated by Armaflex. This is the reason why the coolant loop of BB has a larger heat loss rate than TB which will be presented in section 3.

2.6.3 Conditioning section insulation

Figure 21 shows the insulation and thermocouple insertion of conditioning sections. Nomenclature of conditioning section 1 (Cs1) is used here as an example to illustrate the positional relationship of thermocouples.

The front view of figure 21 shows the vertical relationship of coolant tubes and insulations. The coolant tubes from TB and BB are connected. The top view without top insulation lid shows the coolant tube across the insulation foam. Side insulation is removed from the side view for better illustration. The side view shows how the thermocouple is inserted to measure inlet and outlet temperature. A union cross is used to connect all tubes including a tube to BB, a tube to TB, a tube to inlet/outlet and thermocouple. The tubes and cross are covered by block Armaflex tube insulation.

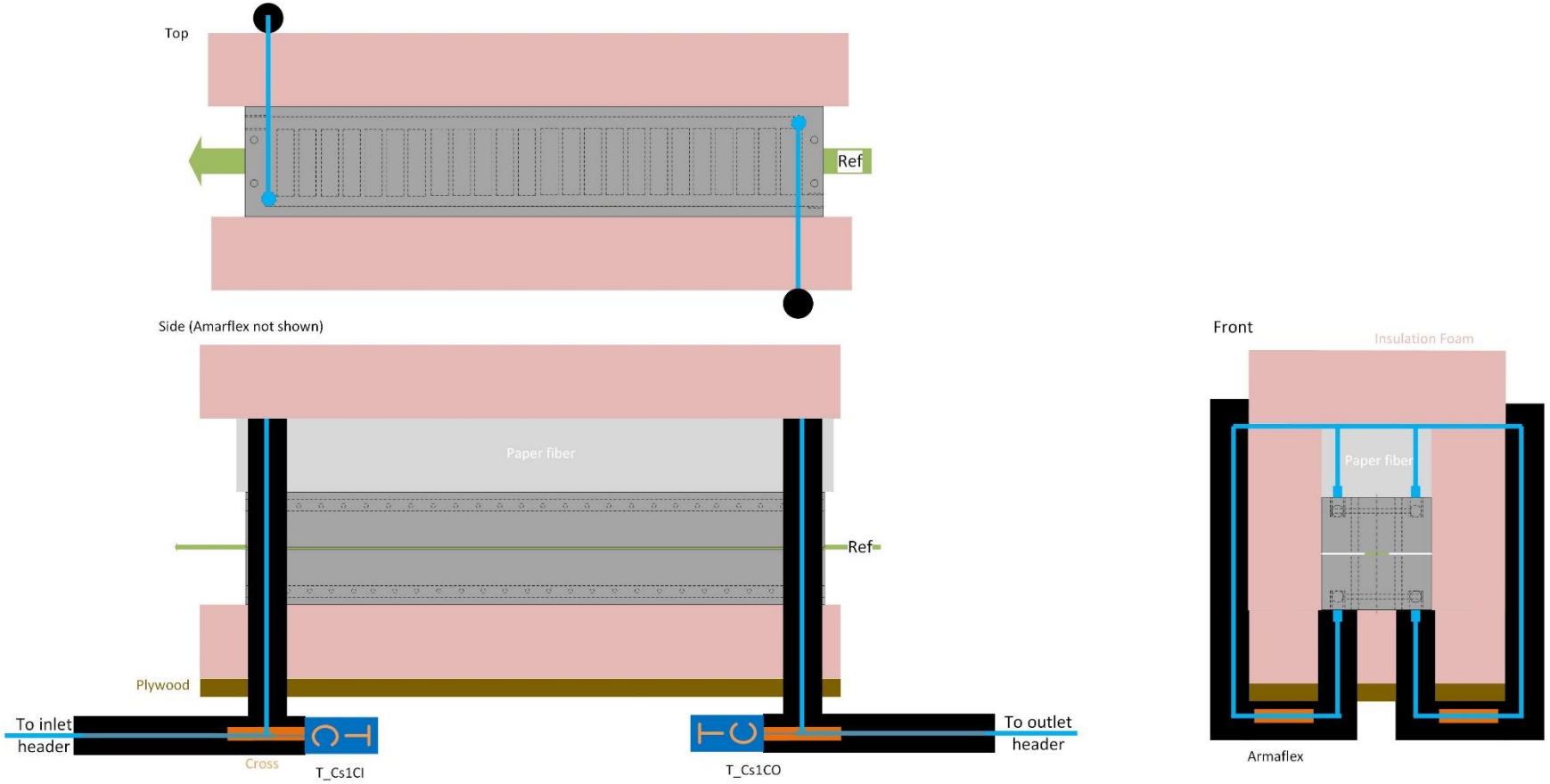

Figure 21 Conditioning section insulation and thermocouples

3. Calibrations and Measurement Process

The calibration has been made to reduce the uncertainty in determining heat transfer coefficient and pressure drop. Thermocouples are calibrated offline in a thermal bath with an accurate RTD thermometer. Pressure transducers, mass flow meters are calibrated online. Heat loss from test line to ambient, the contact resistance of thermal paste contact surface from block to microchannel tube, and temperature uniformity check are made online with testing conditions.

Data reduction processes and equations with uncertainty analysis will be shown later in this section.

3.1 Pressure transducers

The Rosemount pressure transducer is calibrated in situ. The connection of pressure transducer has been discussed above in section 2. With the three-way valve, whether the lower side of the transducer is connected to the atmosphere or system can be changed. During testing, the lower side of the transducer is connected to the system to measure pressure. During calibration, the lower side of the transducer is connected to the atmosphere. As the system pressure changed and was measured by an accurate instrument, a relationship between voltage measured and real gauge/differential pressure can be gained. The Sensotech pressure sensor on the coolant line was calibrated in the calibration room.

A Fluke pressure calibrator 717 and the 700P22 module was used as the reference pressure. The pressure is carefully controlled by an air-piston pressure generator to cover the low range from 0 to 40 kPa so as to calibrate the DP3/DP4/DR2 sensors.

For the two Rosemount sensors GP8 (high range 0 to 3500kPa), a nitrogen tank is used to pressurize the system and Fluke 717 is used as the reference. The calibrator is traceable according to ISO 17025 standard.

All sensors have high side connected to the system and low side to the atmosphere. Gauge pressure in the high side will be readings for both differential pressure transducer and gauge pressure transducer. All transducers will have a 1-5 V DC output corresponding to the pressure. For those transducers with current output, an electrical resistor has been used to convert the signal into a voltage output. With multiple pairs of voltage-to-pressure data, a linear relationship (second order polynomial relationship for model J transducer) can be drawn to convert voltage in V into pressure in kPa. An example of the linearization

process of the signal into pressure of the differential pressure transducer on the evaporator (DP_{Ev}) has been shown in figure 22. The slope of the equation is 0.40, and the intercept is -0.50 as shown in figure 22 and table 9.

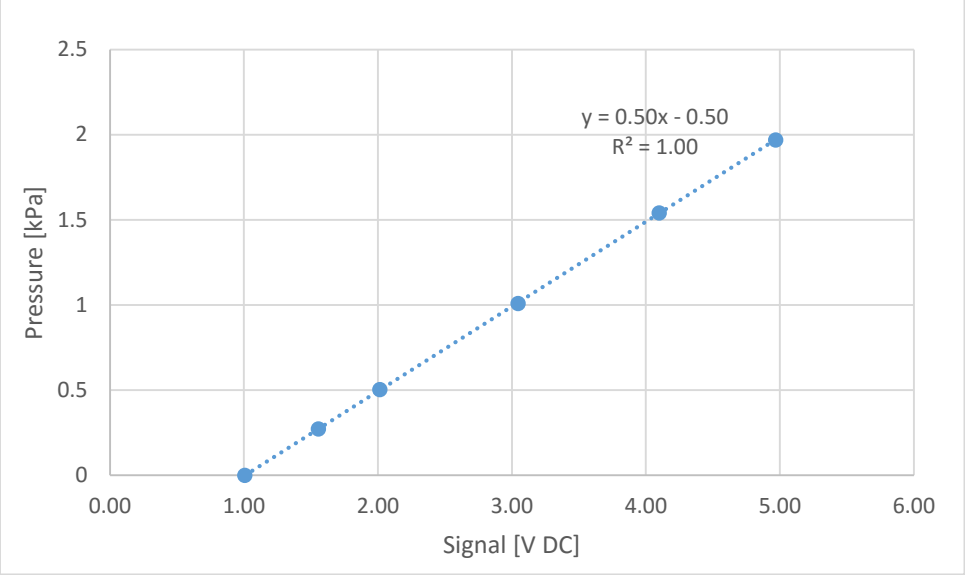

Figure 22 Linear equation of voltage to pressure for sensor DP_{Ev}

Table 9 lists all calibrated span ranges, accuracies, and equations of all differential pressure sensors and gauge pressure sensors. The accuray information is obtained from the statistical calibration data together with the manufacturer's user's manual. The equation for all linear output sensors is:

$$DP\ or\ GP\ [kPa] = Slope \times Voltage[V] + Intercept \quad (3.1)$$

Table 9 Pressure transducer calibration information

Name	Sensor	Location description	Model	Accuracy [kPa]	Range [kPa]	Equation	
						Slope	intercept
DP_Ts1	DP3	Test section 1	S12B1	0.0015	2	0.50	-0.50
	DP4	Test section 1	E12B1	0.015	15	3.73	-3.84
DP_Cs1	DP3	Conditioning Section 1	G22B2	0.008	8	1.95	-1.97
	DP4	Conditioning Section 1	E22T0085B3	0.04	40	9.85	-9.85
DP_Ts2	DP3	Test section 2	E12	0.002	2	0.62	-0.60
	DP4	Test section 2	M12B1I6	0.01	10	2.50	-2.50
DP_Cs2	DP3	Conditioning Section 2	E12	0.008	8	2.00	-2.02
	DP4	Conditioning Section 2	M12B1I6	0.04	40	10.03	-10.06
DP_Ts3	DP3	Test section 2	S12B1	0.0015	2	0.50	-0.50
	DP4	Test section 2	M12B1I6	0.015	15	3.72	-3.78
DP_Cs3	DP3	Conditioning Section 2	S52	0.00555	7.4	1.85	-1.85
	DP4	Conditioning Section 2	M12B1I6	0.04	40	10.01	-10.02
DP_Ts4	DP3	Test section 2	E12	0.002	2	0.49	-0.51
	DP4	Test section 2	M12B1I6	0.015	15	3.71	-3.74
DP_Cs4	DP3	Conditioning Section 2	G22B2	0.008	8	2.00	-2.10
	DP4	Conditioning Section 2	M12B1I6	0.04	40	9.99	-9.99
DP_Ts5	DP3	Test section 2	J22*	0.005	2	$0.12*V^2$-0.24*V+0.12	
	DP4	Test section 2	E22	0.01	10	2.72	-2.85
DP_Cs5	DP3	Conditioning Section 2	S12B1	0.00555	7.4	1.86	-1.88
	DP4	Conditioning Section 2	M12B1I6	0.04	40	10.02	-10.01
DP_Ts6	DP3	Test section 2	E22	0.002	2	0.50	-0.49
	DP4	Test section 2	M12B1I6	0.015	15	3.70	-3.67
P_Ts1RI	GP8	Test Section 1 Inlet	GP8M53B1I6	3.5	3500	867.99	-864.71
P_Ts6RO	GP8	Test Section 6 Outlet	GP8M12B1I6	3.5	3500	865.20	-865.97
DP_Ev	DR2	Evaporator	DR2F22B1	0.005	2	0.50	-0.50
P_PumpCO	Sensotec	Coolant Pump Outlet	Sensotech Z/718	n.a.	598	137.90	0.00

(*This sensor has a polynomial output curve)

3.2 Thermocouples

Thermocouples are calibrated offline in a Neslab thermal bath with temperature control. There are 140 T-type thermocouples and all are calibrated. 133 of them are installed on the facility to measure local temperature while 7 of them are backup thermocouples for replacement of any broken TCs in the future.

During the process of calibration, all thermocouples are put into a thermal bath that can maintain the constant temperature. An ISOTECH TTI-22 standard RTD thermometer is inserted into the bath and is used as reference temperature with an accuracy of 7mK. The bath is filled with 50 percent Ethylene-glycol water solution. For each temperature setting, all thermocouples and the RTD thermometer are kept at the same temperature. Thermocouples are calibrated at thermal bath temperature changing from -10 ^{o}C to 60 ^{o}C with a step of 10 ^{o}C. This range is chosen to cover the experimental condition range.

An example case of all raw temperature reading and RTD thermometer reading is in figure 23. This case shows all raw temperature readings (dots, same color refer to the same sensor) and RTD thermometer average reading (black line). It shows that each thermocouple has a small deviation from the reference of each reading. Average readings from different thermocouples vary slightly. Here the thermometer reads 1.175 ^{o}C.

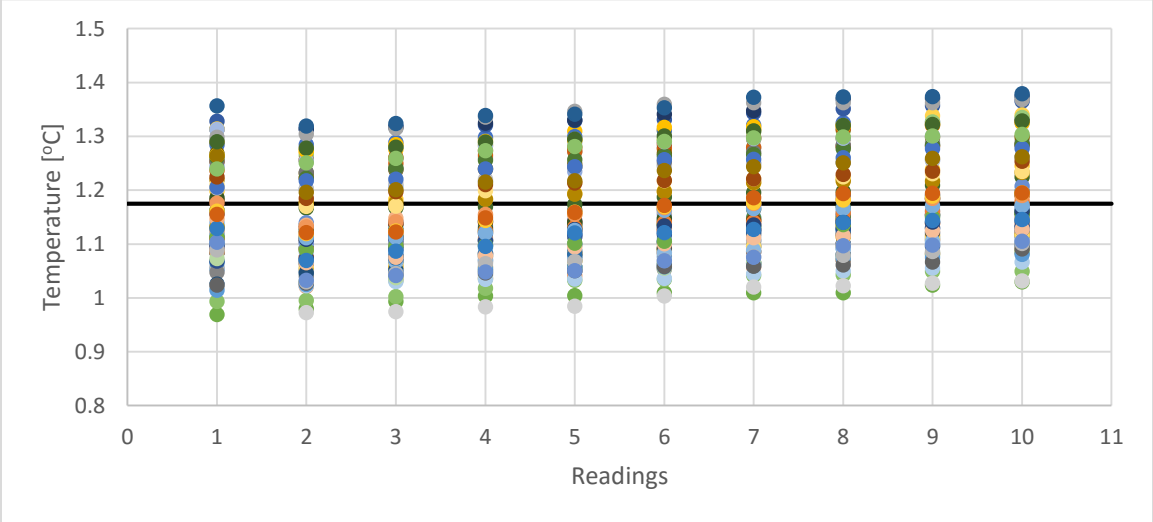

Figure 23 Example of raw temperature reading

By comparing the readings from data logger and the RTD thermometer, a linear equation can be developed to correct the temperature reading more accurately. Figure 24 shows three examples of the equation generation process of thermocouples 1 to 3 in the top block of test section 1 (T_{Ts1WT1}, T_{Ts1WT2}, T_{Ts1WT3}) respectively. In figure 24, the horizontal axis is raw temperature readings in [^{o}C] and the vertical axis is the reading from the thermometer. A linear equation can be generated with the data.

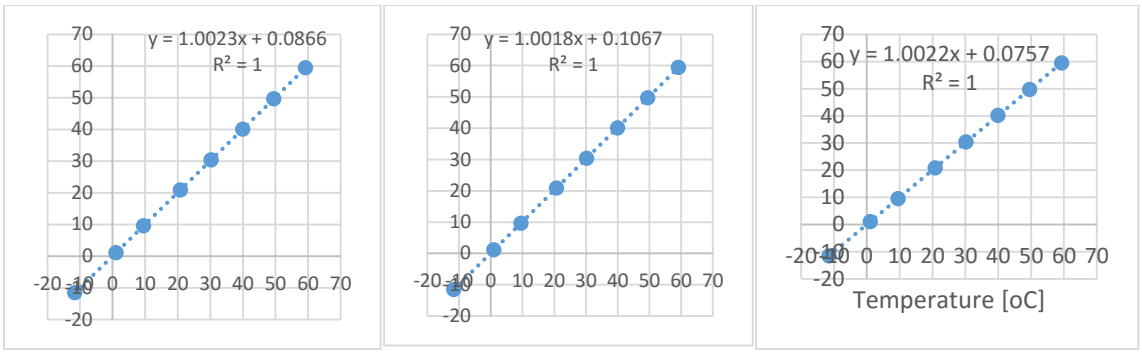

Figure 24 Example of linear relation between raw readings and thermometer readings

The random uncertainty level is measured based on the difference of calibrated temperature of thermocouples to the RTD reading. System uncertainty is gained by data logger testing. After calibration, these thermocouples have uncertainty levels slightly higher than 0.1°C. The standard deviations for these three sensor measurements are 0.0136 °C, 0.0414 °C, and 0.00924 °C respectively. The data logger has a standard deviation level of 0.052 °C. Taking the first thermocouple as an example, the uncertainty will be 0.1053 °C with 95% confidence as calculated in equation (3.2).

$$eT_{Ts1WT1} = 1.96 \times \sqrt{0.052^2 + 0.0136^2} = 0.1053 \quad (3.2)$$

The information including all thermocouples locations, calibrated equations, and accuracies are listed in Appendix A.

$$T\,[^oC] = Slope \times Raw\ reading[^oC] + Intercept \quad (3.3)$$

3.3 Mass flow meter

There are 18 pairs of Micro Motion flow sensors and transmitters on the facility including one pair for refrigerant mass flow rate measurement and 17 pairs for coolant mass flow rate measurement. The transmitter for refrigerant mass flow rate also output density as a second signal. Also, the first transmitter for coolant mass flow rate (Test section 1 bottom line) has density output for coolant information.

All the Micro Motion sensors and transmitters were calibrated/checked before they were put in the facility. The transmitters have a current output of 4 to 20 mA. The electrical resistors of nominally 250 ohms are used to convert the signals to voltages of about 1 to 5 volts.

A model 275 HART Communicator is used to set up the analog output from the transmitter. At least 12 voltage signals for the analog output of 4mA or 20mA are collected. The average of these readings was used to establish correlations between the output parameter and the measured voltage. The transmitter model used for all flow sensors without density measurement is RFT97121PNU. The transmitter used on the refrigerant loop and test section 1 bottom (m_R and m_{Ts1CB}) are RFT9739 so that densities ($\rho_{R,}\, \rho_{Ts1CB}$) can be measured. This information and the corresponding ranges and accuracies of all flow transmitters are listed in Table 10.

The equation will be:

$$m\ [g\ s^{-1}] = Slope \times Voltage[V] + Intercept \tag{3.4}$$

$$\rho\ [g\ cm^{-3}] = Slope \times Voltage[V] + Intercept \tag{3.5}$$

Table 10 Mass flow meter calibration

Sensor				Calibration		Equation	
Name	Location	Fluid	Model	Accuracy (% of rate or g/cm^3)	Range	Slope	Intercept
m_R	-	Refrigerant	CMF010N323NU	0.1%	10g/s	2.50	-2.49
m_Ts1CB	Test Section 1 Bottom	Coolant	CMF010M313MU	0.1%	20g/s	5.00	-5.00
m_Ts1CT	Test Section 1 Top	Coolant	CMF010M313MRAUEZZZ	0.1%	20g/s	4.99	-5.00
m_Cs1C	Conditioning Section 1	Coolant	DS012S109SU	0.15	20g/s	5.00	-5.03
m_Ts2CB	Test Section 2 Bottom	Coolant	CMF010M313MRAUEZZZ	0.1%	20g/s	4.99	-5.03
m_Ts2CT	Test Section 2 Top	Coolant	CMF010M313MU	0.1%	20g/s	5.00	-4.98
m_Cs2C	Conditioning Section 2	Coolant	DS012S109SU	0.15%	20g/s	5.00	-5.00
m_Ts3CB	Test Section 3 Bottom	Coolant	CMF010M999NRAUEZZX	0.1%	20g/s	4.99	-4.99
m_Ts3CT	Test Section 3 Top	Coolant	CMF010M313MU	0.1%	20g/s	5.00	-5.01
m_Cs3C	Conditioning Section 3	Coolant	D3012S109SU	0.15%	20g/s	5.00	-4.99
m_Ts4CB	Test Section 4 Bottom	Coolant	CMF010M520MU	0.1%	20g/s	4.99	-5.02
m_Ts4CT	Test Section 4 Top	Coolant	CMF010M313MU	0.1%	20g/s	5.00	-4.99
m_Cs4C	Conditioning Section 4	Coolant	DS012S109SU	0.15%	20g/s	5.00	-5.00
m_Ts5CB	Test Section 5 Bottom	Coolant	CMF010M321MU	0.1%	20g/s	5.00	-4.99
m_Ts5CT	Test Section 5 Top	Coolant	CMF010M321MU	0.1%	20g/s	5.01	-5.01
m_Cs5C	Conditioning Section 5	Coolant	DS012S109SU	0.15%	20g/s	5.01	-5.00
m_Ts6CB	Test Section 6 Bottom	Coolant	CMF010M321NRAUE22	0.1%	20g/s	5.00	-5.02
m_Ts6CT	Test Section 6 Top	Coolant	CMF010M321MU	0.1%	20g/s	5.03	-5.00
ρ_R	-	Refrigerant	CMF010N323NU	0.0005g/cm^3	2g/cm^3	0.50	-0.50
ρ_Ts1CB	Test Section 1 Bottom	Coolant	CMF010M313MU	0.0005g/cm^3	2g/cm^3	0.50	-0.50

3.4 Heat loss to ambient

Calibration of sectional heat loss is important for the experiment because of its impact on the heat load determination. By looking at the geometry and assembling method of test sections, the total heat loss has been arbitrarily split into 20 parts. Figure 25 shows the location of 20 heat losses. From left to right, the 20 losses are coming from: Inlet, Evaporator, Ts1B, Ts1T, Cs1, Ts2B, Ts2T, Cs2, Ts3B, Ts3T, Cs3, Ts4B, Ts4T, Cs4, Ts5B, Ts5T, Cs5, Ts6B, Ts6T, and Outlet.

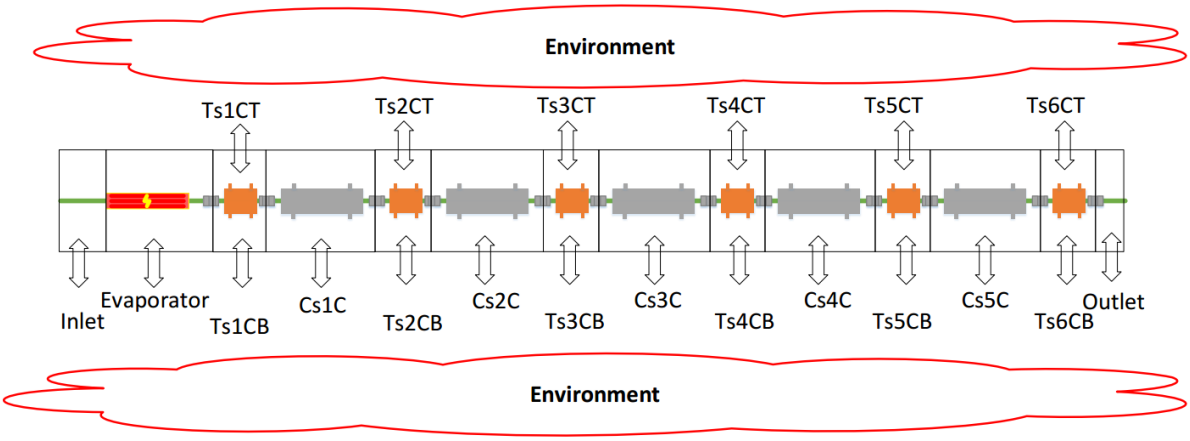

Figure 25 Heat loss sections

Among these heat losses, three of them (Inlet, Evaporator, and Outlet) can be defined as refrigerant line loss. This is due to that in the three section the refrigerant pipe are directly contact with insulation materials. The rest 17 are coolant line losses where the refrigerant line is covered by heat transfer block, so the heat loss will be strongly related to the temperature difference between the coolant and environment. For refrigerant line heat loss, the calibration method is to run liquid phase refrigerant and to measure the temperature change in the heat loss location. By correlating to temperature change, the heat loss can be calculated and it should be a linear function intercepts y-axis at zero of temperature difference to the ambient temperature. For the coolant/water line heat loss, the calibration method is to run liquid phase R134a in refrigerant line and coolant in test or conditioning sections at the same temperature. By measuring the temperature of coolant

line in heat transfer blocks, the heat loss rate can be calculated. Similarly, the heat loss should be a linear function intercepts y-axis at zero of temperature difference to the ambient temperate. The heat losses equation is defined for each top and bottom blocks (TB and BB) as (3.6) and (3.7) and the T in (3.6) is the characteristic temperature.

$$QL = UA(T - T_{amb}) = UA \times dT_{ambient} \tag{3.6}$$

Or

$$QL = UA \frac{\left(T_{ambient} - T_{coolant,in}\right) - \left(T_{ambient} - T_{coolant,out}\right)}{\ln\left(\frac{T_{ambient} - T_{coolant,in}}{T_{ambient} - T_{coolant,out}}\right)} \tag{3.7}$$

The LMTD method (3.7) is used for heat loss from the coolant side, where the inlet and outlet temperature can be measured. Simply temperature difference method (3.6) is used at refrigerant line heat loss where the bulk temperature or block temperature is only known. There is one exception that when one of inlet or outlet temperature of the coolant is higher than ambient temperature and the other is lower, there is no meaning to use LMTD method directly here. In this case, the heat loss will be very small, simply applying the average temperature of inlet and outlet as the characteristic temperature and using equation (3.6) to calculate heat loss. These temperatures used for calculation of heat loss have been listed in table 11.

Equation (3.6) and (3.7) could be also used to define UA. The final calibration results of the heat loss of each section can be determined as shown in table 11 which lists the heat loss UA value and respective temperature for heat loss at different locations. The detailed process of calibration and verification will be reported later in this subsection.

Table 11 Table of calibrated UA value and temperature uses guide

Location	**Temperature of**	**UA value [W K^{-1}]**
Inlet	Refrigerant inlet	0.04368
Evaporator	Evaporator surface	0.17472
Ts1B	Test section 1 bottom coolant side	0.114523
Ts1T	Test section 1 top coolant side	0.090535
Cs1	Conditioning section 1 coolant side	0.436666
Ts2B	Test section 2 bottom coolant side	0.115218
Ts2T	Test section 2 top coolant side	0.020338
Cs2	Conditioning section 2 coolant side	0.346543
Ts3B	Test section 3 bottom coolant side	0.135365
Ts3T	Test section 3 top coolant side	0.025665
Cs3	Conditioning section 3 coolant side	0.277484
Ts4B	Test section 4 bottom coolant side	0.123441
Ts4T	Test section 4 top coolant side	0.022493
Cs4	Conditioning section 4 coolant side	0.325363
Ts5B	Test section 5 bottom coolant side	0.144676
Ts5T	Test section 5 top coolant side	0.007015
Cs5	Conditioning section 5 coolant side	0.365825
Ts6B	Test section 6 bottom coolant side	0.145157
Ts6T	Test section 6 top coolant side	0.020407
Outlet	Refrigerant Outlet	0.089211

With calculation of heat loss and heat transfer rate from coolant side, the total heat transfer rate to the refrigerant line can be defined in (3.8) with test section 1 bottom block

as nomenclature example. Figure 26 shows how the equation works. Detailed equations for data reduction will be discussed later in this section.

$$Q_{Ts1RB} = Q_{Ts1CB} - QL_{Ts1B} \tag{3.8}$$

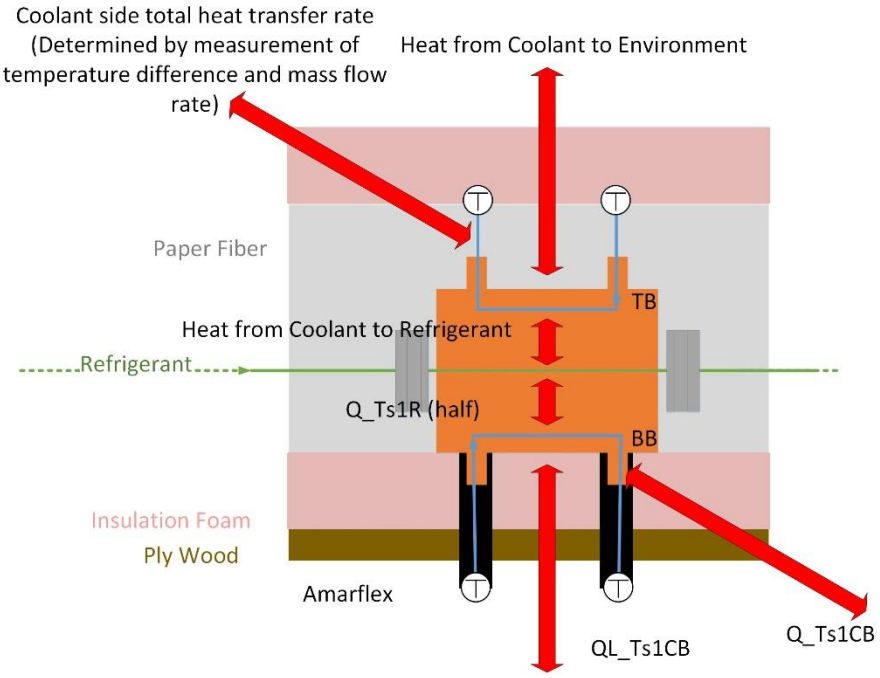

Figure 26 Heat loss example for test section 1

3.4.1 Inlet and evaporator heat loss calibration

Firstly, the inlet and evaporator heat loss have been calibrated. Figure 27 shows how this section looks. Details of insulation have been made previously in this thesis. The whole test line is covered by insulation foam and Armaflex. Paper fiber fills all gaps in the insulation box to prevent any natural convection inside the box. The front surface of inlet connector is covered by black Armaflex. All other parts are in the insulation box and lying on the insulation foam.

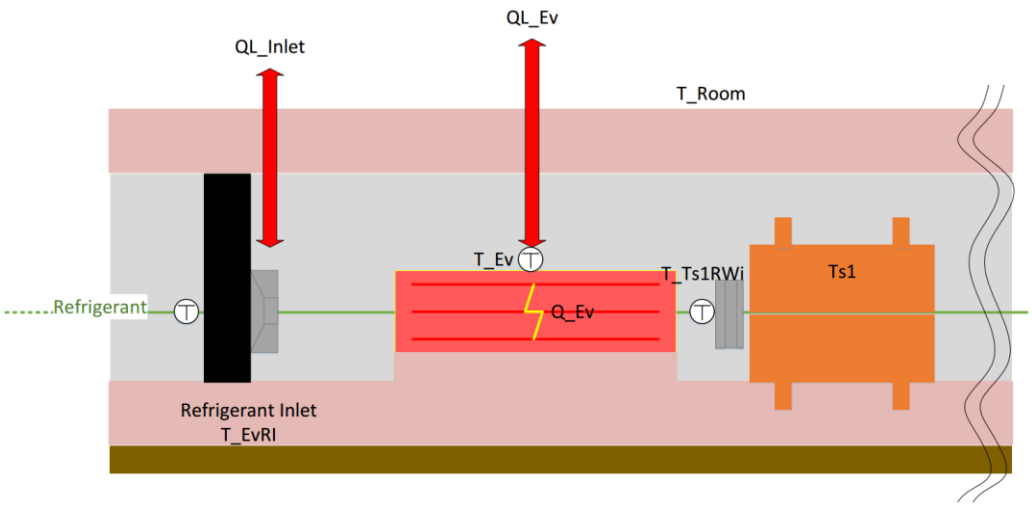

Figure 27 Inlet and evaporator heat loss

The calibration process is that running different combinations of liquid phase refrigerant inlet temperature (T_{EvRI}) and evaporator power supply (Q_{Ev}). Since there is not a thermocouple inserted in the microchannel tube for measuring temperature, a thermocouple is attached to the outer surface of microchannel tube with a clamp to measure the wall temperature. By assuming the heat loss here is small, wall temperature can relatively represent the refrigerant bulk temperature. This assumption is valid because the insulation is thick and outer surface area of the microchannel tube is small. The heat loss then can be measured by knowing the quantity of heat transfer into the refrigerant and power generated from the evaporator.

Table 12 Heat loss of inlet and evaporator

Case	Q_ev [W]	T_ev [°C]	T_in [°C]	T_out [°C]	m_R [g s^{-1}]	P [kPa]	Cp [J g^{-1} K^{-1}]	Q_ref [W]	QL [W]
1	10.42	10.15	6.05	9.22	3.00	484.17	1362	12.95	-2.52
2	28.92	16.17	6.28	13.74	2.98	422.69	1370	30.44	-1.52
3	24.42	49.78	20.54	46.17	0.81	419.71	926.6	19.35	5.08
4	12.82	42.39	27.61	39.19	0.83	421.49	927.4	8.89	3.94
5	18.44	59.65	40.83	55.16	0.83	420.88	934.5	11.10	7.34

Table 12 shows the calibration test's results. By introducing a mix temperature difference to split the loss from the refrigerant line and evaporator (3.9), a total UA value can be gained from linear curve fitting.

$$dT_{mix} = c(T_{Ev} - T_{amb}) + (1 - c)(T_{EvRI} - T_{amb}) \quad (3.9)$$

Here c is taken at 0.8 and the curve fitting has been shown in figure 28.

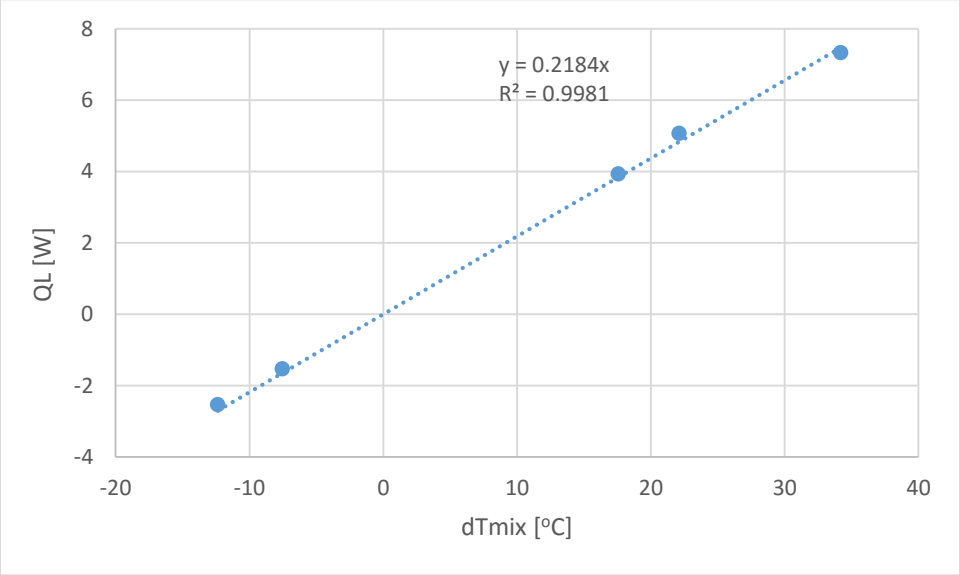

Figure 28 Heat loss calibration curve fitting

In this method, the total UA value is 0.2184 [W K^{-1}]. This value can be separated into 0.2UA and 0.8UA for inlet and evaporator respectively.

3.4.2 Test sections, conditioning sections, and outlet calibration

After calibration of inlet and evaporator, a calibration has been conducted for test sections, conditioning sections, and the outlet of the test line. By running all coolant average temperature as same as the temperature at the inlet of test section 1, an assumption can be made that there is not heat transfer from the coolant to refrigerant side.

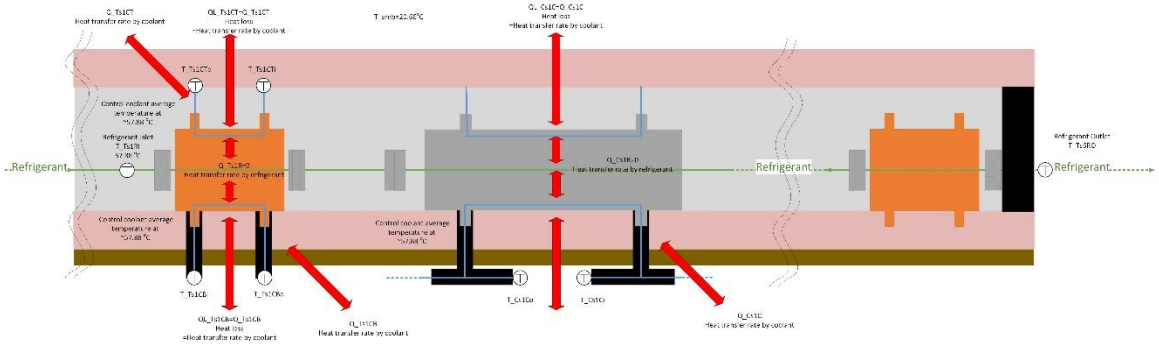

Figure 29 Test line heat loss calibration

Figure 29 shows how calibration is achieved. The inlet temperature is known at 57.88 °C. Average of inlet and outlet of coolant temperature is controlled at 57.88 °C. All

heat transfer rate measured in coolant loop is heat loss to ambient. By applying the data to equation (3.5), the UA value can be determined. Equation (3.10) shows the determination of UA value and the nomenclature comes from test section 1 bottom block. Equation (3.11) uses real values in calibration for test section 1 bottom block and the values are the same as listed in table 11.

$$UA_{Ts1B} = \frac{m_{Ts1CB} \times C_P \times (T_{Ts1CBi} - T_{Ts1CBo})}{\frac{(T_{Ts1CBi} + T_{Ts1CBo})}{2} - T_{amb}} \tag{3.10}$$

$$UA_{Ts1B} = \frac{1.30 \times 4.12 \times (58.37 - 57.57)}{\frac{(58.37 + 57.57)}{2} - 20.66} = 0.11 \tag{3.11}$$

For the outlet part, measured temperature difference with known properties of refrigerant, the UA value can also be determined by equation (3.5).

3.4.3 Heat loss calibration value verification

After calibration, nine tests have been conducted to verify the heat loss calculation. These nine tests are under real experimental conditions. Table 13 and Figure 30 shows the verification results. During the verification, the whole test line inlet and outlet enthalpies are measured by thermocouples and pressure transducers. With the two enthalpies and measured mass flow rate of refrigerant, total heat transfer rate in the refrigerant line can be calculated. In addition, the total heat transfer rate in coolant side can be calculated with known temperature difference and mass flow rate of coolant. Lastly, heat loss from system to ambient can be calculated using the UA parameter mentioned above. In table 6, it shows the combined heat transfer rate (Q) in coolant side and ambient (calibrated heat loss). It also shows the total Q in the refrigerant side. These two Qs should equal to each other after calibration. And the error is defined as:

$$Error\ [\%] = \left| \frac{\text{Total Q in refrigerant side} - \text{Total Q in coolant side}}{\text{Total Q in refrigerant side}} \right| \times 100 \tag{3.12}$$

In table 13, cases are sorted by error from low to high, the last case is the case with the highest error. Figure 30 shows a comparison with error bar.

Table 13 Verification of heat loss calibration

No	Total Q in coolant side and ambient [W]	Uncertainty of total Q in coolant side and ambient [W]	Total Q in refrigerant side [W]	Uncertainty of total Q in refrigerant side [W]	Error [%]
1	254.16	2.42	253.69	0.17	0.18
2	257.46	2.43	258.17	0.14	0.28
3	244.81	2.51	242.76	0.17	0.84
4	250.74	2.52	254.46	0.17	1.46
5	232.39	2.55	237.18	0.17	2.02
6	234.31	2.48	239.17	0.17	2.03
7	249.15	2.51	257.01	0.17	3.06
8	262.74	2.30	254.75	0.18	3.14
9	263.51	2.42	274.52	0.19	4.01

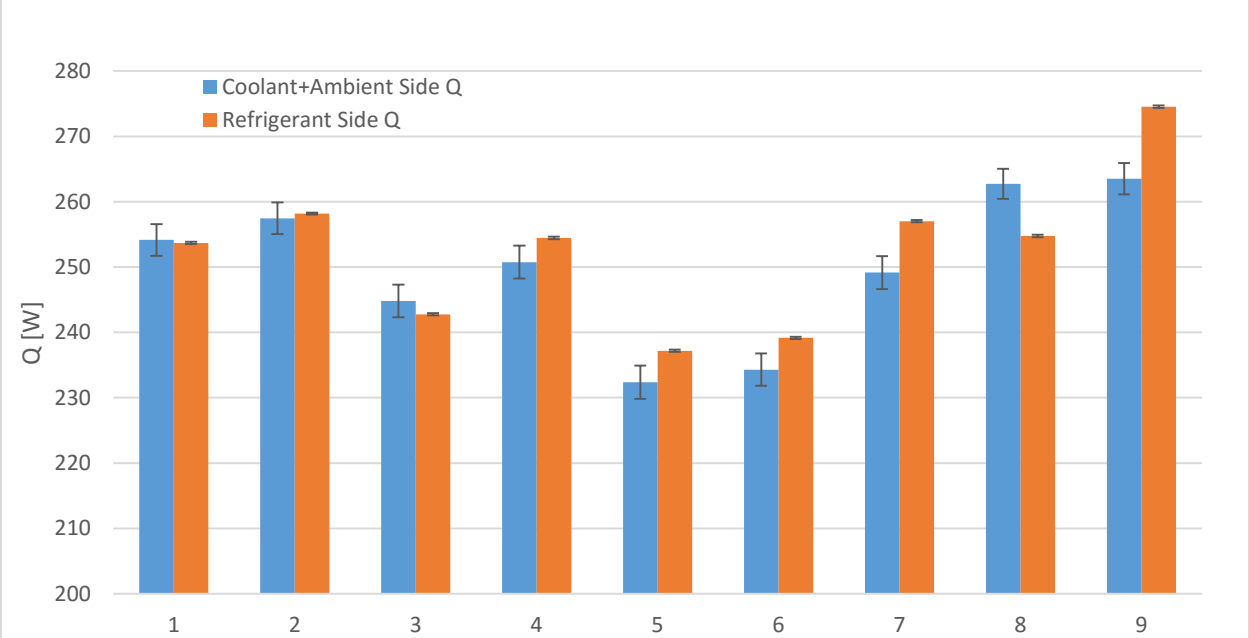

Figure 30 Heat loss verification comparison

Heat loss calibration is very important to obtain actual heat transfer rate from coolant side to refrigerant side. Also, the accuracy level influence how accurate the vapor quality at a certain section can be estimated. Table 14 shows a breakdown analysis of the worst case, case 9.

Table 14 Q loss breakdown of case 9 in heat loss verification (Room temperature is 24.73 ºC)

Location	Coolant Inlet Temperature / Respect Temperature [ºC]	Coolant Outlet Temperature [ºC]	LMTD/ dT [ºC]	UA Value [W K^{-1}]	Heat Loss to ambient [W]	Heat transfer rate calculated in coolant side [W]	Combined heat transfer rate in coolant side and loss to ambient [W]	Ratio of combined Q to Coolant side Q [%]
Inlet	18.13	-	-6.60	0.04	0.29	0.00	-0.29	-100.00
Evaporator	23.76	-	-0.97	0.17	0.17	0.00	-0.17	-100.00
Ts1B	23.81	20.20	-2.27	0.11	0.26	14.66	14.40	1.81
Ts1T	25.13	19.90	-2.22	0.09	0.20	14.78	14.58	1.38
Cs1	27.95	20.97	-0.27	0.44	0.12	35.79	35.67	0.33
Ts2B	24.17	19.30	-2.16	0.12	0.25	14.73	14.48	1.72
Ts2T	22.91	19.12	-3.38	0.02	0.07	14.97	14.90	0.46
Cs2	9.18	14.64	-12.62	0.35	4.38	-17.30	-21.68	-20.18
Ts3B	23.76	18.13	-2.94	0.14	0.40	14.47	14.07	2.83
Ts3T	22.98	18.22	-3.63	0.03	0.09	14.90	14.80	0.63
Cs3	38.47	29.63	8.57	0.28	-2.38	35.72	38.10	-6.24
Ts4B	21.69	16.93	-5.06	0.12	0.62	14.31	13.68	4.56
Ts4T	21.36	16.87	-5.30	0.02	0.12	14.86	14.75	0.81
Cs4	8.28	12.90	-14.02	0.33	4.56	-17.70	-22.26	-20.50
Ts5B	18.04	14.62	-8.29	0.14	1.20	13.78	12.58	9.53
Ts5T	18.38	14.65	-8.08	0.01	0.06	14.94	14.88	0.38
Cs5	39.64	17.49	3.83	0.37	-1.40	51.49	52.90	-2.65
Ts6B	19.89	15.49	-6.81	0.15	0.99	14.05	13.06	7.57
Ts6T	18.98	15.10	-7.53	0.02	0.15	15.08	14.92	1.03
Outlet	14.64	-	-10.09	0.09	0.90	0.00	-0.90	-100.00

From table 6 the heat loss percentage is 100% in the inlet, evaporator, and outlet. This is due to the fact that the only heat transfer in these sections is heat transfer with the environment during verification. The other 17 parts are test sections and conditioning sections. In these sections, the heat transfer rate is calculated from coolant side mass flow rate and temperature difference. For those sections with a temperature close to the room temperature, the heat loss rate is small. The top blocks have a smaller heat loss rate than bottom blocks. For example, the heat loss in TS6T (Test section 6 Topside) is 0.15 watts, in Ts6B (Test section 5 bottom) is 0.99 watts. This is due to that the top blocks have thicker insulation than bottom blocks. For those sections which provide small heat transfer rate but

with huge temperature difference to the environment, the heat loss has taken a huge part of the total heat transfer rate. For example, in Cs4 (conditioning section 4), the heat loss rate is 4.45 watts, and the total heat transfer rate is -22.26 watts. Heat loss rate covers 20.5% of the total heat transfer rate.

When the heat transfer rate in coolant side is large and characteristic temperature in heat loss calculation is close to ambient temperature, heat loss will be small and the uncertainty of determining heat transfer rate to the refrigerant side is maintained at a low level.

3.5 Contact resistance effects on wall temperature measurements and wall temperature uniformity

For the test sections discussed above, the two heat transfer blocks TB and BB sandwich the microchannel tube as shown in Figure 5 previously. In between the block and the tube, a brand thermal paste has been applied to enhance the heat transfer. The thermal paste used here is CHEMPLEX 1381 DE which has a reported thermal conductivity of 0.75 $W\text{-}m^{-1}\text{-}K^{-1}$. However, the thermal contact resistance will still exist which will eventually affect the wall temperature measurement. Therefore, to determine the thermal contact resistance and look into its effect on the heat transfer measurement is important. In the present study, a unique method has been developed to calibrate the contact resistance by comparing the brazed contact (no contact resistance) between the TB and the MC tube and the normal contact between the BB and the MC tube in Test Section 1. Also, it is assumed that all thermal contact resistances in the other test sections will be the same as Test Section 1.

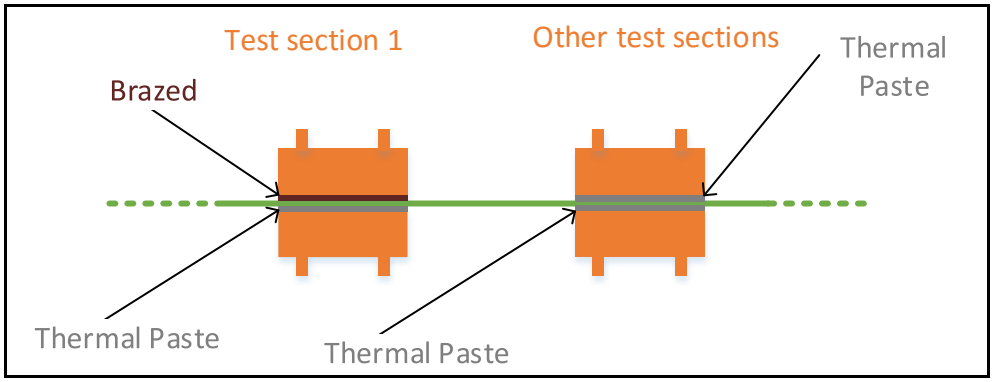

Figure 31 Contact surface treatment to test sections

As shown in Figure 31, Test Section 1 has been slightly modified: its top block brazed directly with the MC tube so that it can be assumed that no thermal contact resistance between the TB and the MC tube exists while the BB is still normally in contact with the MC tube with the thermal paste applied. Four long bolts with nuts are used to assemble the sandwich. The same torque 7.6 [N-m] is applied to all four bolts in each test section assembly. By applying the same torque on the bolts, all contact surfaces can be assumed to have the equal thermal contact resistance.

3.5.1 Calibration theory and process

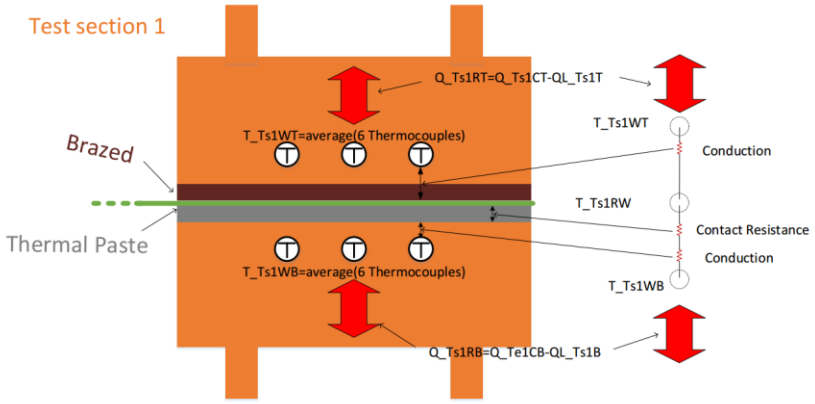

Figure 32 Thermal circuit analysis of test section 1

In the calibration of the thermal contact resistance, coolant temperature and flow rate on both the top and bottom blocks of Test Section 1 are maintained as close as possible to each other. The heater is controlled to make the heat transfer rate to the refrigerant side of TB and BB to be the same (Q_{Ts1RB}=Q_{Ts1RT}). In the ideal cases, they should be kept to be exactly the same. The control on this facility makes close to each other with about 1% difference. Under these conditions, it is assumed that the wall temperatures of the MC tube inner surface on both top and bottom sides are the same. With the same heat flux from block to MC tube on both side, the top and bottom outer surface temperatures of MC tube are assured to be the same as well. A thermal circuit analysis can be drawn as Figure 32. This thermal circuit analysis shows the relationship among thermocouple readings of the TB (T_{Ts1WT}) and the BB (T_{Ts1WB}) and the actual wall temperature (T_{Ts1R}) on microchannel tube.

For the top side of Test Section 1, there is only conductivity resistance between the temperatures at thermocouple measurement locations and the contact wall with the MC

tube. For the bottom side of Test Section 1, however, there are contact resistance and conductivity resistance. For the other five test sections, both contact resistance and conductivity resistance exist for both top and bottom sides and need to be taken into account in correcting the wall temperature.

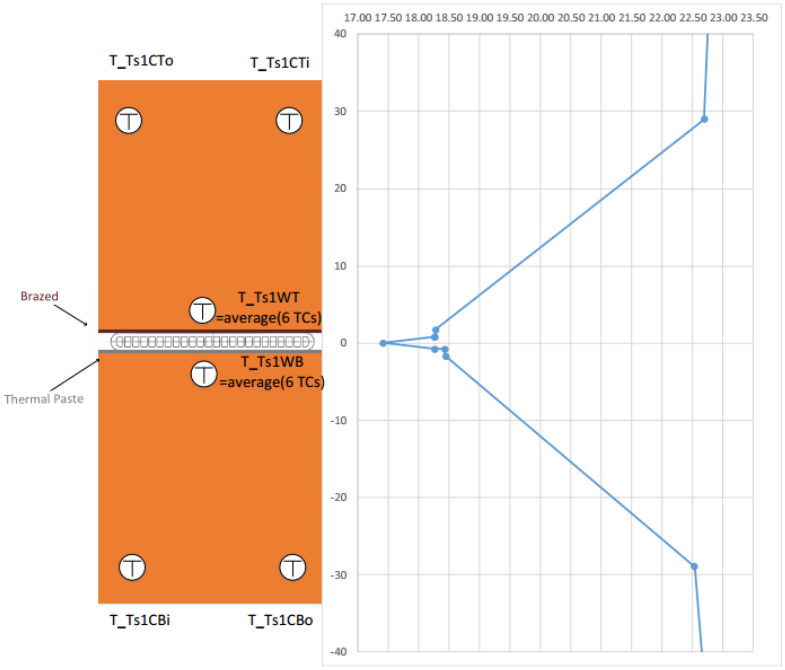

Figure 33 Temperature profile in blocks and microchannel

A temperature profile has been shown in figure 33. The vertical axis is the distance from the center of microchannel tube and horizontal is the temperature in degree Celsius. The temperature at 0 is the refrigerant temperature. At the upper and lower positions of refrigerant temperature show the outer surface temperature of microchannel tube which is calculated. And at the distance of +/- 29.1 mm, it shows the coolant average temperature. This profile does not reflect real temperature distribution in the block, the plot inserted here is for illustrating the influence of contact resistance. A detailed discussion of the numbers in the profile will be made later in this subsection.

With the circuit analysis in Figure 33, following equations can be derived for Test Section 1 and used for the calibration of the thermal contact resistance $R_{contact.}$

First, it is assumed that the wall temperature is uniform in microchannel tube, as shown in equation (3.13):

$$T_{wall,\ top} = T_{wall,\ bottom} = T_{Ts1w} \tag{3.13}$$

For the top side of Test Section 1, only conduction resistance is considered and we have

$$R_{conduction} = \frac{l}{k_{al} * A_{cont}} \tag{3.14}$$

$$R_{conduction} = \frac{(T_{Ts1WT} - T_{Ts1w})}{Q_{Ts1RT}} \tag{3.15}$$

For the bottom side of Test Section 1, both conduction and contact resistance is considered:

$$R_{contact} + R_{conduction} = \frac{(T_{Ts1WB} - T_{Ts1w})}{Q_{Ts1RB}} \tag{3.16}$$

Where T_{Ts1WT} T_{Ts1WB} are the average thermocouple readings of the six TCs on each of the blocks, respectively, k_{al} is the thermal conductivity of aluminum alloy which is a weak function of temperature and is around 177 $Wm^{-1}K^{-1}$, A_{cont} is the contact heat transfer area which equals to contact area 154.2×16.1 mm^2, and l is the distance which is a tine number of 0.93 mm (0.13 mm + 0.8 mm). Q_{Ts1RT} and Q_{Ts1RB} are the heat transfer rates from coolant side to refrigerant side in the TB and BB blocks. Both can be calculated form the coolant (water) balances and the heat loss from the environment to the blocks, respectively. During the calibration and heat transfer measurement, the two values are controlled to be equal to each other. Therefore, in the following analysis, we will use the average of Q_{Ts1RT} and Q_{Ts1RB} to represent the heat transfer rate:

$$Q_{Ts1R\_avg} = \frac{Q_{Ts1RT} + Q_{Ts1RB}}{2} \tag{3.17}$$

Combining the equations above from (3.13) to (3.17):

$$R_{contact} = \frac{1}{hA_{contact}} = \frac{(T_{Ts1WB} - T_{Ts1WT})}{Q_{Ts1R\_avg}} \tag{3.18}$$

It is also assumed that the contact resistance $R_{contact}$ is the same for all test sections since the pressure is the same. For the other test sections, the wall temperature will be calibrated with equation (3.18) which used the nomenclature of test section 1 bottom block as an example.

$$T_{Ts1RW} = T_{Ts1WB} - \left(\frac{l}{k_{al} * A_{cont}} + \frac{1}{hA_{contact}}\right) \times Q_{Ts1RB} \tag{3.19}$$

3.5.2 Results of calibrated contact resistance

The average value of $hA_{contact}$ gained experimentally is 120 [W K^{-1}]. The contact resistance $R_{contact}$ is 0.00833 [K W^{-1}]. Appendix B shows all calibrated value. The first two columns show case number and blocks. From left to right of the rest of header row, there is coolant side heat transfer rate, refrigerant side heat transfer rate after heat loss calibration (equation 3.8), wall temperature reading from thermocouples inserted into block, variance of the 6 thermocouple readings, sample standard deviation of the 6 thermocouple readings, estimated wall temperature without contact resistance, estimated wall temperature with contact resistance (equation 3.19), contact heat transfer coefficient with area (equation 3.18), calculated heat transfer coefficient without considering contact resistance, and heat transfer coefficient with contact resistance taken into account.

In Appendix B, the first two cases are heating of liquid refrigerant R134a, the third case is cooling vapor refrigerant R134a, and the other 13 are evaporating two-phase R134a.

By looking at variance and standard deviation of wall thermocouple readings, it is shown that the temperature distribution in wall temperature measurement is uniform. For the first two heating cases, the variance is about 0.5 ^{o}C and small standard deviation. For the third one, cooling of vapor, the variance is relatively large because refrigerant temperature is changing. For the rest of the cases, evaporating R134a, there should not be a temperature difference in refrigerant in theory. So the variance of temperature reading is affected by coolant temperature distribution and uncertainty of thermocouple readings.

By comparing the estimated temperature w/ or w/o contact resistance, the effect of contact resistance can be shown. Approximately speaking, there is about 0.083 ^{o}C of

difference for 10 W of heat transfer rate from the coolant to refrigerant because the contact resistance is about 0.0083 K/W. The last two column shows how contact resistance can effect calculation of heat transfer coefficient. In two phase cases (case 4 to 16), the heat transfer coefficient is corrected by about 10% to 20% larger after considering contact resistance effects.

Noted that when the assumption of uniform wall temperature on microchannel tube is held, test section 1 can always serve as a calibration section to correct all other section's wall temperatures. The procedure will be the same as the calibration, but the contact resistance (or contact heat transfer coefficient $hA_{contact}$) will be calculated simultaneously during experiments.

Case 1 and 13 are selected for case details illustration and will be presented. Both vertical and horizontal wall temperature distribution will be discussed here.

3.5.3 Case 1 details of wall temperature uniformity and calibrated contact resistance

Table 15 shows the information listed in Appendix B for case 1. Case one is a liquid phase heating case with a heat transfer rate of about 40 watts in total from the coolant to refrigerant. The refrigerant is heated from 5.73 ^{o}C to 10.6 ^{o}C. From figure 34, it is shown that the temperature of thermocouple reading is effected by refrigerant temperature change. The variance of thermocouple readings on the top block is 0.324 and 0.226 ^{o}C for the lower block. After taking contact resistance into account, the BB wall temperature is corrected from 13.714 to 13.627 degree Celsius. The heat transfer coefficient of BB is corrected from 488 to 499 [$WK^{-1}m^{-2}$] with 2.2% of changes.

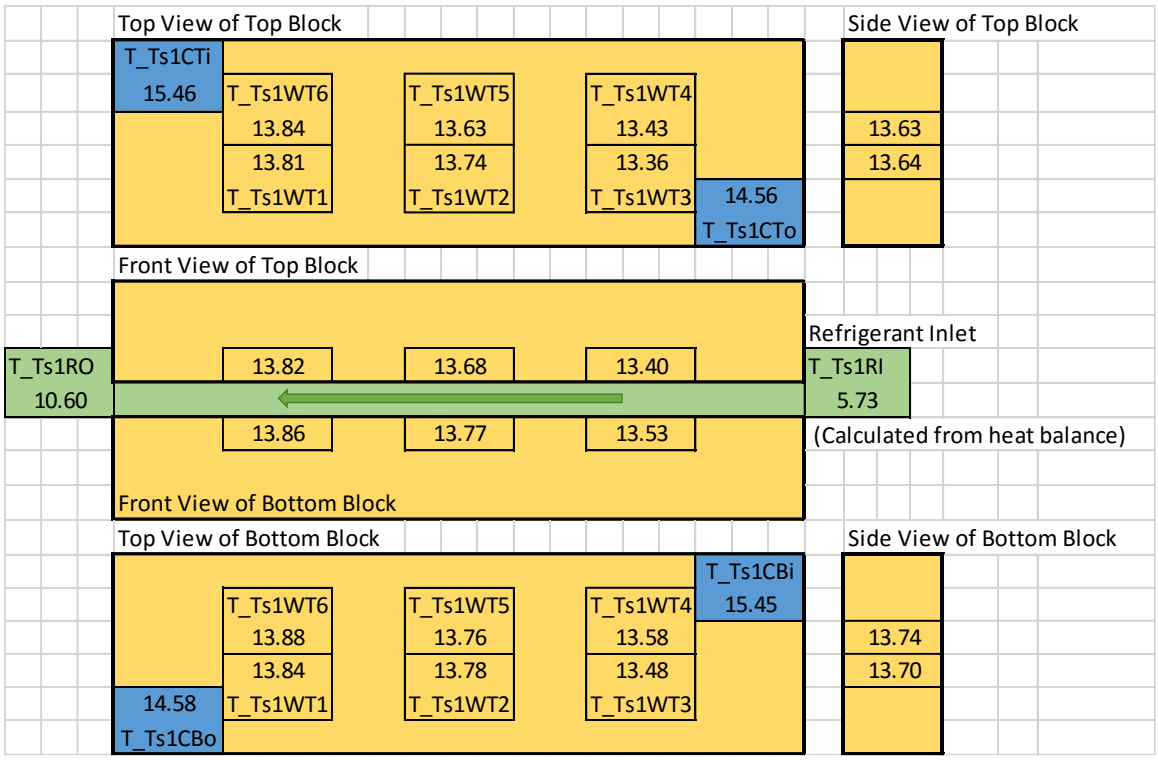

Figure 34 Temperature distribution

Table 15 Case 1 in Appendix B

Test case	Block	Coolant side Q [W]	Calibrated Q [W]	Average of 6 Thermocouples [°C]	Variance of 6 Thermocouples [°C]	Standard Deviation of 6 Thermocouples [°C]	Estimated T_wall (w/o contact resistance) [°C]	Estimated T_wall (w/ contact resistance) [°C]	hA_contact [W/K]	Heat Transfer Coefficient (w/o calibration) [W/Km^2]	Heat Transfer Coefficient (w/ calibration) [W/Km^2]
1	Top	11.550	11.988	13.634	0.474	0.200	13.609	13.609	0.000	482.211	482.211
	Bottom	11.019	11.572	13.722	0.398	0.155	13.697	13.609	131.454	488.413	499.539
Errors	Top	0.702		0.017						33.117	33.117
	Bottom	1.173		0.019						49.852	51.131

Figure 35 (a) shows the vertical temperature profile in the block. 35 (b) is a detailed profile for near wall temperature of (a). The vertical axis shows distance in mm and horizontal axis shows temperature in ^{o}C.

In this single phase heating condition, the average refrigerant temperature is used at position 0. A laminar temperature profile has been made in the tube. On the top surface of the microchannel tube, which is brazed to the block (0.775 mm), the temperature is 13.61 ^{o}C. Above the surface (1.705mm), the average value of thermocouple reading is 13.63 ^{o}C. In the bottom block the temperature on the surface (-0.775 mm), where the thermal paste is, the temperature is 13.61 ^{o}C and the same as the top block; and at the same position (-0.775mm) but with effect of contact resistance the temperature is 13.71 ^{o}C. The

thermocouple reading (-1.705 mm) is 13.7 ^{o}C. Average coolant temperature at TB and BB (+/- 29.1 mm) is 15.01 and 15.02 ^{o}C respectively. The ambient temperature, in this case, is 19.84 ^{o}C.

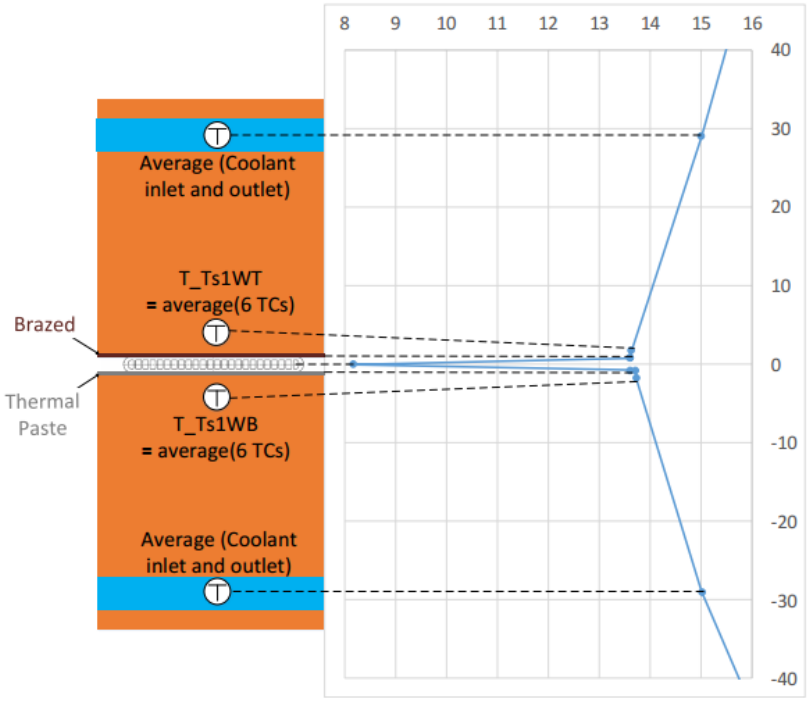

(a)

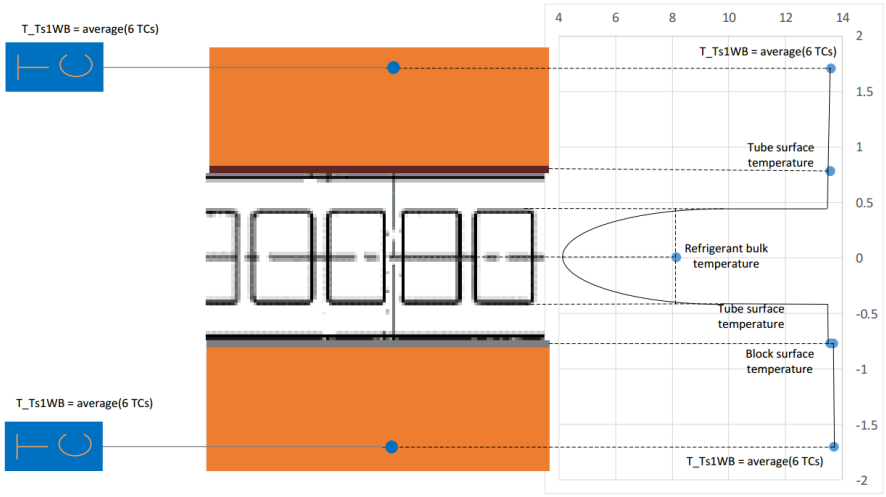

(b)

Figure 35 Vertical temperature profile of case 1

3.5.4 Case 13 details of wall temperature uniformity and calibrated contact resistance

Table 16 shows the information listed in Appendix B case 13. Case 13 is a two-phase R134a evaporating case with a heat transfer rate of about 40 watts in total from the coolant to the refrigerant side. The refrigerant temperature drops slightly from 17.43 to 17.41 ^{o}C due to pressure drop. From figure 36, it is shown that the temperature of thermocouple reading is not affected by refrigerant temperature change. The variance is only due to uncertainty and coolant temperature distribution. The variance of thermocouple readings on top block is 0.175 and 0.098 ^{o}C for the bottom block. After taking contact resistance into account, the wall temperature of BB is corrected from 18.398 to 18.237 degree Celsius. The heat transfer coefficient is corrected from 3190 to 3742 [W $K^{-1}m^{-2}$] with 15% of changes.

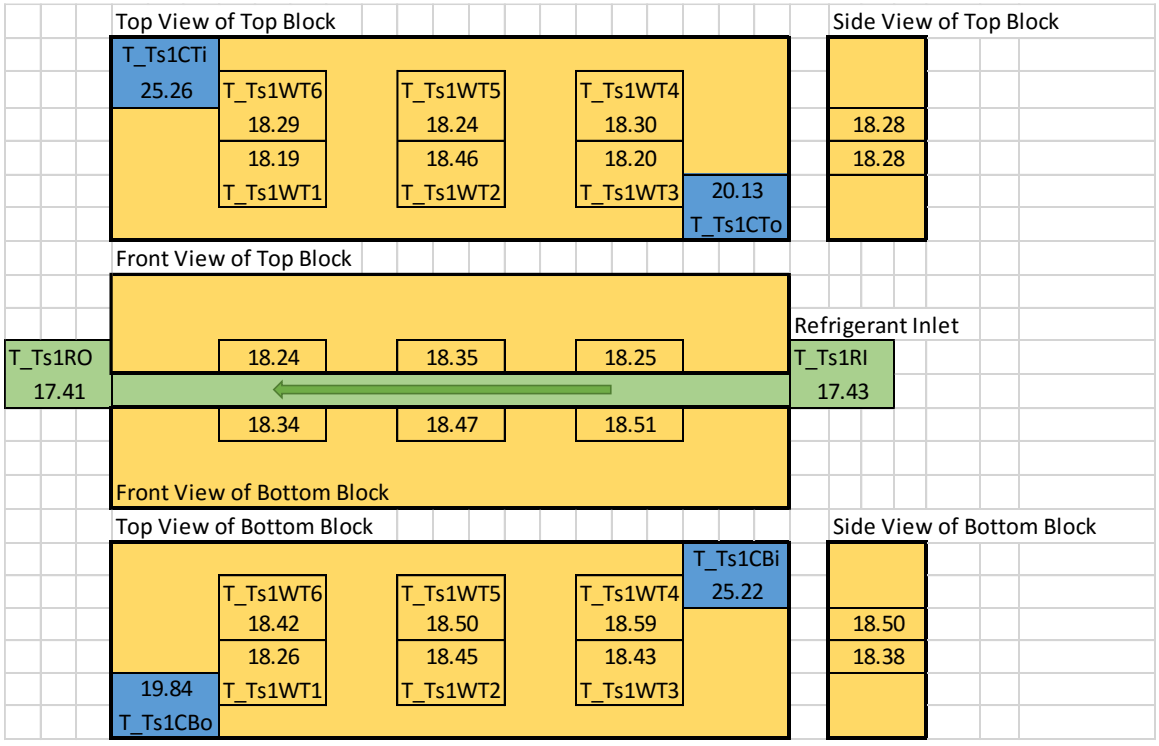

Figure 36 Temperature distribution

Table 16 Case 13 in Appendix B

Test case	Block	Coolant side Q [W]	Calibrated Q [W]	Average of 6 Thermocouples [°C]	Variance of 6 Thermocouples [°C]	Standard Deviation of 6 Thermocouples [°C]	Estimated T_wall (w/o contact resistance) [°C]	Estimated T_wall (w/ contact resistance) [°C]	hA_contact [W/K]	Heat Transfer Coefficient (w/o calibration) [W/Km^2]	Heat Transfer Coefficient (w/ calibration) [W/Km^2]
13	Top	19.794	19.936	18.279	0.175	0.099	18.237	18.237	0.000	3748.445	3748.445
	Bottom	19.729	19.928	18.440	0.098	0.107	18.398	18.237	123.277	3190.237	3742.574
Errors	Top	0.600	0.600				0.045	0.045	0.000	698.086	698.086
	Bottom	0.638	0.638				0.046	0.046	0.000	524.306	706.726

Figure 37 (a) shows the vertical temperature profile in the block. 37 (b) is a detailed profile for near wall temperature of (a). The vertical axis shows distance in mm and horizontal axis shows temperature in ^{o}C.

In this single-phase heating condition, Average refrigerant temperature (17.42 ^{o}C) is used at position 0. A laminar temperature profile has been made in the tube (noted that it is two-phase and probably bubble/slug flow in reality). On the top surface of the microchannel tube, which is brazed to the block (0.775 mm), the temperature is 18.24 ^{o}C. Above the surface (1.705mm), the average value of thermocouple reading is 18.28 ^{o}C. In the bottom block the temperature on the surface (-0.775 mm), where the thermal paste is located, the temperature is 18.24 ^{o}C, the same as the top block; and at the same position (-0.775mm) but with the effect of contact resistance the temperature is 18.43 ^{o}C. The thermocouple reading (-1.705 mm) is 18.44 ^{o}C. Average coolant temperature at TB and BB (+/- 29.1 mm) is 22.69 and 22.53 ^{o}C respectively. The ambient temperature, in this case, is 23.29 ^{o}C.

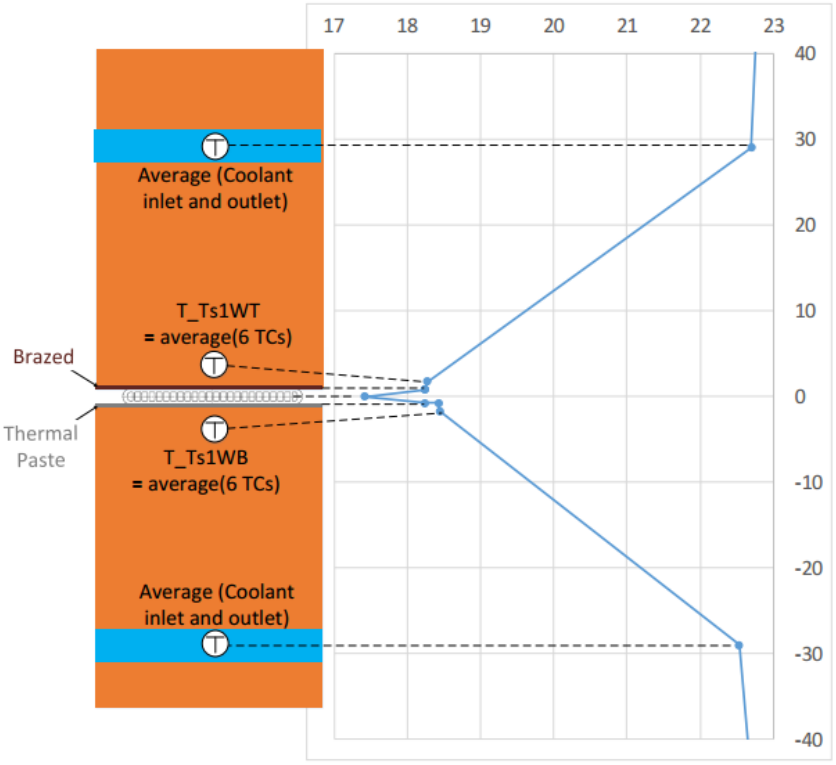

(a)

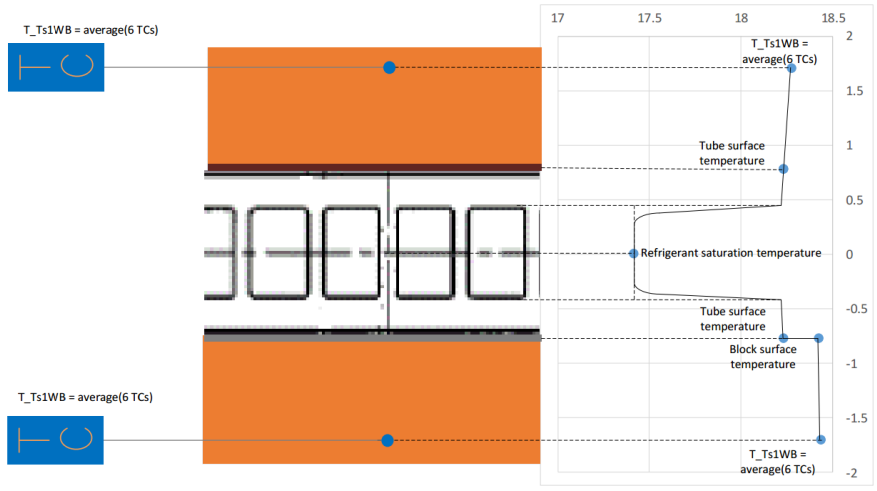

(b)

Figure 37 Vertical temperature profile of case 13

3.6 Measurement of HTC and PD and data reduction

Heat transfer coefficient (HTC) and pressure drop (PD) are the two primary measurements to be obtained in this facility. HTC and PD are measured by the definition:

$$HTC = \frac{Q}{A_s(T_{wall} - T_{ref})} \tag{3.20}$$

$$PD = \frac{P_{out} - P_{in}}{L} \tag{3.21}$$

In equation (3.20), A_s is the surface area which is the total port surface area in most cases. T_{wall} is a calibrated wall temperature defined previously. T_{ref} is the bulk refrigerant temperature and is equal to saturation temperature in two phase. Q is the total heat transfer rate which is measured in the coolant loop.

In equation (3.21), the pressure difference (P_{out}-P_{in}) is directly measured by differential pressure transducers. L is the length of the test section which is a known.

Six thermocouples are placed at each of the top and bottom blocks which are close to the tube surface at three locations of the test section. The thermocouple location and calibration process can be found previously in this section. After calibration (equation 3.19), the wall temperature in equation (3.20) can be obtained:

$$T_{TsiRW} = \frac{\left[\frac{\sum_{n=1}^{6} T_{TsiWTn}}{6} - R_{cond} \times \frac{Q_{TsiR}}{2} - R_{cont} \times \frac{Q_{TsiR}}{2}\right] + \left[\frac{\sum_{n=1}^{6} T_{TsiWTn}}{6} - R_{cond} \times \frac{Q_{TsiR}}{2} - R_{cont} \times \frac{Q_{TsiR}}{2}\right]}{2} \tag{3.22}$$

Refrigerant temperature (T_{ref}) is the equilibrium saturation temperature in two-phase experiments. The temperature comes from a database which uses the equation of states of parameters to determine the value. The inlet and outlet saturation pressures are actually measured. A gauge pressure transducer measures the pressure at the inlet of the test line. A series of differential pressure transducers measures the pressure difference from inlet to the test section and has been shown in figure 12. Combining the gauge and differential pressures, the saturation pressure is determined:

$$P_{TsjRI} = P_{Ts1RI} - \sum_{i=1}^{j} DP_{Tsi} + DP_{Csi} \tag{3.23}$$

Heat transfer rate from the coolant to refrigerant is calibrated with heat loss. The value is determined by equation (3.8). Coolant side heat transfer rate is determined in (test section 1 BB nomenclature as example):

$$Q_{Ts1CB} = m_{Ts1CB} \times C_p \times (T_{Ts1CBi} - T_{Ts1CBo}) \tag{3.24}$$

Combing equation (3.8) and (3.23):

$$Q_{Ts1RB} = m_{Ts1CB} \times C_p \times (T_{Ts1CBi} - T_{Ts1CBo}) - UA_{Ts1B} \frac{(T_{amb} - T_{Ts1CBi}) - (T_{amb} - T_{Ts1CBo})}{\ln\left(\frac{T_{amb} - T_{Ts1CBi}}{T_{amb} - T_{Ts1CBo}}\right)} \tag{3.25}$$

Substituting equation (3.19), (3.22), (3.23), (3.24) and the database of refrigerant properties, HTC can be determined and written in general form:

$$HTC_{Tsi} = \frac{Q_{TsiRB} + Q_{TsiRT}}{A_s(T_{TsiRW} - \frac{T_{TsiRI} + T_{TsiRO}}{2})} \tag{3.26}$$

The pressure drop equation (3.21) can be rewritten into:

$$PD_{Tsi} = \frac{DP_{Tsi}}{L} \tag{3.27}$$

In two phase heat transfer experiments, heat transfer coefficient is typically plotted versus vapor quality (x). x is determined by a database for refrigerant properties. By putting in enthalpy and saturation pressure into the database, quality can be calculated as $x=(P, h)$.

Enthalpy is calculated by the heat balance method. With the temperature and pressure measurements in single-phase refrigerant, an inlet enthalpy can be determined. By adding or subtracting heat from the inlet enthalpy value so that the enthalpy at test section can be calculated:

$$h_{TsjRI} = h_{EvRI} + \frac{Q_{Ev} + \sum_{i=1}^{j} Q_{TsiR} + Q_{CsiR}}{m_R} \tag{3.28}$$

Both evaporation and condensation experiments can be conducted by this facility. Under evaporation test mode, the sub-cooled single-phase refrigerant is supplied to the evaporator which controls the inlet state of sub-cooling (SC) of the refrigerant to Test Section 1. Under condensation test mode, the sub-cooled single-phase refrigerant is

supplied to the pre-heater which heats the refrigerant into the desired superheat (SH) at the inlet of Test Section 1. Refrigerant leaving one test section runs into the following conditioning section. In the test section, the refrigerant is heated/cooled under a constant wall temperature condition controlled by the two aluminum blocks with coolant/heating fluid (water in this thesis). The MC tube is located between the two aluminum blocks, which supplies heat/cooling on both sides of the tube. All gaps among the two aluminum blocks and the tube are filled with high thermal conductivity paste to reduce the contact thermal resistance while the upper and lower parts of aluminum blocks are tightened with four bolts and nuts at the four corners. One exception is that the top block of Test Section 1 is brazed to the MC tube in order to determine the contact resistance which has been discussed in detail in the thesis.

3.7 Uncertainty analysis

All system and random uncertainties of instrumental measurements will contribute to final results. The uncertainties are determined from calibration tests in labotaries or reported by the manufacturer. Values of uncertainties have already been reported in this thesis and this subsection will talk about the analysis of uncertainties in the result.

According to the NIST standard of uncertainty, the uncertainty is done by summarizing the root sum square combinations. The overall uncertainty (eR) of a result (R) with a known function F of n variables x_i with known uncertainties (ex_i) could be expressed in equation (3.29). This equation is under assumptions that all variables are independent, repeated measurements show Gaussian distribution, and all uncertainties of variables are in the same level of confidence. In this thesis, the level of confidence is 95%.

$$R = F(x_1, x_2, \dots x_i, \dots)$$

$$eR = \sqrt{\sum_{i=1}^{n} \left(\frac{\partial F}{\partial x_i} ex_i\right)^2} \tag{3.29}$$

With equation (3.29) and (3.20), the uncertainty of heat transfer coefficient can be expressed in:

$$eHTC = \sqrt{\left(\frac{eQ}{A_s(T_{wall} - T_{ref})}\right)^2 + \left(-\frac{Q \times eT_{ref}}{A_s(T_{wall} - T_{ref})^2}\right)^2 + \left(-\frac{Q \times eT_{wall}}{A_s(T_{wall} - T_{ref})^2}\right)^2} \tag{3.30}$$

Where eQ, eT_{ref}, and eT_{wall} are the uncertainty of heat transfer rate, temperature of the refrigerant, and temperature of wall respectively. Uncertainty of heat transfer rate to refrigerant can be determined in (take test section 1 bottom as example):

$$eQ_{Ts1RB} = \left\{ \left(em_{Ts1CB} \times C_p \times (T_{Ts1CBi} - T_{Ts1CBo}) \right)^2 + \left(m_{Ts1CB} \times C_p \times eT_{Ts1CBi} \right)^2 + \left(-m_{Ts1CB} \times C_p \times eT_{Ts1CBo} \right)^2 \right\}^{\frac{1}{2}} \quad (3.31)$$

In equation (3.31): em_{Ts1CB}, eT_{Ts1CBi}, eT_{Ts1cbo} are uncertainties of coolant mass flow rate of test section 1 bottom, coolant temperature inlet of test section 1 bottom block, and outlet temperature respectively. These values are all listed in this thesis.

When averaging several readings, i.e, averaging 6 TCs reading for wall temperature, the uncertainty drops to about 1/6 of the original as shown in equation (3.32). Here all uncertainties of each individual thermocouple have been listed in this thesis.

$$eT_{wall} = \sqrt{\frac{(eT_1)^2 + (eT_2)^2 + (eT_3)^2 + (eT_4)^2 + (eT_5)^2 + (eT_6)^2}{6}} \quad (3.32)$$

As mentioned above, the refrigerant temperature is only a function of saturation pressure in two phase. A central differencing method has been used to calculate the uncertainty when using a database:

$$eT_{ref} = \frac{T(P_{sat} + \delta P) - T(P_{sat} - \delta P)}{2\delta P \times P_{sat}} \times eP_{sat} \quad (3.33)$$

Here, δP is a small value to add bias numerically for finding out the differentiate of function $T(P)$ at P_{sat}.

Since the pressure drop determined by equation (3.21) has only one measurement variable, the uncertainty will be just the uncertainty of differential pressure transducer readings (eDP) divided by the length (L).

$$ePD = \frac{eDP}{L} \quad (3.34)$$

4. R134a results and discussion

R134a is the first refrigerant running in the facility for testing. Two-phase pressure drop and two-phase heat transfer coefficient have been obtained. The homogeneous model has been applied to predict two-phase pressure drop and compared with data. 5 prediction models have been applied to predict heat transfer coefficient data and compared to measurements.

Original results can be found in Appendix C.

4.1 Two-phase pressure drop homogeneous model

The total pressure drop (PD_{total}) in two phase flow can be broken down into three parts: frictional pressure drop ($PD_{friction}$), momentum pressure drop ($PD_{momentum}$), and static pressure drop (PD_{static}).

$$PD_{total} = PD_{friction} + PD_{momemtum} + PD_{static} \tag{4.1}$$

Carey (1992) introduced a simple homogenous model to model the frictional and momentum pressure drop. Hartnett and Kostic (1993) have developed a model to predict the fully developed laminar flow in rectangular ducts.

The frictional pressure drop is represented as:

$$PD_{friction} = \frac{2fG^2}{D \times \rho_{TP}} \tag{4.2}$$

In equation (4.2), f is a non-dimensional number, the friction factor, determined implicitly from equation (4.3) and (4.4) for laminar and turbulent flow respectively.

$$f_l = \frac{96(1 - 1.3553\beta + 1.9467\beta^2 - 1.7012\beta^3 + 0.9546\beta^4 - 0.2573\beta^5)}{Re_{TP}} \tag{4.3}$$

$$f_t = 8 * \left(\left(\frac{8}{Re_{TP}}\right)^{12} + \frac{1}{\left(\left(\frac{37530}{Re_{tp}}\right)^{16} + \left[2.457 \ln \left(\frac{1}{\left(\frac{7}{Re_{TP}}\right)^{0.9} + 0.27\frac{\varepsilon}{D}} \right) \right]^{16} \right)^{1.5}} \right)^{\frac{1}{12}} \quad (4.4)$$

From equation (4.3), it can be concluded that by defining a two-phase Reynolds number Re_{TP}, the friction coefficient $f_l Re_{TP}$ is a constant in prediction. The constant is a function of the aspect ratio of the channel (β).

In equation (4.4), friction factor is a function of two-phase Reynolds number. This non-dimensional number is defined as:

$$Re_{TP} = \frac{GD}{\mu_{TP}} \quad (4.5)$$

G is mass flux, *D* is the diameter of tube, and μ_{TP} is the two-phase viscosity defined as:

$$\mu_{TP} = \rho_{TP} \left[\frac{x}{\rho_g}\mu_g + \frac{1-x}{\rho_f}\mu_f \right] \quad (4.6)$$

$$\rho_{TP} = \rho_g \left[\frac{\rho_f}{x\rho_f + (1-x)\rho_g} \right] \quad (4.7)$$

In equation (4.6), ρ_{TP} is a two-phase density defined in equation (4.7), *x* is the quality, ρ_g and ρ_f are the vapor and liquid phase density, μ_g and μ_f are the vapor and liquid phase dynamic viscosity.

The accelerating pressure drop (PD_a) is the main contributor to momentum pressure drop which is defined as:

$$PD_a = \int \frac{dP}{dz} dz \quad (4.8)$$

$$\frac{dP}{dz} = \frac{d(\frac{x}{\rho_g} + \frac{1-x}{\rho_f})}{dz} \quad (4.9)$$

The accelerating pressure will be integrated along the heated length of tube. Summary of (4.2) and (4.8) will be the predicted pressure drop.

The results and comparison to experimental data will be presented later in this section.

4.2 Two phase evaporation heat transfer coefficient models

Most correlations of two-phase evaporation heat transfer coefficient are developed for round tubes. Qu and Mudawar (2003) presented a correction to modify the round tube heat transfer coefficient prediction into a rectangular channel as equation (4.10).

$$HTC_{rec} = HTC_{round}\frac{Nu_3}{Nu_4} \tag{4.10}$$

Nu_3 and Nu_4 are the single-phase fully developed laminar Nusselt numbers for different wall heating conditions respectively.

$$Nu_3 = 8.235(1 - 1.883\beta + 3.767\beta^2 - 5.814\beta^3 + 5.361\beta^4 - 2.0\beta^5) \tag{4.11}$$

$$Nu_4 = 8.235(1 - 2.042\beta + 3.085\beta^2 - 2.477\beta^3 + 1.058\beta^4 - 0.186\beta^5) \tag{4.12}$$

Five models of HTC_{round} with correction to rectangular tube have been used.

Table 17 Table of heat transfer coefficient predictions

Chen (1966)	$HTC = \frac{Nu_3}{NU_4}(Eh_{sp} + Sh_{nb})$ $h_{sp} = 0.023(Re_f)^{0.8}(\mathrm{Pr}_f)^{0.4}\frac{k_f}{D}$ $h_{nb} = 0.00122\frac{k_f^{0.79}C_{Pf}^{0.45}\rho_f^{0.49}}{\sigma^{0.5}\mu_f^{0.29}h_{fg}^{0.24}\rho_g^{0.24}}\Delta T_{sat}^{0.24}\Delta P_{sat}^{0.75}$ $E = \left(1 + \frac{1}{Xtt^{0.5}}\right)^{1.78}, S = 0.9622 - 0.5822\tan^{-1}(\frac{Re_f E^{1.25}}{6.18e4})$ $Re_f = \frac{G(1-x)D}{\mu_f}, Pr_f = \frac{C_{Pf}\mu_f}{k_f}, X_{tt} = \left(\frac{1-x}{x}\right)^{0.9}\left(\frac{\rho_g}{\rho_f}\right)^{0.5}\left(\frac{\mu_f}{\mu_g}\right)^{0.1}$
Shah (1982)	$HTC = \frac{Nu_3}{NU_4}max(E,S)h_{sp}$ $h_{sp} = 0.023(Re_f)^{0.8}(\mathrm{Pr}_f)^{0.4}\frac{k_f}{D}$ $F = 1.47\ (Bo \geq 11e-4) or\ 15.43(Bo < 11e-4)$

Table 17 (cont'd)

	$NN = Co\ (Fr_f \geq 0.04) or\ 0.38 Fr_f^{-0.3} Co (Fr_f < 0.04)$ $Co = \left(\frac{1-x}{x}\right)^{0.8} \left(\frac{\rho_g}{\rho_f}\right)^{0.5}, Fr_f = \frac{\rho_f^2 G^2}{9.81D}, S = \frac{1.8}{NN^{0.8}}, Bo = \frac{Q''}{G\, h_{fg}}$ *NN>1:* $E = 230 Bo^{0.5}\ (Bo > 3e-5)\ or\ 1 + 46 Bo^{0.5}\ (Bo < 3e-5)$ *1>NN>0.1:* $E = FBo^{0.5} \exp(2.74 NN^{-0.1})$ *0.1>NN:* $E = FBo^{0.5} \exp(2.74 NN^{-0.15})$
Gungor and Winterton (1986)	$HTC = \frac{Nu_3}{NU_4}(Eh_{sp} + Sh_{nb})$ $h_{sp} = 0.023 (Re_f)^{0.8} (\mathrm{Pr}_f)^{0.4} \frac{k_f}{D}$ $h_{nb} = 55 \mathrm{P_r}^{0.12} (-\log_{10} P_r)^{-0.55} M_W^{-0.5} Q''^{0.67}$ $E = 1 + 24000 Bo^{1.16} + 1.37 \left(\frac{1}{X_{tt}}\right)^{0.86}$ $S = \left(1 + 1.15e-6 E^2 Re_f^{1.17}\right)^{-1}$
Kandlikar (1990)	$HTC = \frac{Nu_3}{NU_4} max(E, S) h_{sp}$ $h_{sp} = 0.023 (Re_f)^{0.8} (\mathrm{Pr}_f)^{0.4} \frac{k_f}{D}$ $E = 0.6683 Co^{-0.2} f(Fr_f) + 1058 Bo^{0.7}$ $S = 1.136 Co^{-0.9} f(Fr_f) + 667.2 Bo^{0.7}$ $f(Fr_f) = 1\ (Fr_f \geq 0.04) or\ (25 Fr_f)^{0.3}\ (Fr_f < 0.04), Fr_f = \frac{\rho_f^2 G^2}{9.81D}$
Trans et al. (1996)	$HTC = \frac{Nu_3}{Nu_4}\left[8.4e5 (Bo^2 We_f)^{0.3} \left(\frac{\rho_f}{\rho_g}\right)^{0.4}\right]$ $We_f = \frac{v_f G^2 D}{\sigma}$

A comparison of prediction models to experimental data and discussion will be presented later in this section.

4.3 Two-phase (evaporating) pressure drop

Figure 38 shows the evaporating pressure drop. The horizontal error bar is the quality change in the test section. Each test produces six pressure drop data points from test section 1 to 6. The heat flux and mass flux in each test are identical in each test sections. However, heat flux is changed among three tests.

When mass flux is fixed at 121 $kgm^{-2}s^{-1}$, pressure drop slightly increases as the heat fluxes are increasing from1798 to 3608 Wm^{-2}. This is due to the fact that the accelerating pressure drop contributes more in the higher heat fluxes case.

At the beginning, the pressure drop is small in the liquid phase in the bubbly flow. Pressure drop starts to increase as vapor quality goes higher because of more frictional loss from vapor phase than the liquid phase. Also, the friction between liquid and vapor can contribute to pressure drop.

Figure 38 also shows the corresponding saturation pressure at each data points. The overall pressure drops from about 530 to 440 kPa from test section 1 to 6.

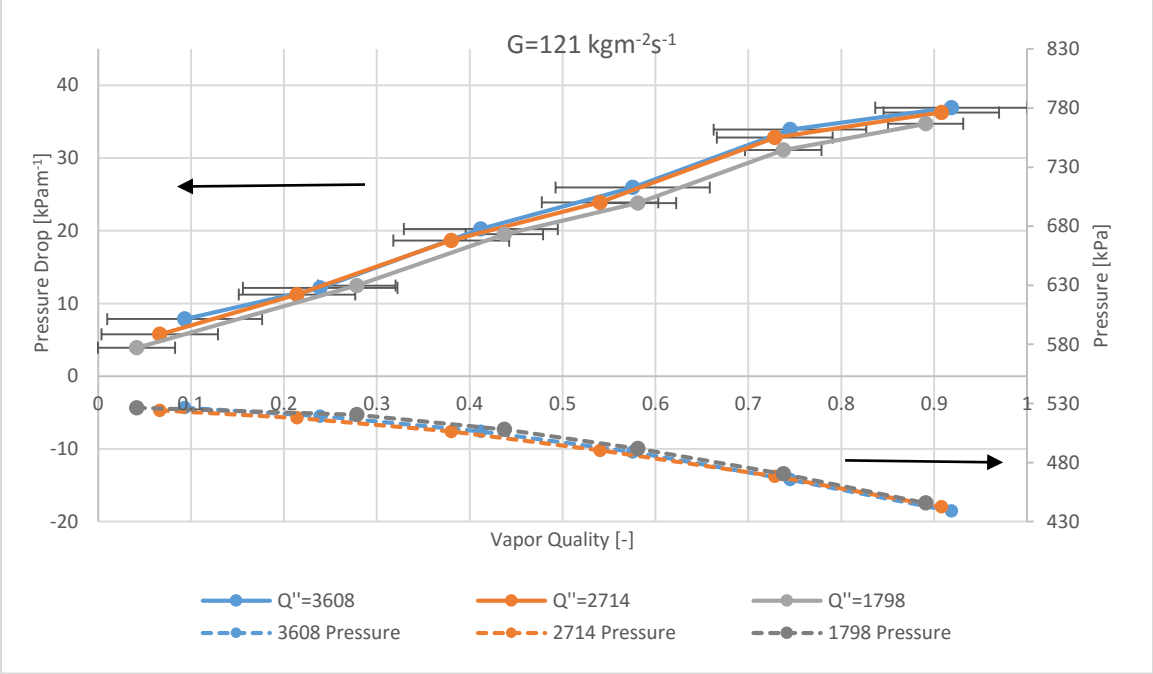

Figure 38 Diabatic pressure drop of R134a at fixed mass flux and different heat fluxes

Figure 39 shows pressure drop measurements compared with the prediction of the homogeneous model. As can be observed, the prediction is lower than the measurements.

The mean absolute error (MAE) of the homogeneous model is 24% and the error is defined as:

$$MAE = \frac{\sum_{i=1}^{n} \left| \frac{Measurement - Prediction}{Measurement} \right|}{N} \times 100\% \tag{4.13}$$

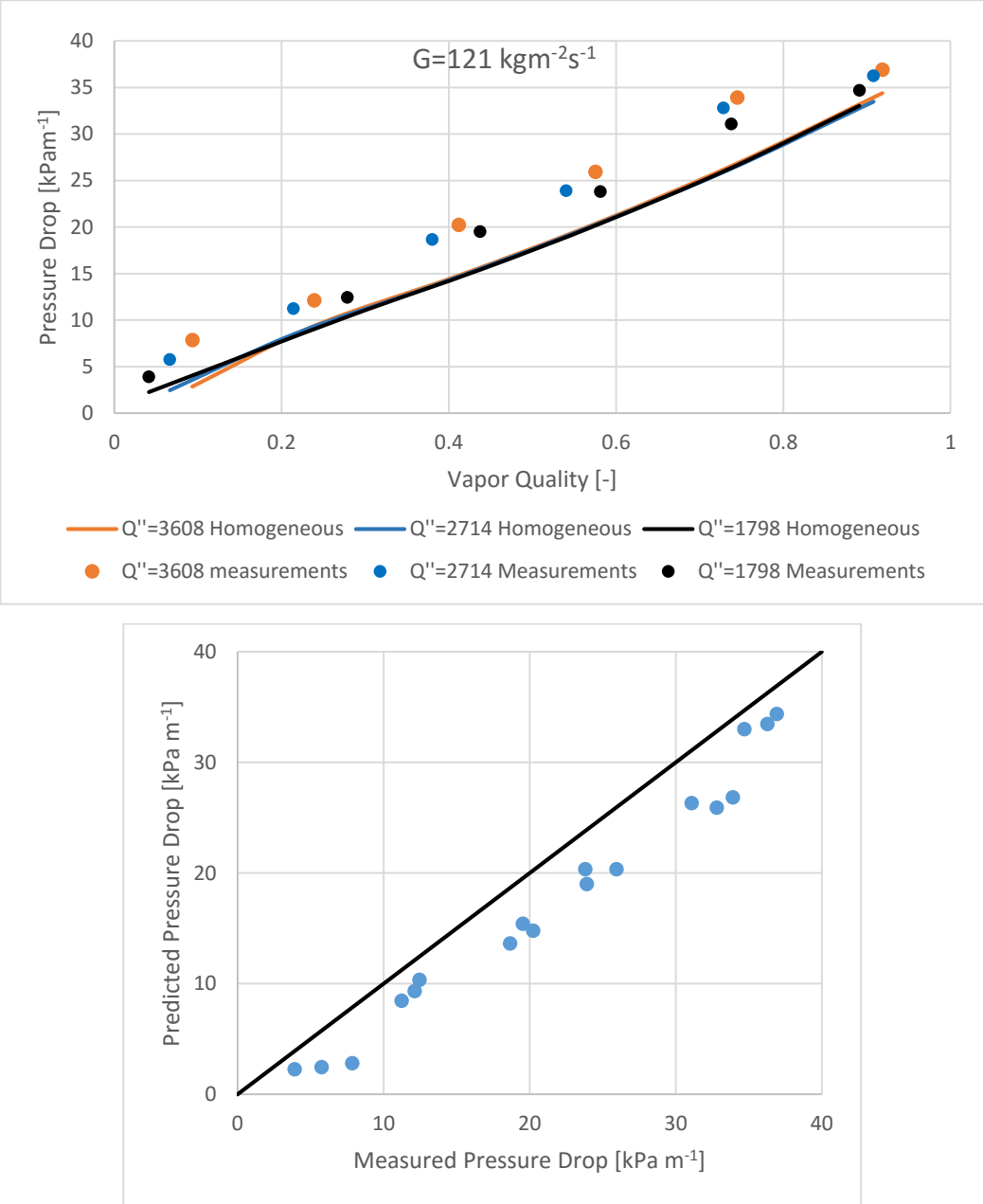

Figure 39 Pressure drop measurement and prediction comparison

4.4 Two-phase heat transfer coefficient

Figure 40 shows the heat transfer coefficient at fixed mass flux and different heat fluxes. As with the pressure drop experiments, each line has six data points collected from test section 1 to 6. These heat transfer coefficient data points are gained at the same time of measuring pressure drop.

Three tests are conducted and each test has an identical mass flux of 121 $kgm^{-2}s^{-1}$. Heat transfer coefficient increases when the heat fluxes are increasing from 1798 to 3608 Wm^{-2}. As vapor quality increases, the heat transfer coefficient starts to increase. But the heat transfer coefficient is not a strong function of quality in a moderate range of quality (0.2 to 0.7) for small heat fluxes. At about the quality of 0.75, heat transfer coefficient reaches the highest value and starts to drop due to depression of boiling and dry out effects. HTC drops after it reaches the maximum points.

The saturation pressure is also shown in figure 40. The pressure in test section 1 is about 530 kPa and in the last test section it is about 440 kPa.

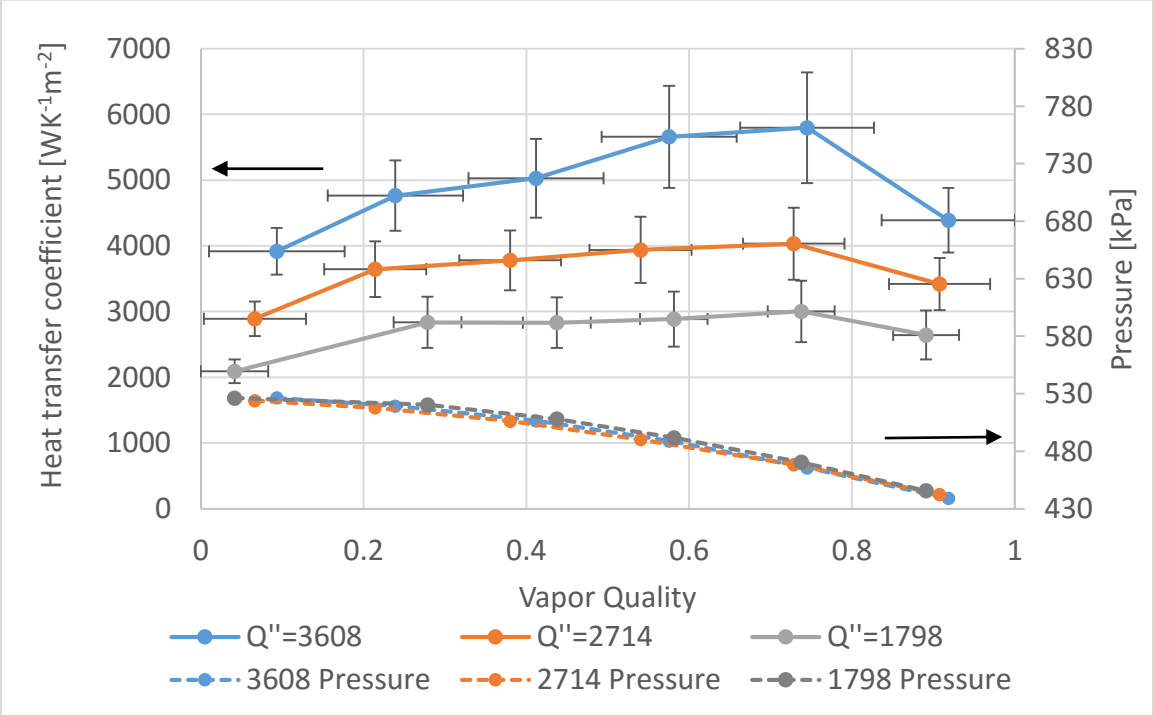

Figure 40 Heat transfer coefficient at fixed mass flux and different heat fluxes

Data from the three tests are plotted with five heat transfer coefficient prediction model in figure 41. It shows that all models have under-predicted the heat transfer coefficient. Figure 42 plot predicted heat transfer coefficient versus measurement.

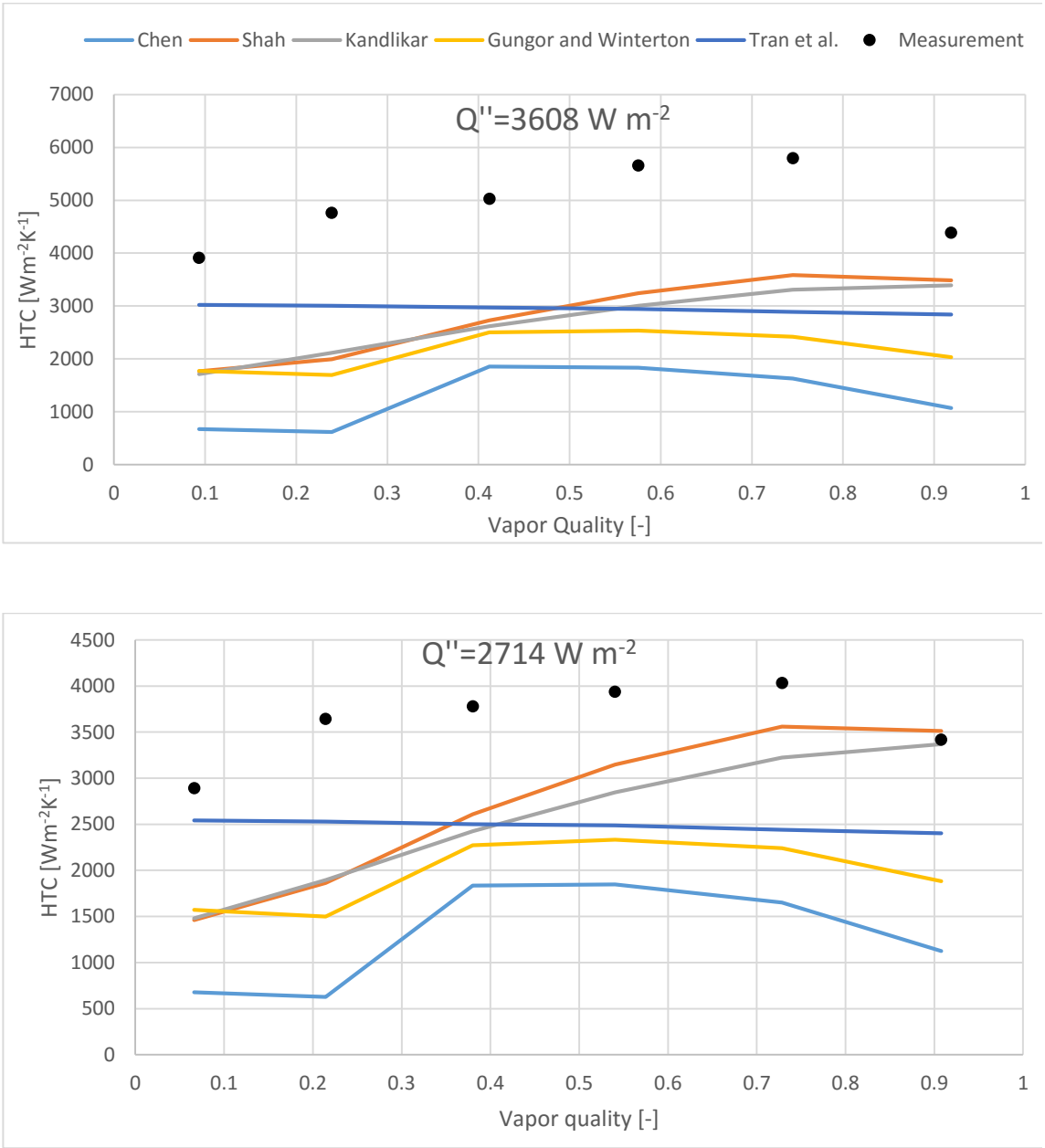

Figure 41 Comparison of measurement to prediction of the three tests

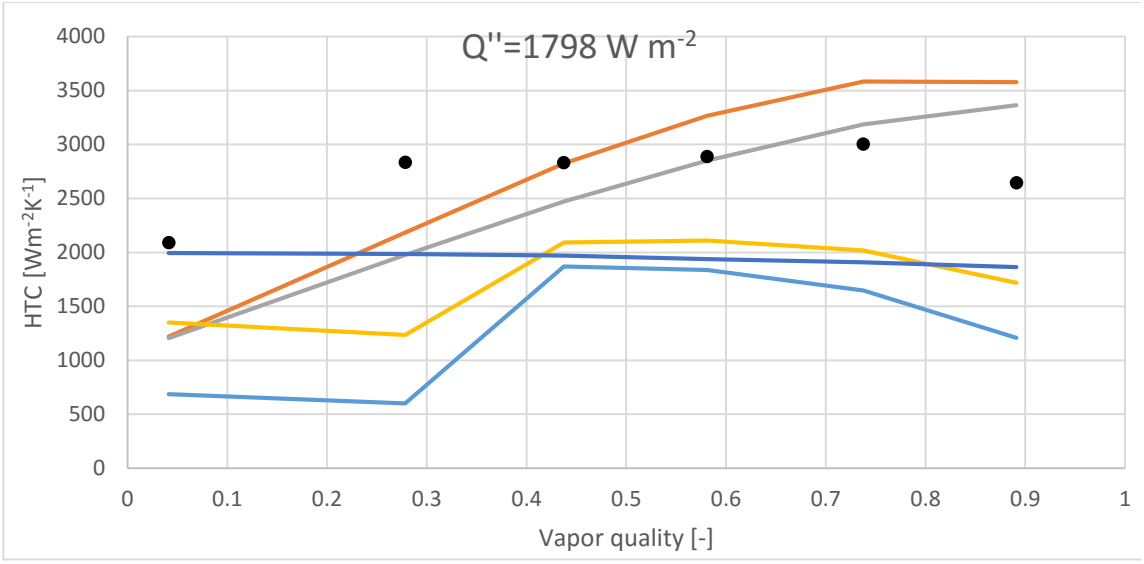

Figure 41 (cont'd)

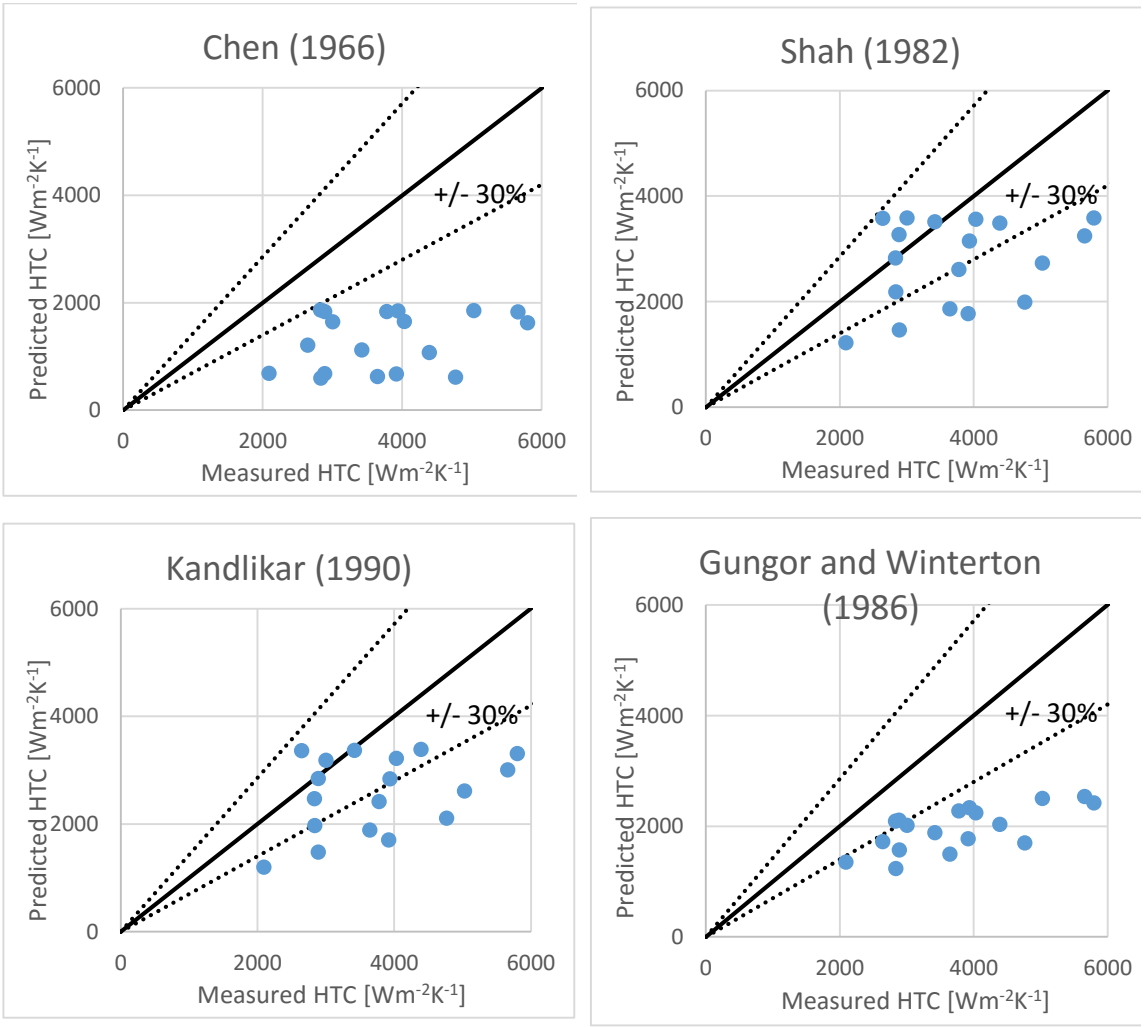

Figure 42 Comparison of prediction model to measurements

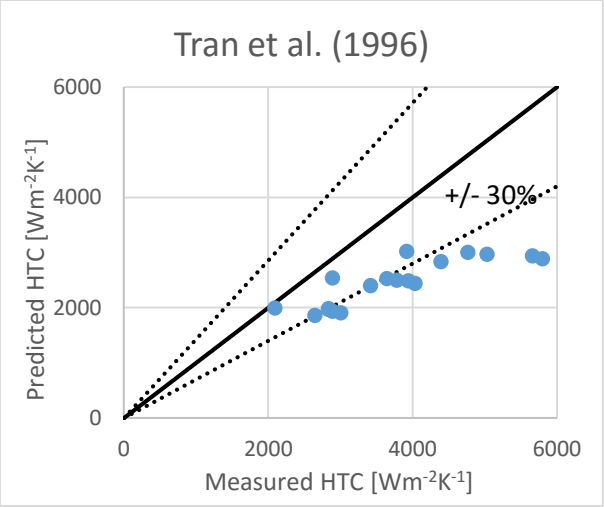

Figure 42 (cont'd)

According to figures 41 and 42, Chen (1966)'s model under predicts the heat transfer coefficient but with the same trends. The same situation for Gungor and Winterton (1986) can be observed. The models from Shah (1982) and Kandlikar (1990) predict an increasing curve till very high-quality zone. Tran et al. (1996) predicts the enlargement of boiling effect at low quality but with a different trend over the whole quality change. Table 18 shows the 5 models and their MAE to measurement data.

Table 18 Each model and the MAE

Model	**MAE [%]**
Chen (1966)	64.1
Shah (1982)	30.9
Kandlikar (1990)	31.9
Gungor and Winterton (1986)	45.2
Tran et al. (1996)	32.3

Conclusions

A heat transfer coefficient and pressure drop measurement facility has been designed and built. Literature studies of the experimental facility have been made. How the facility was built and instructions of important parts of the facility have been reported in this thesis. Details of the test line structure have been reported including test section, conditioning section, pressure transducer installation, etc.

Calibration process on the facility has been reported. Calibrated parameters of instruments including the pressure transducers, mass flow meters, and thermocouples have been reported in this report. Calibration of heat losses and contact resistance have been made and introduced. The heat loss calibration has been verified by nine cases. Two cases in contact resistance calibration experiments have been discussed and the uniformity of wall temperature measurements has been proved.

Heat transfer coefficient and pressure drop are measured in R134a in three different conditions. The measurements are shown and compared to prediction models. It is shown that heat transfer coefficient is a function of heat fluxes. Pressure drop is a weak function of heat fluxes because the only component different in theory is the acceleration pressure drop. It has been shown that all prediction model has under-predicted heat transfer coefficients. The model with smallest MAE comes from Shah (1982), Kandlikar (1990), and Tran et al. (1996).

Future work of the research is:

1) Collecting more data on the new facility on R134a.
2) Collecting heat transfer coefficient and pressure drop for other low GPW refrigerants, blends, with or without oil.
3) Building a new model for heat transfer coefficient and pressure drop in microchannel tubes.

References

Anowar Hossain, M., Onaka, Y., Afroz, H. M. M., & Miyara, A. (2013). Heat transfer during evaporation of R1234ze(E), R32, R410A and a mixture of R1234ze(E) and R32 inside a horizontal smooth tube. International Journal of Refrigeration, 36(2), 465–477.

Anwar, Z., Palm, B., & Khodabandeh, R. (2015). Flow boiling heat transfer, pressure drop and dryout characteristics of R1234yf: Experimental results and predictions. Experimental Thermal and Fluid Science, 66, 137–149.

Carey, V.P., (1992). Liquid-vapor phase-change phenomena, Hemisphere Publishing Co.

Chen, J. C. (1966). Correlation for boiling heat transfer to saturated fluids in convective flow. Industrial & Engineering Chemistry Process Design and Development, 5(3), 322–329.

Garimella, S., & Bandhauer, T. M. (2001). Measurement of condensation heat transfer coefficients in microchannel tubes. In *Proceedings of the 2001 International Mechanical Engineering Congress and Exposition*.

Gungor, K.E. Winterton, R.H.S. (1986) A general correlation for flow boiling in tubes and annuli, Int. J. Heat Mass Transfer 29 351–358.

Harley, J. C. (1993). Compressible gas flows in microchannel and microjets. University of Pennsylvania.

Hartnett, J. P., & Kostic, M. (1989). Heat transfer to newtonian and non-newtonian fluids in rectangular ducts. Advances in Heat Transfer, 19, 247–356.

Hrnjak, P., & Litch, A. D. (2008). Microchannel heat exchangers for charge minimization in air-cooled ammonia condensers and chillers. International Journal of Refrigeration, 31(4), 658–668.

Kandlikar, S.G. (1990). A general correlation for saturated two- phase flow boiling heat transfer inside horizontal and vertical tubes, J. Heat Transfer 112 219–228.

Kandlikar, S. G., & Grande, W. J. (2003). Evolution of Microchannel Flow Passages--Thermohydraulic Performance and Fabrication Technology. Heat Transfer

Mehendale, S. S., Jacobi, a. M., & Shah, R. K. (2000). Fluid Flow and Heat Transfer at Micro- and Meso-Scales With Application to Heat Exchanger Design. Applied

Mortada, S., Zoughaib, a., Arzano-Daurelle, C., & Clodic, D. (2012). Boiling heat transfer and pressure drop of R-134a and R-1234yf in minichannels for low mass fluxes. International Journal of Refrigeration, 35(4), 962–973.

Qu, W., & Mudawar, I. (2003). Flow boiling heat transfer in two-phase micro-channel heat sinks-I. Experimental investigation and assessment of correlation methods. International Journal of Heat and Mass Transfer.

Serizawa, A., Feng, Z., & Kawara, Z. (2002). Two-phase flow in microchannels. Experimental Thermal and Fluid Science, 26(6-7), 703–714.

Shah, M.M. (1982). Chart correlation for saturated boiling heat transfer: equations and further study, ASHRAE Trans. 88 185–196.

Szczukiewicz, S., Borhani, N., & Thome, J. R. (2012). Two-phase flow boiling in a single layer of future high-performance 3D stacked computer chips. InterSociety Conference on Thermal and Thermomechanical Phenomena in Electronic Systems, ITHERM, 597–605.

Tran, T.N. M.W. Wambsganss, D.M. France, (1996). Small circular- and rectangular-channel boiling with two refrig- erants, Int. J. Multiphase Flow 22 485–498.

Triplett, K. a., Ghiaasiaan, S. M., Abdel-Khalik, S. I., & Sadowski, D. L. (1999). Gas–liquid two-phase flow in microchannels Part I: two-phase flow patterns. International Journal of Multiphase Flow, 25(3), 377–394.

Tu, X., & Hrnjak, P. S. (2004). Flow and Heat Transfer in Microchannels 30 to 300 Microns in Hydraulic Diameter. Air Conditioning and Refrigeration Center.

Wilson, E.E. (1915) A Basis for Rational Design of Heat Transfer Apparatus, Trans. ASME J. Heat Transfer, vol. 37: p. 47-82.Garimella, S., & Bandhauer, T. M. (2001). Measurement of condensation heat transfer coefficients in microchannel tubes. Proceedings of the 2001 International Mechanical Engineering Congress and Exposition.

Zhang, J., Parakash, S., Jaluria, Y., & Lin, L. (2010). An Experimental Study on the Effect of Configuration of Multiple. In Proceedings of the 14th International Heat Transfer Conference. Washington, DC, USA.

Appendix A Thermocouple calibration results

Name	Component	Fluid/Material	Location	Slope	Intercept	Accuracy [°C]
Backup	-	-	-	1.004	0.0567	0.1761
Backup	-	-	-	1.0022	-0.2648	0.1406
Backup	-	-	-	0.9978	-0.0225	0.1371
Backup	-	-	-	0.9976	0.016	0.1443
Backup	-	-	-	0.9991	0.1334	0.1352
Backup	-	-	-	0.9985	0.1339	0.1738
Backup	-	-	-	0.9985	0.1237	0.1351
Backup	-	-	-	1.0031	0.0365	0.1653
Backup	-	-	-	0.9961	0.1687	0.1553
T_Cs1CI	Conditioning Section 1	Coolant	Inlet	1.003	-0.1124	0.1079
T_Cs1CO	Conditioning Section 1	Coolant	Outlet	1.0007	-0.0614	0.1057
T_Cs1WI	Conditioning Section 1	Wall	Inlet	0.9989	0.1132	0.2246
T_Cs2CI	Conditioning Section 2	Coolant	Inlet	1.0004	-0.0417	0.1128
T_Cs2CO	Conditioning Section 2	Coolant	Outlet	1.0013	-0.0635	0.1146
T_Cs2WI	Conditioning Section 2	Wall	Inlet	0.9981	0.1448	0.2052
T_Cs3CI	Conditioning Section 3	Coolant	Inlet	1.0017	-0.0877	0.1066
T_Cs3CO	Conditioning Section 3	Coolant	Outlet	1.0044	-0.1299	0.1057
T_Cs3WI	Conditioning Section 3	Wall	Inlet	0.9989	0.1361	0.182
T_Cs4CI	Conditioning Section 4	Coolant	Inlet	1.0045	-0.1525	0.1295
T_Cs4CO	Conditioning Section 4	Coolant	Outlet	1.0032	-0.0923	0.1269
T_Cs4WI	Conditioning Section 4	Wall	Inlet	0.9986	0.1433	0.1957
T_Cs5CI	Conditioning Section 5	Coolant	Inlet	1.0041	-0.1354	0.1076
T_Cs5CO	Conditioning Section 5	Coolant	Outlet	1.0001	-0.0683	0.1057
T_Cs5WI	Conditioning Section 5	Wall	Inlet	0.9979	0.1457	0.2273
T_EvRI	Evaporator	Refrigerant	Inlet	1.0023	0.0286	0.1277
T_GhGO	Glycol Heater	Glycol	Outlet	1	0	0.9852
T_PhxCI	Plate Heat Exchanger	Coolant	Inlet	1	0	0.9852
T_PhxCO	Plate Heat Exchanger	Coolant	Outlet	1	0	0.9852

Name	Component	Fluid/Material	Location	Slope	Intercept	Accuracy [ºC]
T_Pump	Pump	Refrigerant	Outlet	1	0	0.9853
T_RWi	-	Refrigerant	Wall Inlet	1.0003	-0.2306	0.1639
T_RWo	-	Refrigerant	Wall outlet	1.0025	0.1007	0.1577
T_Ts1CBi	Test Section 1	Coolant	Bottom Inlet	1.007	-0.1532	0.139
T_Ts1CBo	Test Section 1	Coolant	Bottom Outlet	1.004	-0.1188	0.1039
T_Ts1CTi	Test Section 1	Coolant	Top Inlet	1.0023	-0.0885	0.1022
T_Ts1CTo	Test Section 1	Coolant	Top Outlet	1.0056	-0.1688	0.117
T_Ts1WB1	Test Section 1	Wall	Bottom 1	1.0021	0.0875	0.1094
T_Ts1WB2	Test Section 1	Wall	Bottom 2	0.9991	0.147	0.1154
T_Ts1WB3	Test Section 1	Wall	Bottom 3	1.0017	0.0858	0.1095
T_Ts1WB4	Test Section 1	Wall	Bottom 4	1.0023	0.0634	0.1184
T_Ts1WB5	Test Section 1	Wall	Bottom 5	1.0043	-0.0051	0.1134
T_Ts1WB6	Test Section 1	Wall	Bottom 6	1.005	-0.0133	0.1133
T_Ts1WI	Test Section 1	Wall	Inlet	1.0011	-0.0444	0.4011
T_Ts1WO	Test Section 1	Wall	Outlet	1.0001	0.0818	0.149
T_Ts1WT1	Test Section 1	Wall	Top 1	1.0023	0.0866	0.1053
T_Ts1WT2	Test Section 1	Wall	Top 2	1.0018	0.1067	0.1303
T_Ts1WT3	Test Section 1	Wall	Top 3	1.0022	0.0757	0.1035
T_Ts1WT4	Test Section 1	Wall	Top 4	1.0025	0.0483	0.1045
T_Ts1WT5	Test Section 1	Wall	Top 5	1.0042	0.034	0.107
T_Ts1WT6	Test Section 1	Wall	Top 6	1.0028	0.0414	0.1178
T_Ts2CBi	Test Section 2	Coolant	Bottom Inlet	1.0008	-0.0652	0.135
T_Ts2CBo	Test Section 2	Coolant	Bottom Outlet	1.002	-0.0959	0.1023
T_Ts2CTi	Test Section 2	Coolant	Top Inlet	1.0045	-0.1726	0.1106
T_Ts2CTo	Test Section 2	Coolant	Top Outlet	1.0072	-0.1935	0.1175
T_Ts2WB1	Test Section 2	Wall	Bottom 1	1.0019	0.083	0.1042
T_Ts2WB2	Test Section 2	Wall	Bottom 2	1.0036	0.0644	0.114
T_Ts2WB3	Test Section 2	Wall	Bottom 3	1.003	0.0458	0.1119
T_Ts2WB4	Test Section 2	Wall	Bottom 4	1.0044	-0.0018	0.1426
T_Ts2WB5	Test Section 2	Wall	Bottom 5	1.0054	0.0017	0.1212
T_Ts2WB6	Test Section 2	Wall	Bottom 6	1.0037	0.0318	0.1226

Name	Component	Fluid/Material	Location	Slope	Intercept	Accuracy [ºC]
T_Ts2WI	Test Section 2	Wall	Inlet	0.9988	0.1188	0.2006
T_Ts2WO	Test Section 2	Wall	Outlet	0.9986	0.1332	0.2241
T_Ts2WT1	Test Section 2	Wall	Top 1	1.0079	-0.0271	0.1364
T_Ts2WT2	Test Section 2	Wall	Top 2	1.0014	0.0855	0.1143
T_Ts2WT3	Test Section 2	Wall	Top 3	1.0056	-0.0004	0.1278
T_Ts2WT4	Test Section 2	Wall	Top 4	1.0038	0.0233	0.1285
T_Ts2WT5	Test Section 2	Wall	Top 5	1.0034	0.0522	0.1255
T_Ts2WT6	Test Section 2	Wall	Top 6	1.0034	0.04	0.1263
T_Ts3CBi	Test Section 3	Coolant	Bottom Inlet	1.0031	-0.0774	0.1135
T_Ts3CBo	Test Section 3	Coolant	Bottom Outlet	1.002	-0.0667	0.1132
T_Ts3CTi	Test Section 3	Coolant	Top Inlet	1.0018	-0.0734	0.1063
T_Ts3CTo	Test Section 3	Coolant	Top Outlet	1.0008	-0.0227	0.1198
T_Ts3WB1	Test Section 3	Wall	Bottom 1	1.0007	0.1027	0.1134
T_Ts3WB2	Test Section 3	Wall	Bottom 2	1.001	0.1052	0.1136
T_Ts3WB3	Test Section 3	Wall	Bottom 3	0.9989	0.1466	0.1165
T_Ts3WB4	Test Section 3	Wall	Bottom 4	1.0048	-0.0137	0.1085
T_Ts3WB5	Test Section 3	Wall	Bottom 5	1.0032	0.0217	0.1226
T_Ts3WB6	Test Section 3	Wall	Bottom 6	1.0042	-0.0058	0.113
T_Ts3WI	Test Section 3	Wall	Inlet	0.9982	0.1411	0.2178
T_Ts3WO	Test Section 3	Wall	Outlet	1.007	-0.0913	0.2829
T_Ts3WT1	Test Section 3	Wall	Top 1	1	0.123	0.1293
T_Ts3WT2	Test Section 3	Wall	Top 2	1.0004	0.1464	0.1215
T_Ts3WT3	Test Section 3	Wall	Top 3	1.0026	0.0774	0.1186
T_Ts3WT4	Test Section 3	Wall	Top 4	1.0048	-0.3772	0.1068
T_Ts3WT5	Test Section 3	Wall	Top 5	1.0039	-0.0606	0.1176
T_Ts3WT6	Test Section 3	Wall	Top 6	1.004	-0.0311	0.1138
T_Ts4CBi	Test Section 4	Coolant	Bottom Inlet	1.002	-0.0747	0.1042
T_Ts4CBo	Test Section 4	Coolant	Bottom Outlet	1.0045	-0.1782	0.1068
T_Ts4CTi	Test Section 4	Coolant	Top Inlet	1.0058	-0.1882	0.115
T_Ts4CTo	Test Section 4	Coolant	Top Outlet	1.0033	-0.1076	0.1105
T_Ts4WB1	Test Section 4	Wall	Bottom 1	1	0.0607	0.1177

Name	Component	Fluid/Material	Location	Slope	Intercept	Accuracy [ºC]
T_Ts4WB2	Test Section 4	Wall	Bottom 2	0.9988	0.1685	0.1521
T_Ts4WB3	Test Section 4	Wall	Bottom 3	1.0028	0.0219	0.1132
T_Ts4WB4	Test Section 4	Wall	Bottom 4	1.0039	-0.0028	0.1051
T_Ts4WB5	Test Section 4	Wall	Bottom 5	1.0012	0.0571	0.1104
T_Ts4WB6	Test Section 4	Wall	Bottom 6	1.0042	-0.0166	0.1067
T_Ts4WI	Test Section 4	Wall	Inlet	0.9988	0.1375	0.1912
T_Ts4WO	Test Section 4	Wall	Outlet	0.9984	0.139	0.2111
T_Ts4WT1	Test Section 4	Wall	Top 1	1.0017	0.0199	0.1164
T_Ts4WT2	Test Section 4	Wall	Top 2	0.9996	0.1574	0.1402
T_Ts4WT3	Test Section 4	Wall	Top 3	0.9993	0.0777	0.1118
T_Ts4WT4	Test Section 4	Wall	Top 4	1.0047	-0.05	0.1265
T_Ts4WT5	Test Section 4	Wall	Top 5	1.0036	-0.012	0.1256
T_Ts4WT6	Test Section 4	Wall	Top 6	1.0025	0.0265	0.132
T_Ts5CBi	Test Section 5	Coolant	Bottom Inlet	1.002	-0.1177	0.1069
T_Ts5CBo	Test Section 5	Coolant	Bottom Outlet	1.0039	-0.1619	0.117
T_Ts5CTi	Test Section 5	Coolant	Top Inlet	1.0048	-0.1385	0.1294
T_Ts5CTo	Test Section 5	Coolant	Top Outlet	1.0072	-0.2049	0.1728
T_Ts5WB1	Test Section 5	Wall	Bottom 1	1.0029	0.0405	0.1075
T_Ts5WB2	Test Section 5	Wall	Bottom 2	1.0022	0.0626	0.1116
T_Ts5WB3	Test Section 5	Wall	Bottom 3	1.0024	0.0315	0.1086
T_Ts5WB4	Test Section 5	Wall	Bottom 4	1.0033	0.0021	0.1151
T_Ts5WB5	Test Section 5	Wall	Bottom 5	1.0024	0.0137	0.1111
T_Ts5WB6	Test Section 5	Wall	Bottom 6	1.0014	0.037	0.1142
T_Ts5WI	Test Section 5	Wall	Inlet	0.9983	0.1419	0.2185
T_Ts5WO	Test Section 5	Wall	Outlet	0.9987	0.1421	0.1614
T_Ts5WT1	Test Section 5	Wall	Top 1	1.0016	0.0762	0.1219
T_Ts5WT2	Test Section 5	Wall	Top 2	1.0042	-0.0093	0.1086
T_Ts5WT3	Test Section 5	Wall	Top 3	1.0034	-0.0035	0.1724
T_Ts5WT4	Test Section 5	Wall	Top 4	1.0019	0.0445	0.1233
T_Ts5WT5	Test Section 5	Wall	Top 5	1.002	0.056	0.1086
T_Ts5WT6	Test Section 5	Wall	Top 6	1.0044	0.0107	0.1066

Name	Component	Fluid/Material	Location	Slope	Intercept	Accuracy [ºC]
T_Ts6CBi	Test Section 6	Coolant	Bottom Inlet	1.0023	-0.1106	0.1077
T_Ts6CBo	Test Section 6	Coolant	Bottom Outlet	1.0012	-0.1374	0.105
T_Ts6CTi	Test Section 6	Coolant	Top Inlet	1.0053	-0.1406	0.1108
T_Ts6CTo	Test Section 6	Coolant	Top Outlet	1.0033	-0.1184	0.105
T_TS6RO	Test Section 6	Refrigerant	Outlet	1.0031	0.0587	0.1274
T_Ts6WB1	Test Section 6	Wall	Bottom 1	1.0015	0.0798	0.1239
T_Ts6WB2	Test Section 6	Wall	Bottom 2	1.0032	0.0288	0.1269
T_Ts6WB3	Test Section 6	Wall	Bottom 3	1.0015	0.0662	0.1183
T_Ts6WB4	Test Section 6	Wall	Bottom 4	1.0045	0.001	0.1072
T_Ts6WB5	Test Section 6	Wall	Bottom 5	1.0013	0.067	0.1143
T_Ts6WB6	Test Section 6	Wall	Bottom 6	1.0023	0.0362	0.1067
T_Ts6WI	Test Section 6	Wall	Inlet	1	0.1232	0.1484
T_Ts6WO	Test Section 6	Wall	Outlet	1.0019	0.1047	0.1355
T_Ts6WT1	Test Section 6	Wall	Top 1	1.0024	0.0078	0.1069
T_Ts6WT2	Test Section 6	Wall	Top 2	1.0019	0.0375	0.1194
T_Ts6WT3	Test Section 6	Wall	Top 3	1.0032	0.0404	0.131
T_Ts6WT4	Test Section 6	Wall	Top 4	1.0026	0.0616	0.1147
T_Ts6WT5	Test Section 6	Wall	Top 5	1.001	0.0874	0.109
T_Ts6WT6	Test Section 6	Wall	Top 6	1.0029	0.0341	0.117

Appendix B Contact resistance and temperature uniformity data

Test case	Block	Coolant side Q [W]	Refrigerant side Q [W]	Average of 6 TCs [oC]	Variance of 6 TCs[oC]	Standard Deviation of 6 TCs [oC]	Estimated T_{wall} (w/o contact resistance) [oC]	Estimated T_{wall} (w/ contact resistance) [oC]	$hA_{contact}$ [W-K^{-1}]	Heat Transfer Coefficient (w/o calibration) [W-K^{-1}-m^{-2}]	Heat Transfer Coefficient (w/ calibration) [W-K^{-1}-m^{-2}]
1	Top	11.55	11.99	13.63	0.47	0.20	13.63	13.63	0.00	482.21	482.21
	Bottom	11.02	11.57	13.72	0.40	0.16	13.71	13.63	132.39	488.41	499.54
Errors	Top	0.70								33.12	33.12
	Bottom	1.17								49.85	51.13
2	Top	19.58	19.55	17.74	0.51	0.22	17.73	17.73	0.00	619.43	619.43
	Bottom	19.20	19.16	17.88	0.45	0.17	17.87	17.73	139.43	613.52	632.01
Errors	Top	0.71								29.03	29.03
	Bottom	1.19								40.63	42.19
3	Top	-17.27	-16.85	16.85	0.80	0.33	16.86	16.86	0.00	395.98	395.98
	Bottom	-15.32	-14.80	16.75	0.70	0.29	16.76	16.86	145.44	460.47	450.86
Errors	Top	0.70								21.75	21.75
	Bottom	1.13								32.59	31.71
4	Top	25.33	25.40	19.57	0.31	0.11	19.56	19.56	0.00	4860.71	4860.71
	Bottom	25.22	25.27	19.81	0.44	0.14	19.79	19.56	109.75	3934.98	4884.61
Errors	Top	0.19								382.53	382.53
	Bottom	0.38								254.45	388.29
5	Top	9.88	10.06	19.18	0.10	0.04	19.18	19.18	0.00	3727.87	3727.87
	Bottom	9.67	9.91	19.28	0.12	0.05	19.27	19.18	102.05	3155.16	3783.19
Errors	Top	0.20								580.40	580.40
	Bottom	0.33								410.30	584.12
6	Top	9.75	9.97	19.04	0.12	0.04	19.03	19.03	0.00	4229.44	4229.44

Test case	Block	Coolant side Q [W]	Refrigerant side Q [W]	Average of 6 TCs [oC]	Variance of 6 TCs[oC]	Standard Deviation of 6 TCs [oC]	Estimated T_{wall} (w/o contact resistance) [oC]	Estimated T_{wall} (w/ contact resistance) [oC]	$hA_{contact}$ [$W\text{-}K^{-1}$]	Heat Transfer Coefficient (w/o calibration) [$W\text{-}K^{-1}\text{-}m^{-2}$]	Heat Transfer Coefficient (w/ calibration) [$W\text{-}K^{-1}\text{-}m^{-2}$]
	Bottom	9.75	10.03	19.14	0.13	0.05	19.13	19.03	100.27	3418.52	4204.27
Errors	Top	0.56								858.20	858.20
	Bottom	0.62								590.70	873.61
7	Top	9.72	10.01	18.54	0.12	0.05	18.53	18.53	0.00	4260.85	4260.85
	Bottom	9.61	9.94	18.63	0.14	0.05	18.62	18.53	108.61	3532.84	4288.08
Errors	Top	0.20								757.95	757.95
	Bottom	0.33								524.24	766.16
8	Top	19.79	19.94	18.28	0.28	0.10	18.24	18.24	0.00	3957.84	3957.84
	Bottom	19.73	19.93	18.44	0.32	0.11	18.40	18.24	123.28	3369.92	3959.47
Errors	Top	0.60								392.80	392.80
	Bottom	0.64								292.54	396.23
9	Top	10.06	10.00	19.44	0.14	0.05	19.18	19.43	0.00	2333.00	2333.00
	Bottom	10.01	9.98	19.52	0.11	0.04	19.27	19.43	129.44	2128.89	2337.97
Errors	Top	0.46								275.58	275.58
	Bottom	0.62								248.87	292.87
10	Top	20.08	19.92	20.06	0.29	0.10	19.18	20.05	0.00	3160.19	3160.19
	Bottom	20.15	20.01	20.24	0.27	0.10	19.27	20.05	112.55	2728.69	3146.18
Errors	Top	0.49								242.75	242.75
	Bottom	0.62								194.18	251.95
11	Top	20.04	19.91	20.14	0.32	0.12	19.18	20.12	0.00	3781.96	3781.96
	Bottom	20.10	20.02	20.32	0.23	0.09	19.27	20.12	109.50	3166.08	3761.97
Errors	Top	0.49								340.33	340.33
	Bottom	0.62								254.17	350.89

Test case	Block	Coolant side Q [W]	Refrigerant side Q [W]	Average of 6 TCs [oC]	Variance of 6 TCs[oC]	Standard Deviation of 6 TCs [oC]	Estimated T_{wall} (w/o contact resistance) [oC]	Estimated T_{wall} (w/ contact resistance) [oC]	$hA_{contact}$ [$W\text{-}K^{-1}$]	Heat Transfer Coefficient (w/o calibration) [$W\text{-}K^{-1}\text{-}m^{-2}$]	Heat Transfer Coefficient (w/ calibration) [$W\text{-}K^{-1}\text{-}m^{-2}$]
12	Top	20.08	19.92	20.06	0.29	0.10	20.02	20.02	0.00	3243.35	3243.35
	Bottom	20.15	20.00	20.24	0.27	0.10	20.20	20.02	112.63	2791.03	3228.97
Errors	Top	0.49								255.04	255.04
	Bottom	0.62								202.30	264.37
13	Top	19.79	19.94	18.28	0.18	0.10	18.24	18.24	0.00	3957.84	3957.84
	Bottom	19.73	19.93	18.44	0.10	0.11	18.40	18.24	123.28	3369.92	3959.47
Errors	Top	0.60	0.60							392.80	392.80
	Bottom	0.64	0.64							292.54	396.23
14	Top	14.86	14.97	18.17	0.17	0.06	18.04	18.04	0.00	3748.44	3748.44
	Bottom	14.85	15.01	18.26	0.10	0.04	18.12	18.04	117.98	3190.24	3742.57
Errors	Top	0.59	0.59							698.09	698.09
	Bottom	0.62	0.62							524.31	706.73
15	Top	14.66	14.92	18.15	0.32	0.08	18.12	18.12	0.00	4089.77	4089.77
	Bottom	14.64	14.94	18.27	0.27	0.07	18.24	18.12	124.51	3463.93	4083.91
Errors	Top	0.60	0.60							555.42	555.42
	Bottom	0.64	0.64							411.67	561.59
16	Top	19.82	19.98	18.58	0.32	0.11	18.53	18.53	0.00	2389.95	2389.95
	Bottom	19.77	19.96	18.73	0.27	0.10	18.69	18.53	128.50	2171.85	2391.94
Errors	Top	0.61								132.60	132.60
	Bottom	0.65								115.87	135.89

Appendix C Original data of experiments

G [$kgm^{-2}s^{-1}$]	Q" [Wm^{-2}]	x [-]	dx [-]	T_{wall} [^oC]	T_{ref} [^oC]	P_{sat} [kPa]	Q [W]	HTC [$Wm^{-2}K^{-1}$]	eHTC [$Wm^{-2}K^{-1}$]	PD [kPa m^{-1}]	ePD [kPa m^{-1}]
120.8	3610.1	0.093	0.167	18.2	17.3	526.4	39.9	3907.0	354.4	7.847	0.008
120.8	3608.0	0.239	0.166	17.6	16.9	519.2	39.8	4750.7	531.6	12.133	0.055
120.8	3594.4	0.412	0.166	16.7	16.0	506.4	39.7	5012.1	594.5	20.238	0.083
120.8	3613.7	0.575	0.166	15.5	14.9	488.9	39.9	5551.8	748.2	25.945	0.083
120.8	3604.3	0.745	0.164	13.9	13.3	465.5	39.8	5752.8	829.7	33.906	0.055
120.8	3621.9	0.919	0.164	12.0	11.1	439.0	40.0	4336.0	478.7	36.918	0.083
120.6	2714.3	0.066	0.126	18.1	17.2	524.0	30.0	2843.9	256.2	5.753	0.008
120.6	2710.0	0.214	0.125	17.5	16.8	517.7	29.9	3569.9	405.7	11.235	0.055
120.6	2697.8	0.380	0.125	16.7	16.0	506.3	29.8	3695.9	435.2	18.654	0.083
120.6	2723.8	0.540	0.126	15.8	15.0	490.2	30.1	3496.4	400.3	23.904	0.083
120.6	2711.7	0.729	0.125	14.2	13.5	468.3	29.9	3837.1	497.2	32.816	0.055
120.6	2728.9	0.908	0.124	12.4	11.5	442.5	30.1	3133.9	336.2	36.262	0.083
121.5	1806.3	0.041	0.083	18.2	17.3	526.3	19.9	2049.0	172.1	3.900	0.008
121.5	1803.4	0.278	0.083	17.6	16.9	520.4	19.9	2758.7	370.3	12.457	0.055
121.5	1809.0	0.437	0.084	16.8	16.1	508.0	20.0	2750.3	365.0	19.523	0.083
121.5	1796.0	0.581	0.083	15.8	15.1	491.7	19.8	2488.5	315.7	23.812	0.083
121.5	1795.9	0.738	0.082	14.3	13.7	470.4	19.8	2818.3	414.1	31.090	0.055
121.5	1780.5	0.891	0.081	12.5	11.8	445.6	19.7	2357.8	298.0	34.706	0.083